Master Thesis in Geosciences

Argentine margin (north of 48°S): regional tectonic evolution based on integrated analysis of seismic reflection and potential field data and modelling

by

Enric León

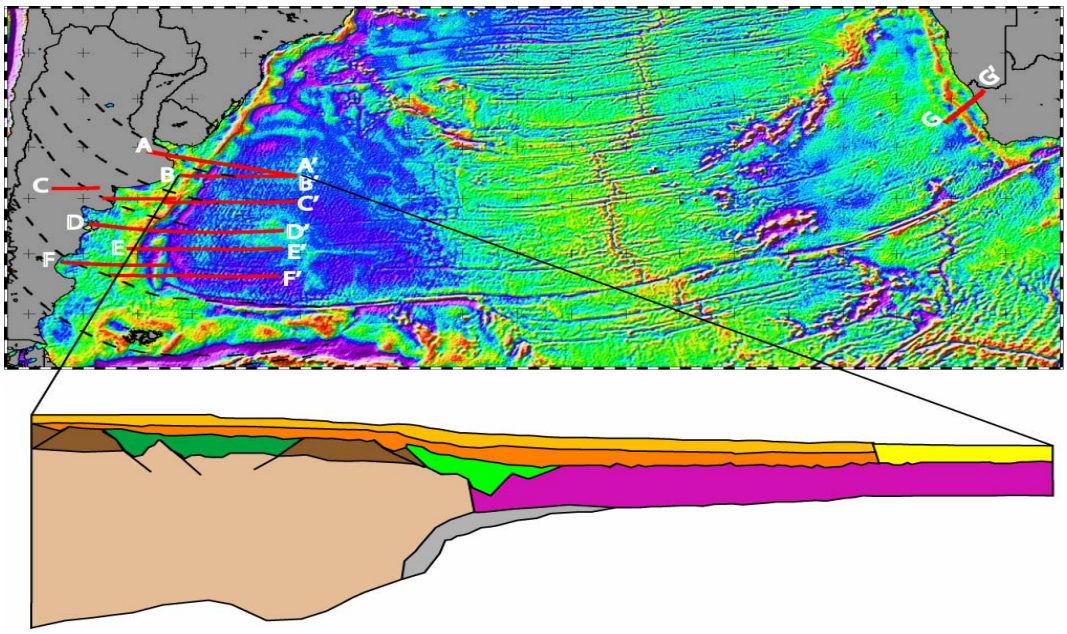

UNIVERSITY OF OSLO

FACULTY OF MATHEMATICS AND NATURAL SCIENCES

Argentine margin (north of 48°S): regional tectonic evolution based on integrated analysis of seismic reflection and potential field data and modelling

by

Enric León

Master Thesis in Geosciences

Discipline: Petroleum Geology and Geophysics

Department of Geosciences

Faculty of Mathematics and Natural Sciences

UNIVERSITY OF OSLO

[June 2007]

Tutor(s): Assoc. Prof. Filippos Tsikalas and Prof. Jan Inge Faleide, UiO

This work is published digitally through DUO – Digitale Utgivelser ved UiO

http://www.duo.uio.no

It is also catalogued in BIBSYS (http://www.bibsys.no/english)

Contents

Preface

This Master Thesis culminates the two-year Master Program on Petroleum Geology and Geophysics, carried out at the Department of Geosciences, University of Oslo, and supervised by Assoc. Prof. Filippos Tsikalas and Prof. Jan Inge Faleide. The study is based on the analysis of integrated seismic and potential field data and modelling on the Argentine margin.

Acknowledgements

First of all, I want to express my gratitude to Assoc. Prof. Filippos Tsikalas for the technical support and his devoted dedication during the continuous evaluation of the work. I am also grateful to Prof. Jan Inge Faleide for the interesting suggestions on the discussion and the final corrections. I would like to thank Ph.D.-candidate Olav Antonio Blaich for his kind help, technical support and discussions. Finally, I want to thank Sille for her patience and support during these years.

University of Oslo, June 2007

Enric León Sistach

Chapter 1
Introduction

The opening of the South Atlantic Ocean followed the fragmentation of Gondwana super-continent in Late Jurassic-Early Cretaceous times and resulted in the development of conjugate passive continental margins (Hinz et al., 1999). The South Atlantic oceanic basin extends over the vast area between Africa and South America, between the Equator and 50ºS approximately. The main bathymetric features (Fig. 1.1) reveal fairly symmetrical margins, with the axis centred along the mid-oceanic ridge. The abyssal plain at both sides of the ridge is interrupted by two conspicuous bathymetric structures: the Río Grande Rise and the Walvis Ridge (Fig. 1.1). On the South American side, the NW-SE trending Río Grande Rise separates the Brazil Basin to the north from the Argentine Basin to the south, while on the conjugate African side, the Angola Basin and the Cape Basin are separated by the NE-SW trending Walvis Ridge. Farther south, two prominent linear features extend transversally to the ridge trend: the Falkland/Malvinas Escarpment and the Agulhas Fracture Zone (Fig. 1.1). The Argentine continental margin is one of the most extensive margins in the world, as it extends over a length of 2300 km and a width of 350 km (to the 200-m isobath) (Keeley et al., 1993). Despite the intense exploration activity that has taken place since the 1960's, the Argentine continental margin is still considered to be in its initial stage of exploration (Lesta, 2003), confirmed at present, by the low density coverage of geophysical and geological data across the area.

The final break-up of SW Gondwana and subsequent opening of the South Atlantic has been dated around 130 Ma (Early Cretaceous) from different authors, based on identified magnetic anomalies on oceanic floor (e.g. Nürnberg, 1997). The opening of the South Atlantic started as a combined rift motion and strike-slip deformation. At Campanian time (84 Ma), the African and South American plates separated by simple divergence (Nürnberg, 1991). Breakup was accompanied by massive, transient magmatic activity. This magmatism is recognized by the continental flood basalt provinces of Paraná and Etendeka (Gladczenko et al., 1997). The Río Grande Rise and the Walvis Ridge connect these two provinces through the Tristan da Cunha hotspot trail (Fig. 1.1). A common tectono-volcanic crustal structure has been identified in both conjugate margins across the South Atlantic (Hinz et al. 1999; Gladczenko et al. 1997), characterized by a voluminous volcanic wedge of seaward-dipping

reflectors. On the outer South American margin, it stretches over a distance of 3500 km from 48°S to 20°S. The volume of these volcanic extrusions decreases southward on the Argentine Margin, as they approach the transform margin of the Falkland/Malvinas Plateau (Hinz et al., 1999).

The formation of the basins on the Argentine margin has been attributed at least to two rifting episodes. The first one, during Late Triassic-Early Jurassic time (Urién & Zambrano, 1996), created the basins of San Jorge (Fig. 1.1), San Julián and Northern Malvinas (cfr. Fig. 2.6), in an intracratonic setting of southern Gondwana prior to breakup. The extensive, Late Jurassic-Early Cretaceous rifting episode that resulted in the breakup of South America and Africa, gave rise to the Salado, Colorado, Valdés-Rawson (Fig. 1.1) and Malvinas (cfr. Fig. 2.6) basins, evolving in a passive margin setting. The origin of the Salado and Colorado basins is still under discussion. Their particular orientation and the fact that they are not deepening regularly towards the continental margin led some authors to interpret them as failed rift arms (Max et al., 1999), extending westward from a triple point in the incipient Gondwana rift.

The hydrocarbon exploration on the Argentine Margin is still in a relatively early stage. By the end of 2001, ten basins were under development, with a total of 300.000 km of 2D seismic lines and 182 exploration wells. These numbers are small, considering the extension of the Argentine continental margin (3.000.000 km²) (Lesta, 2003). The exploration activity offshore Argentina has not been regular through time, nor for the different basins. The lack of early success and adequate technology may have been one of the causes of the delay in the exploration process. To date, only a few wells have been drilled at water-depths greater than 100 m. The location of the continent-ocean boundary/transition (COB/COT) is of main interest for the hydrocarbon exploration in offshore frontier areas, since it is considered to mark the limit of the exploration zone. Locating the correct position of this boundary/zone is a controversial issue, which is in part dealt with by potential field methods.

Potential field gravity and magnetic data and modelling are valuable tools that complement the imaging of the crust provided by seismic reflection/refraction methods. By integrating seismic reflection/refraction data, gravity, magnetics, bathymetry and sediment thickness, the objective of this study is to provide a wider constraint spectrum to the understanding of the continental margin evolution. In particular, the analysis aims to the understanding of the crustal structure and basin architecture. The focus of this study is on: gravity modelling across

the margin; better definition of the COB/COT; redefinition/improvement of the structural setting; discussion of the basin architecture across the conjugate margins.

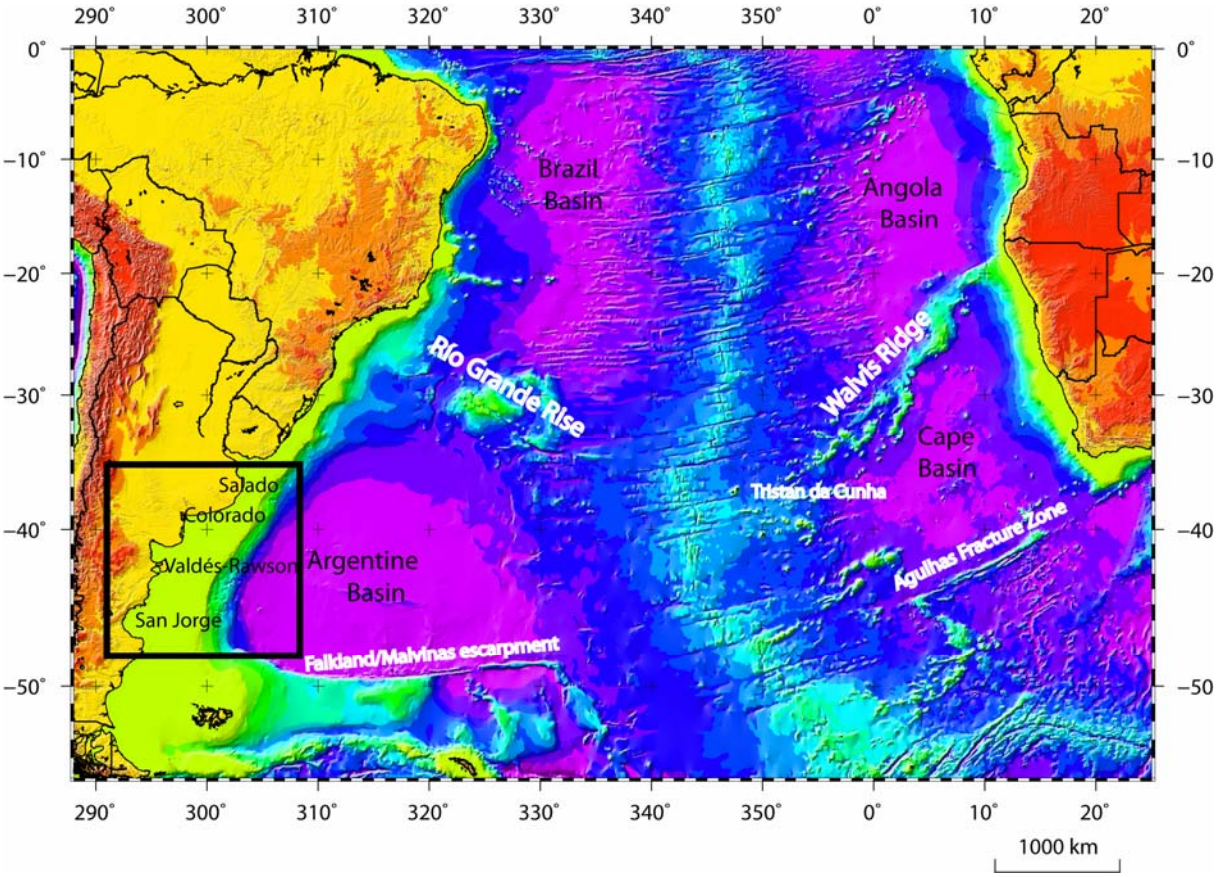

Fig 1.1. 1x1' GEBCO elevation grid (General Bathymetric Chart of the Oceans, Jakobsson et al., 2000). Study area outlined with rectangle.

Chapter 2
Geological background

The present tectono-sedimentary configuration of the Argentinian continental margin is the result of a long and complex geological history, culminating in the separation between South America and Africa. The creation of the South Atlantic margins as a result of the Mesozoic breakup of Gondwana has been strongly influenced by the structural inheritance of this supercontinent. Hence, it is very important to understand the geological features and structural trends of the reconstructed Gondwana before breakup, as well as the pattern of separation followed during the opening of the South Atlantic. Pre-existing (mostly Precambrian) structures have played a large part in determining the line of continental breakup. The positions of boundaries between different age basement blocks and the structural grain of the basement controlled the line of separation and the position of the failed rifts (Macdonald, 2003).

2.1. SW Gondwana before breakup (pre-rift phase)

After breakup of the supercontinent Rodinia in the end Mesoproterozoic, a subsequent drifting and later amalgamation of several cratonic blocks resulted in the formation of the Gondwana supercontinent in the end Neoproterozoic-Paleozoic (Cawood, 2005). The assembly of these continental blocks is related to different orogenies that have been recognized throughout Gondwana. The Panafrican orogenies (East African, Pinjarra, Damara and Braziliano) during the early Paleozoic, are related to multiple assembly of East and West Gondwana into a supercontinent. The so-called Gondwanide Orogeny took place in latest Paleozoic to early Mesozoic (Dalziel, 2005). Gondwana was then a mosaic of many highly varied Precambrian terrains, separated by late Proterozoic-early Paleozoic orogenic belts (Fig. 2.1). These belts can be traced across Africa, South America, Antarctica and Australia (de Wit, 1999). The southern margin of Gondwana was dominated by Cordillera-type tectonics probably since Precambrian times, with convergent and/or strike-slip translation settings (de Wit, 1999).

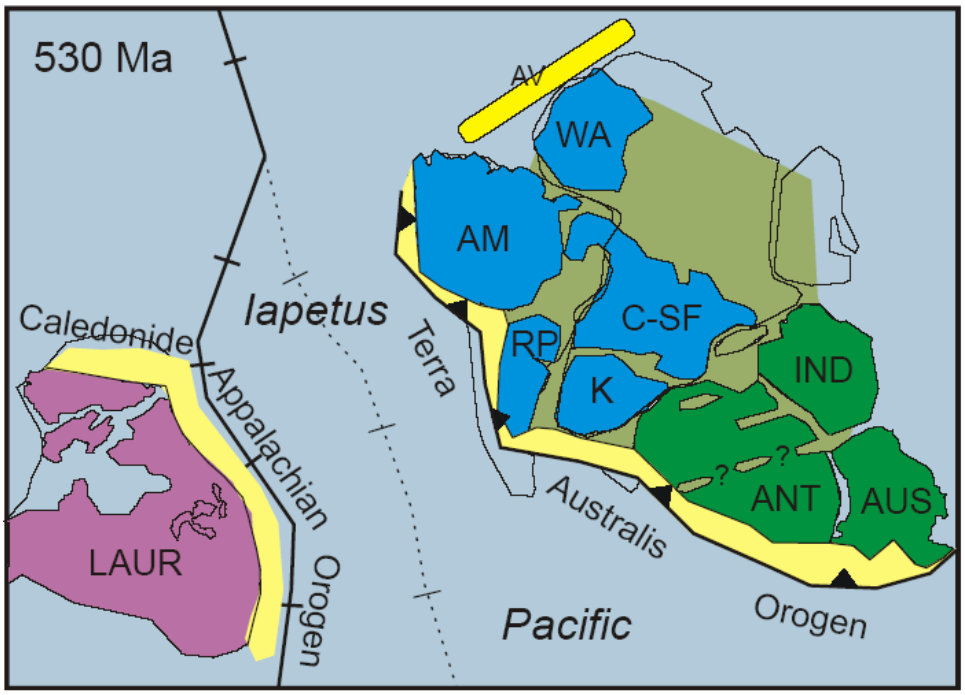

Fig. 2.1. Paleogeographic reconstruction of Gondwana at around 530 Ma, after final assembly of the West (blue) and the East (green) segments, each of which is composed of several cratonic blocks (AM-Amazonia, ANT-Antarctica, AUS-Australia, AV-Avalonia, C-SF-Congo-San Francisco, IND-India, K-Kalahari, LAUR-Laurentia, RP-Río de la Plata, WA-West Africa) (after Cawood et al. 2005).

2.1.1 Gondwanide Orogeny

A deformation belt of latest Paleozoic to early Mesozoic age within the former Gondwana continent has been described across parts of South America (Sierra de la Ventana, in southern Tandil High, cfr. Fig. 2.7), the Cape mountains of southern South Africa, eastern Australia and presumably, in Antarctica (Fig. 2.2). The origin of these fold belts has been historically attributed to the amalgamation of the Patagonia Terrane against the Río de la Plata craton (Urién & Zambrano, 1996) although other hypothesis have been proposed.

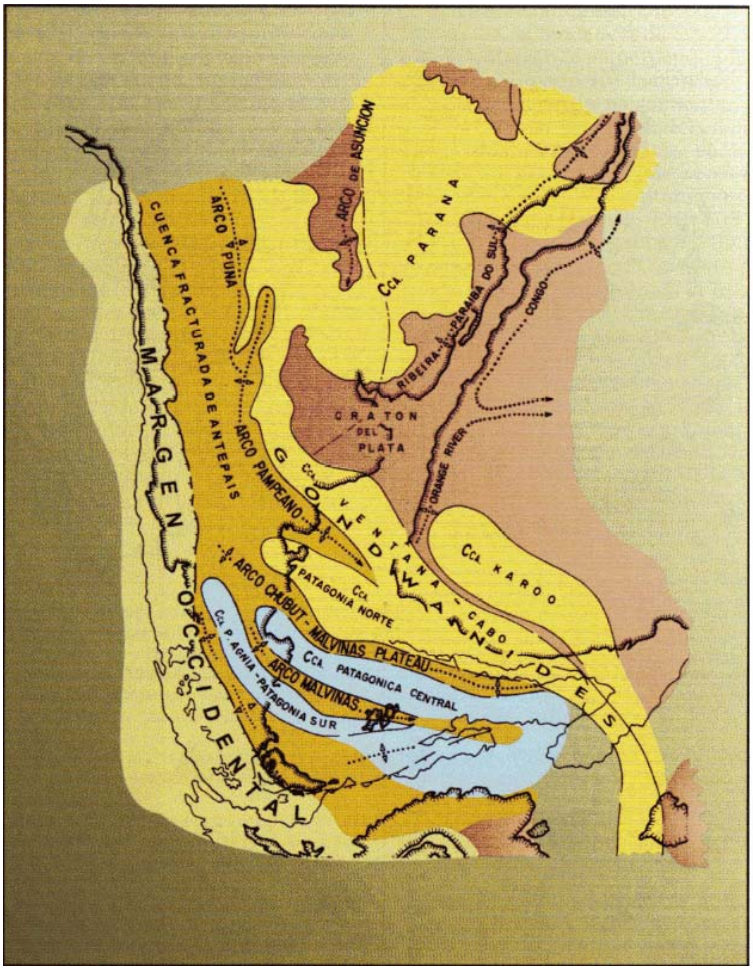

Fig. 2.2. Paleogeographic reconstruction of SW Gondwana prior to separation at 162 Ma (Middle-Late Jurassic). The Gondwana fold belt ("Gondwanides" in figure) are shown as a NW-SE oriented yellow strip to the south of the "Río de la Plata" craton in South America, and along southern South Africa (after Urien & Zambrano, 1996).

Cawood et al. (2005) suggested an accretionary model in which small continent terranes where acreted at different positions and times against SW Gondwana during Paleozoic times. Pankhurst et al. 2006 reviewed previous hypothesis of continental accretion involving the collision of the Patagonia terrane with Gondwana during Late Paleozoic to explain the fold belts of South America and South Africa. These authors repositioned the northern boundary of the Patagonia terrane along the Huincul Fault (Fig. 2.3). Moreover, the so-called Southern Patagonia terrane, represented by the Deseado Massif, is believed to have collided with the North Patagonian Massif in mid-Carboniferous times as a result of a NE directed ocean floor subduction (Pankhurst et al., 2006). The suture zone would lie beneath the Mesozoic sediments of the San Jorge Basin. As a consequence of this collision, a belt of deformed

Paleozoic sedimentary sequences of the Sierra de la Ventana (Cape region of South Africa, the Falkland Islands and the Ellsworth Mountains of West Antarctica) was formed, as they were forced up against the Río de la Plata and Kaapvaal cratons (Pankhurst et al., 2006). The granitic intrusives of the North-Patagonian Massif and the Deseado Massif can be attributed to this orogeny. It is likely that other intrusives from the core of the orogen are found beneath the Agulhas Plateau and the Malvinas/Falkland Platform (Ramos & Turic, 1996). Furthermore, based on magnetic studies over the Argentine continental shelf, Max et al. (1999) proposed multiple accretion of microcontinent fragments termed the Patagonia Platform, against the southern margin of the Río de la Plata craton, during Late Paleozoic. The line of suture has been placed along the Colorado Discontinuity (cfr. Fig. 2.6) by Ghidella et al. (1995), representing a NW-SE oriented line separating two regions with very contrasting magnetic responses.

Another hypothesis that explains the formation of the Gondwanide fold belts is presented by Dalziel et al. (2000), by which a hot mantle plume beneath the subduction zone produced a flattening of a segment of oceanic lithosphere being subducted beneath Gondwanaland. The flattening produced tractions that were transmitted to the base of the overriding plate far into the interior of the supercontinent, with associated deformation of basement and supracrustal sediments. This model provides a casual linking between the Gondwanide Orogeny and the Karroo-Ferrar Large Igneous Province (LIP). The early Mesozoic Gondwanide Orogeny in South America, southern Africa and Antarctica immediately preceded the emplacement of a LIP associated with the initial fragmentation of Gondwana (Dalziel et al. 2000).

2.2 Break-up of southern Gondwana (syn-rift phase)

The rift in the South Atlantic propagated stepwise northward, starting in the southernmost Atlantic. Recent reconstructions of Gondwana prior to break-up have achieved a better fit between Africa and South America by treating the latter as a non-rigid single block, as well as by considering the presence of micro-continents within the plate setting (Macdonald, 2003). That is, a split of the South American plate into at least four sub-plates separated by strike-slip fractures or by dyke swarms (Fig. 2.3): a northern (Brazilian) plate, bounded to the south by the line of the Paraná dyke swarm; a north-central (Paraná) plate, bounded to the south by the Colorado-Huincul line; a south-central (Río Negro) plate, bounded to the south by the Gastre

Fault System; and a southern (Patagonian) plate. This configuration of South America is in agreement with the reconstructed position of the Falkland/Malvinas islands in the Early Jurassic, east of South Africa and rotated 180 to 190 degrees from its actual position.

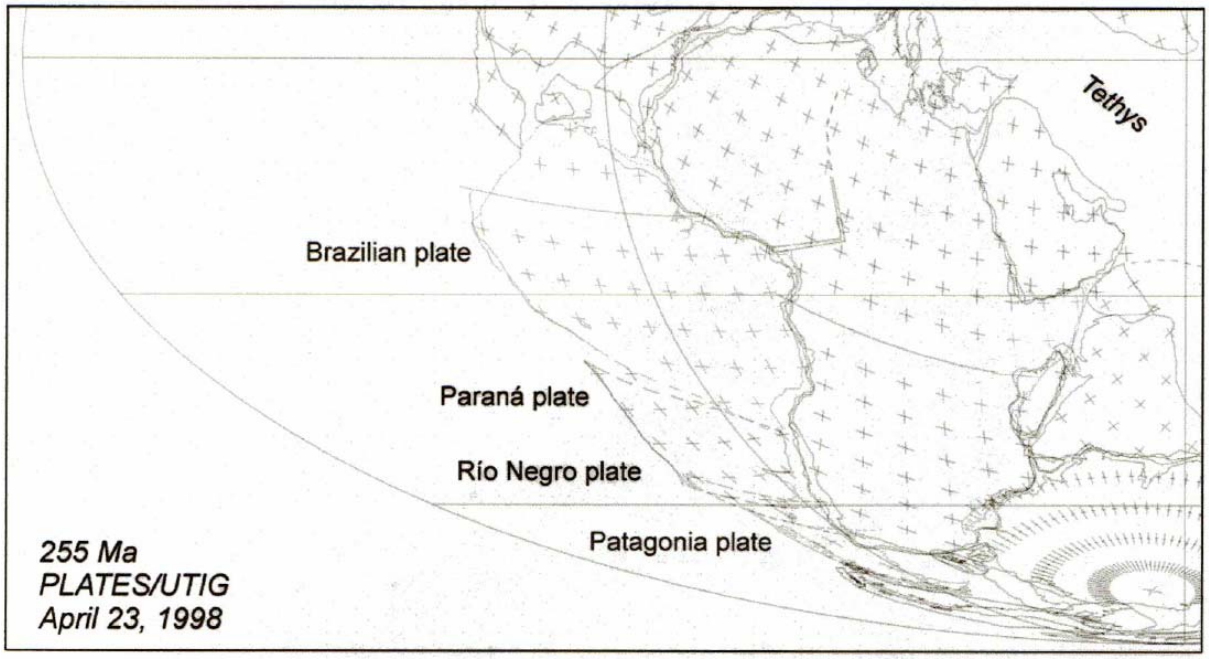

Fig. 2.3. Reconstruction of SW Gondwana at 255 Ma based on a four-plate South America (after Macdonald et al., 2003).

From Early Permian, regional extension created a rift system in Gondwana, which propagated from eastern Africa in a SW direction towards the Malvinas/Falkland Plateau region. The continental extension in South America began in the Late Triassic, with the formation of some intracratonic basins in Patagonia (San Jorge, Northern Malvinas, San Julián). At that time, a mantle plume created the large magmatic province of Karoo-Ferrar over most of South Africa and an extense part of East Antarctica (Macdonald et al. 2003). By Late Jurassic (150 Ma), the evolving rifting resulted in the separation of Gondwana in two parts: a western Gondwana which included Africa and South America, and an eastern Gondwana, made up of Antarctica, Australia, India, Malagasy (Madagascar) and New Zealand (Fig. 2.4) (de Wit, 1999). The next phase in the breakup was more complex due to simultaneous rifting between Africa and South America and between (Antarctica-Australia) and (India-Malagasy) in Early Cretaceous times, at about 135-120 Ma (Fig. 2.5).

Antarctica started moving eastward as southern South America moved westward from a fixed Africa. The Falkland/Malvinas block rotated by 180 and the Patagonia block moved dextrally along the Gastre Fault System.

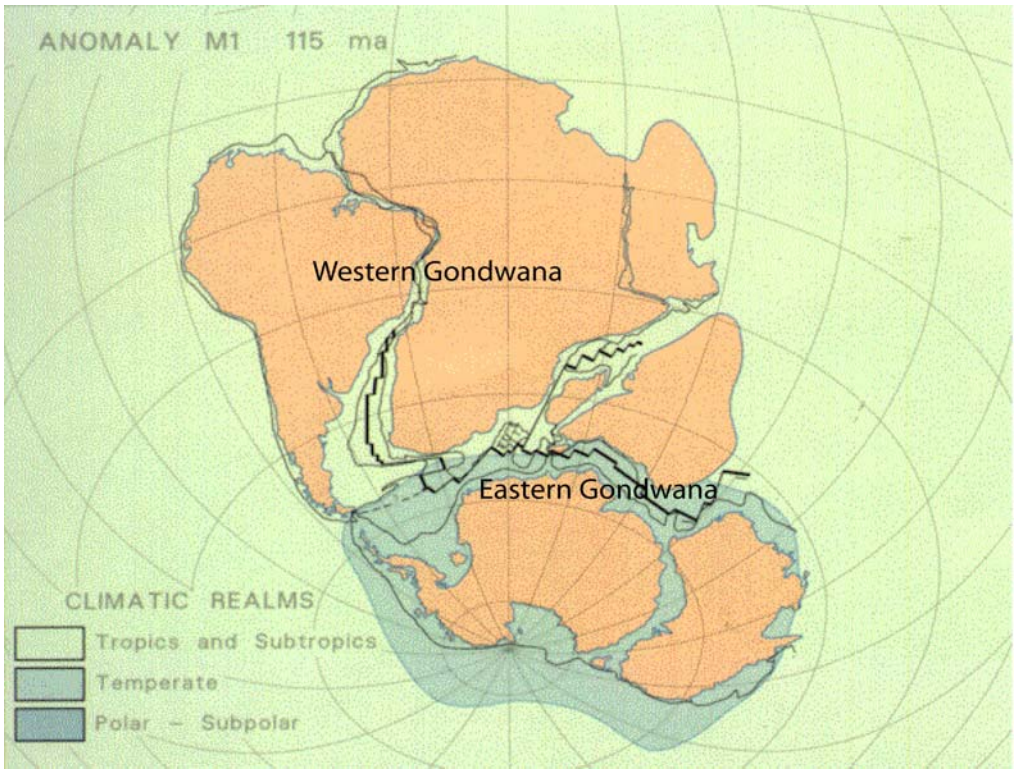

Fig. 2.4. Early Cretaceous reconstruction of Gondwana. Simultaneous break-up of South America and Africa and Antarctica-Australia from India-Malagasy (de Wit et al., 1993).

A fit reconstruction of the South Atlantic can only be achieved by considering intracontinental deformation during initial opening (Nürnberg & Müller, 1991). These authors suggested rift motion combined with minor strike-slip movement along intracontinental zones of weakness across Gondwana. These zones are found in Africa (the Benue Trough/Niger Rift system) and also in South America: intracontinental deformation has been described along the Parana and Chacos Basin shear zone and in the Salado and Colorado rift basins (Fig. 2.5). The two latter basins, oriented almost perpendicular to the Atlantic margin, are described as aulacogenic rift basins (Urien & Zambrano, 1996). Their orientation, transversal to the continental margin, is attributed to the structural control of the Paleozoic Gondwanide fold belt, with oblique extension resulting in rotation of the NE Brazil microplate, and strike-slip movements along the Pernambuco Shear Zone, with creation of transtensional depocentres.

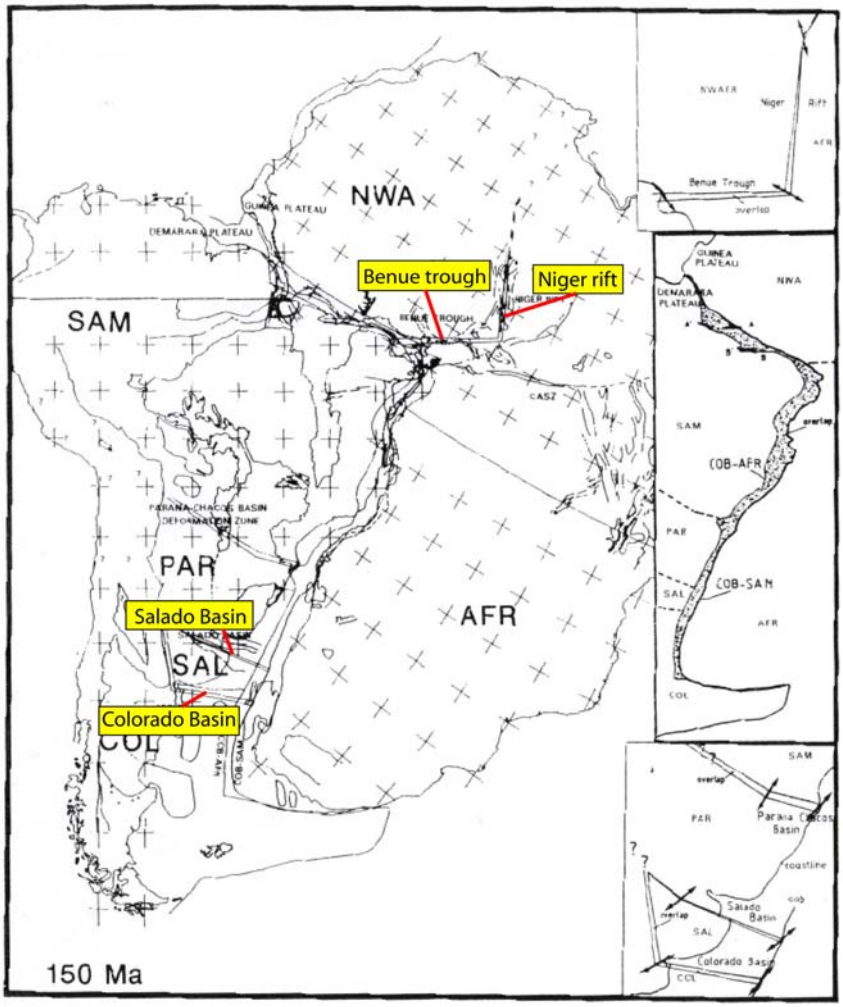

Fig. 2.5. Reconstruction of SW Gondwana at 150 Ma (Latest Jurassic). Intracontinental deformation zones which developed in transtensional basins are shown (modified after Nürnberg & Müller, 1991).

During the first rift phase (150-130 Ma), the rift propagated to about 38°S, in the vicinity of the Salado Basin. It caused continental stretching and minor dextral strike-slip motion within the Colorado and Salado basins, and continued at 130 Ma along the Paraná-Chacos Basin deformation zone. At 130 Ma, widespread rifting led to continental break-up. The Paraná-Etendeka mantle-plume, centred on Brazil and Namibia, generated extensive volcanism with flood basalts in the Paraná and Parnaíba basins. Between Chron M4 (126.5 Ma) and Chron M0 (118.7 Ma), rifting ceased in the Salado and Colorado basins and propagated northward into the Benue through (Nürnberg & Müller, 1991).

2.3 Post-rift

At Chron M0 (118.7 Ma), the Equatorial Atlantic begun to open and by Late Albian-Early Cenomanian, extension in the South Atlantic changed from oblique to normal to the margin and total separation between Africa and South America was consumated, allowing to full connection between the central and the South Atlantic (Nürnberg & Müller, 1991). Most of the marginal basins were now in a thermal sag phase and had been transgressed, but interior basins had no marine influence yet. After total separation between Africa and South America (Chron 34 – Santonian), the opening of the South Atlantic was characterized by simple divergence of two plates, only complicated by variations in seafloor spreading rate and direction and by fracture zone and ridge jumps (Nürnberg, 1991). The extension changed from oblique to normal to the margin by Albian to Cenomanian times (Macdonald, 2003). The atlantic margins were under a thermal sag phase and most of the basins had been transgressed. Salt tectonism took place in the basins to the North of the Río Grande Rise – Walvis Ridge.

2.4 Argentine margin

The Argentine Margin exhibits a characteristic configuration in a set of sedimentarty basins and highs, with a dominant elongation trend at high angle to the margin edge, which has been attributed to the inheritance of pre-breakup structural trends of former Gondwana. This type of basin configuration differs with that of the Brazilian and its conjugate southern African margin, where the basins constitute a narrow belt paralleling the shelf edge. The simplified tectonic map of the Argentine margin (Fig. 2.6) reveals the presence of several Mesozoic basins related to extension and breakup of Gondwana, separated by structural highs of mostly Paleozoic and Precambrian rocks. The main extensional faults are marked, and the direction of the pre-breakup tectonic grain is defined by the elongation of the basement highs. The width of the margin is marked by the 500 m bathymetry contour. The general structural trend (W-E, NW-SE) displayed by the elongation of the basins and highs is orthogonal to the continental margin. The main basins within the study area include, from north to south, the Salado, Colorado. Valdés-Rawson, San Jorge and San Julián basins. South of the study area, along 48ºS, a first order E-W trending geomorphological feature, the Falkland /Malvinas Escarpment, separates the Argentine Basin from the Falkland/Malvinas Plateau (Fig. 2.6). The

Falkland Escarpment has been interpreted as a first order fault zone (Falkland/Malvinas Fault Zone), separating oceanic crust in the Argentine Basin, from continental crust in the Falkland Plateau, the latter being a submerged part of South America (Rabinowitz & LaBrecque, 1979). Paleomagnetic studies in the Falkland Islands suggested that the Falkland Plateau was an assemblage of several microplates that suffered 180º clockwise rotation (Biddle et al., 1996).

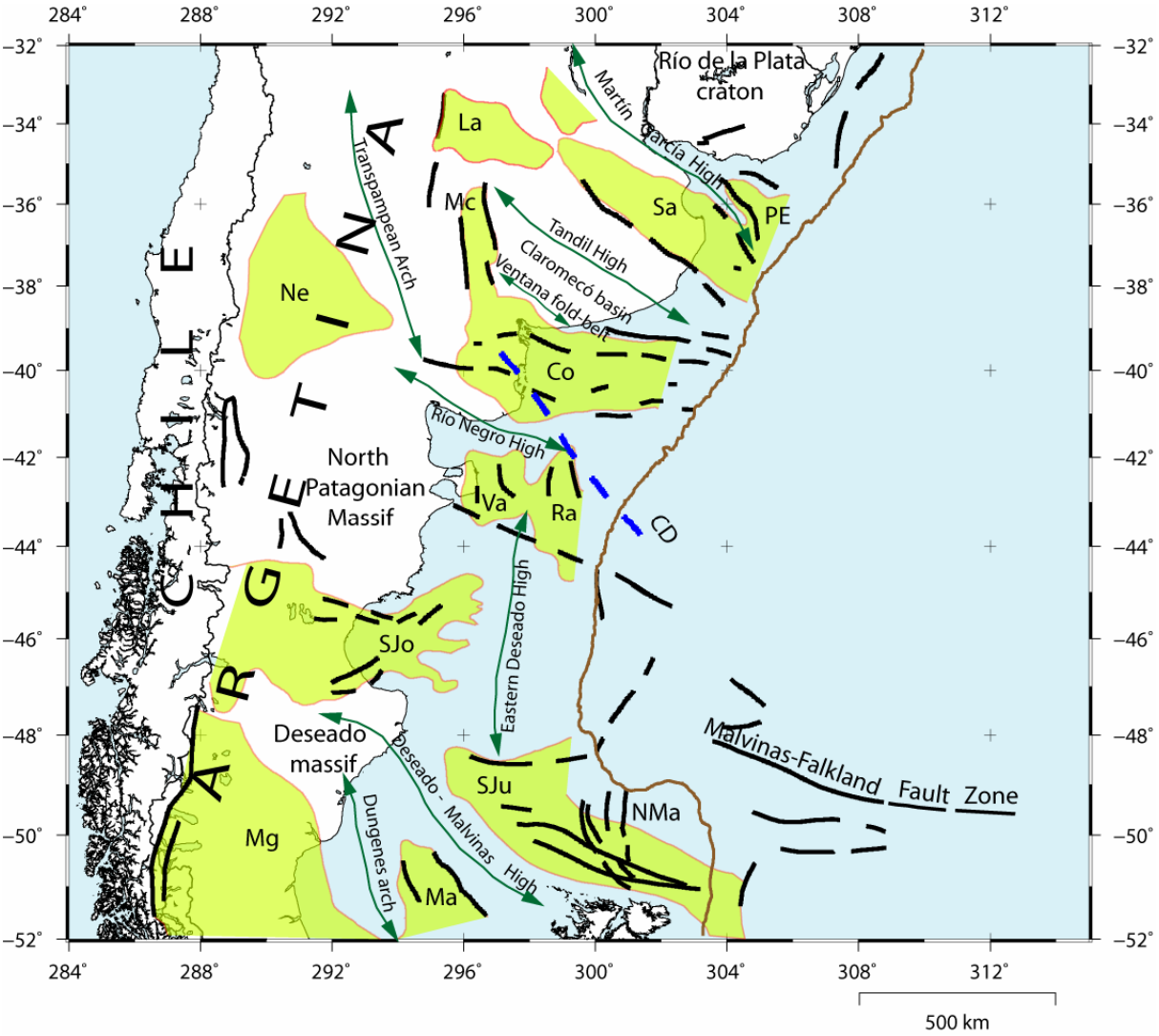

Fig. 2.6. General geologic map of the Argentine margin. Basin contours and faulting generalized from Ramos & Turic (1996). Arrowed axis show elongation of the main basement highs. Brown line represents the 500 m bathymetric curve. Dashed blue line is the Colorado Discontinuity (CD) of Ghidella et al. (1995). Basins: Co, Colorado; La, Laboulaye; Ma, Malvinas; Mc, Macachín; Mg, Magallanes; Ne, Neuquén; NMa, Northern Malvinas; PE, Punta del Este; Ra, Rawson; Sa, Salado; SJo, San Jorge; SJu, San Julián; Va, Valdés.

2.4.1 Salado and Colorado basins

These two basins are treated together because of their common genesis. They were originated simultaneously in Late Jurassic to Early Cretaceous (Lesta et al., 1977), together with the Santa Lucía Basin, in Uruguay. Their development in elongated troughs along WNW-ESE and W-E trending axes, at a high-angle of intersection with the continental margin trend, led to interpret them as intracontinental sag basins. Other speculations regarded them as pull-apart basins due to oblique extension, or as failed rift structures (aulacogens) joining in a triple point to the east (Max et al., 1999). The latter seems unlikely, since no volcanic activity appears to have taken place along the main basin faults. Recent studies (Franke et al., 2006) support the idea that the Salado and Colorado basins are typical rift basins, the orientation of which was controlled by the prevailing Paleozoic fabric. Both basins extend partially into the continent and exhibit similar sediment thicknesses, with depocentres in the order of 6 to 8 km. Another common remark is the presence of an outer basement high positioned on the continental slope. This structure separated the basins from fully open marine conditions until the end of the Cretaceous (Stoakes et al., 1991).

Two basement provinces have been identified within the area of the Colorado/Salado basin: an igneous and metamorphic province of Permian and older age, and a Late Paleozoic province, mainly made up of Permian sedimentary rocks (Fryklund et al., 1996). Keeley & Light (1993) described for that area a Precambrian basement, exposed on the Uruguayan side of the Río de la Plata and in the Tandilia Hills (Southern Buenos Aires province) and a Paleozoic sedimentary basement. Well-data suggest an offshore extension of the Paleozoic Claromecó Basin, beneath the sediments of the Colorado Basin (Fryklund et al., 1996). Franke et al. (2006) interpretED the basement as a continuation of the Ventana Hills, the Claromecó depocentre and Paleozoic to Middle Mesozoic rocks of the Patagonia terrane.

Salado Basin

This NW-SE elongated narrow basin is located on the northern part of the study area. It extends over a distance of more than 500 km, partly under the emerged continent and partly under the continental shelf. Genetically, it is related to the Punta del Este Basin, in the Uruguayan shelf, both basins being separated by a basement high (Martín García High and its SW extension, La Plata High) (Fig. 2.6). The Salado Basin narrows towards its onshore NW end and opens to the SW towards the continental slope, where it connects with the slope sediments. It accumulates a maximum thickness of 6000 m. A basement high (La Plata High)

separates the Salado Basin from the deep Argentine Basin (Fig. 2.7). The basin was regarded as a graben-shaped structure originated by faults trending NW-SE (Zambrano & Urién, 1970).

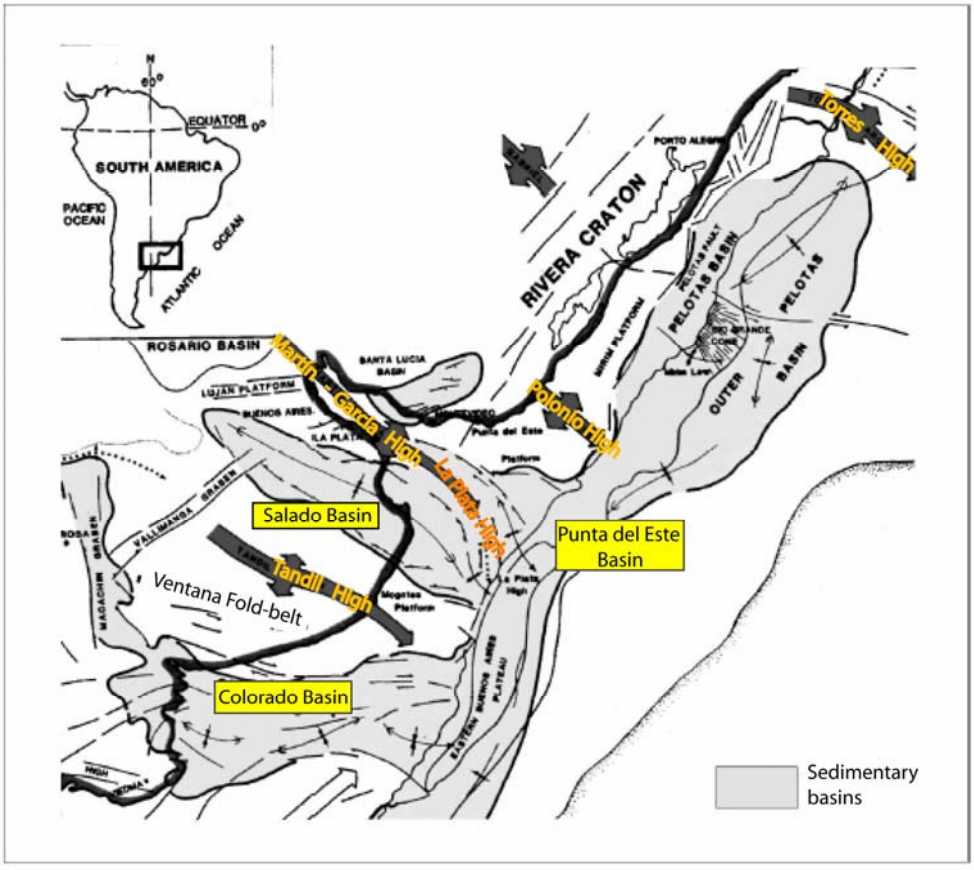

Fig. 2.7. Outline of the marginal basins of Northern Argentina, offshore Uruguay and southernmost Brazil (after de Santa Ana et al., 2005)

Colorado Basin

Located south of the Salado Basin, the Colorado Basin shows a similar orientation (W-E), at high-angle of intersection with the continental margin. This basin extends mainly beneath the broad continental shelf with dimensions of 500 x 200 km. It is separated from the Argentinian Basin by a basement high paralleling the continental margin, which represents the southward continuation of the La Plata High in the Salado Basin (Fig. 2.6). The Colorado and Salado basins are separated by a NW-SE basement high (Tandilia High) of Precambrian rocks. Furthermore, the basin has three main depocentres, elongated in a NW-SE direction, subparallel to the axis of the underlying Claromecó depocentre (Fryklund et al., 1996). These depocentres are controlled by basement faulting, and resulted from segmentation of the basin

by transverse faults lying parallel to the present margin. The Colorado Basin contains a thick succession (up to 7 km) of Jurassic through Recent continental to neritic sediments (Urién & Zambrano, 1996).

2.4.2 Valdés-Rawson basins

Located to the east of the Valdés Peninsula, the Valdés and Rawson composite basins consist of several sub-basins that extend entirely within the continental shelf, and were made up of several poorly interconnected half-grabens. They were formed during the rifting phase between Africa and South America, that at these latitudes, took place earlier than the previous Salado and Colorado basins, in Middle to Late Jurassic. The Valdés and Rawson basins show similar structural style, dominated by a typical extensional faulting (Marinelli & Franzin, 1996), controlled by NNW trending faults. In the Rawson Basin, the main tectonic fabric is NNW-SSE, suggesting control by Triassic-Jurassic accretionary back-arc fabrics (Keeley et al., 1993). During Atlantic rifting, this trend was modified, producing N-S extensional strain like in the Macachín Basin (Keeley et al., 1993). The Valdés Basin, inshore of the Rawson basins, shows a NW-SE oriented fault pattern, a trend that persists to the south towards the San Jorge Basin. The stratigraphy of the two basins is dominated by Late Jurassic pyroclastic rocks and Cretaceous continental sediments, topped by marine sediments during Tertiary time (Lesta et al., 1977).

2.4.3 San Jorge Basin

The San Jorge Basin is a dominantly extensional basin superimposed on Precambrian to Paleozoic continental crust (Rodríguez et al., 2001). The basin is located in Central Patagonia, and covers an area of 180.000 km². It extends over the continent from the Atlantic coast to the Andes fold belt, and over the continental shelf until 65ºW longitude (Fig. 2.6). It has an irregular outline shape and an overall E-W trend. In the continental part, it is bounded to the south by the Deseado Massif and to the north, several basement highs separate it from the Cañadón Asfalto Basin (Fig. 2.8). The Somuncura Massif (Fig. 2.8) represents also a northern boundary, farther east. The basin is divided in two sub-basins by the N-S trending San Bernardo fold belt: to the west, the so-called Río Mayo sub-basin, and to the east, the most developed part of the basin, reaching sediment thickness of over 7 km. This is also where most of the hydrocarbon production takes place representing the most prolific basins of Argentina. Although the San Jorge Basin extends partly over the continental shelf, it does not reach the outer shelf margin, separated by the prominent Eastern Deseado High (Fig. 2.6).

The basin was originated by a Late Triassic–Early Jurassic extensional phase, in a intracratonic sag setting, prior to the breakup of Gondwana (Baldi & Nevistic, 1996). This event caused the formation of numerous basins in Patagonia, in a "Basin and Range" igneous setting, with widespread distribution of rhyolitic volcanism. The late rift phase, from Late Jurassic to Early Cretaceous times resulted in attenuation of the extensional faulting, with the configuration of the basin into a single entity and the deposition of a thick lacustrine sedimentary unit (Baldi & Nevistic, 1996). This phase was followed by a long sag phase, when subsidence was mainly driven by thermal contraction. The Pozo D-129 Formation represents the first sedimentary unit totally integrated in the basin. During Lower Tertiary, regional compression caused by subduction along the western margin of South America created the San Bernardo fold belt.

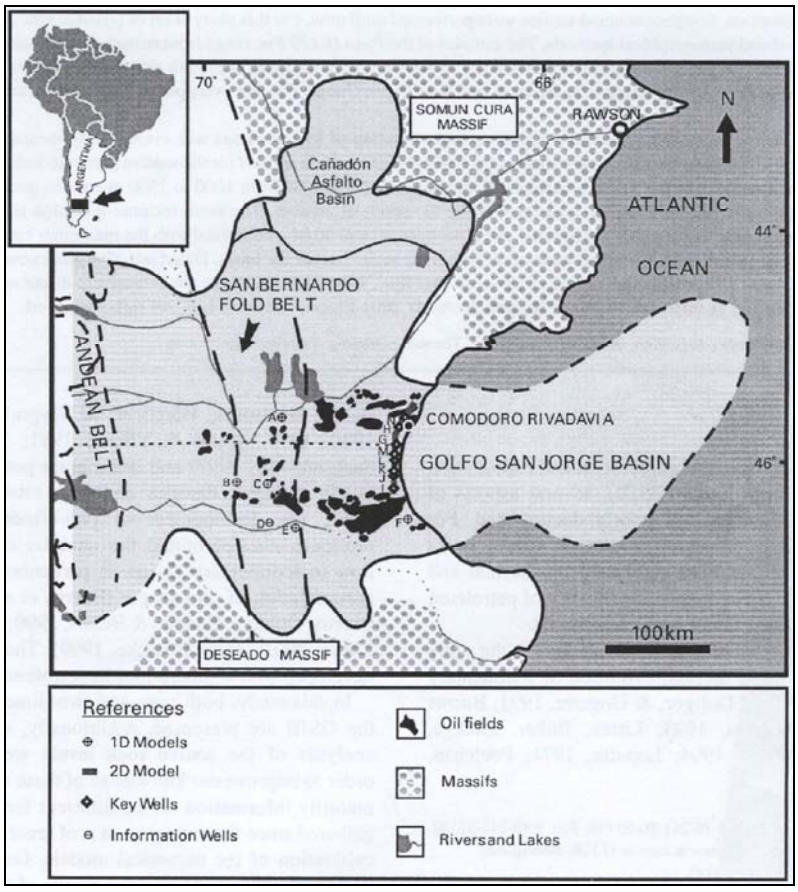

Fig. 2.8. Location of the San Jorge Basin (modified after Bianchi (1981), in Rodríguez et al., 2000).

2.4.4 San Julián Basin

Located to the south of the San Jorge basin, the San Julián Basin is entirely developed in the continental shelf (Fig. 2.6). The Basin was formed at the northern edge of the Deseado/Malvinas microplate, which collided against the southern margin of Gondwana during Permian (Figuereido et al., 1996). Its development was related to a Triassic through Middle Jurassic phase of oblique extension, creating a series of ENE-trending grabens under intense volcanic activity. The basin was affected by tectonic inversion during Cretaceous times (Aptian?), caused by collisions of Pacific microplates with the continent as it drifted westward, and by compressional stresses related to the movement of the Malvinas-Agulhas Fracture Zone. The subsequent uplift of the area resulted in the development of a regional unconformity.

2.4.5 North Malvinas Basin

This basin is situated to the north of the Malvinas/Falkland islands (Fig. 2.6), stretching along a distance of 270 km in a general N-S direction, with a width of 100 km. The basin consists of two major tectonic structures: a N-S trending graben (the northern graben) and a set of NW-SE trending, less developed southern hemi-grabens. A total thickness of over 9000 m of sediments has been measured, predominantly of fluvial origin (Ross et al., 1996). The North Malvinas Basin was created by two successive rifting episodes (Fig. 2.9): the first one, during Early-Middle Jurassic times, was related to crustal extension to the norh-east of the old subduction zone of Samfrau, in SW Gondwana, and produced the NW-SE trending hemi-grabens; the second rift phase, in Late Jurassic-Early Cretaceous times was related to the opening of the South Atlantic and created wider structures trending in a N-S direction (Ross et al., 1996).

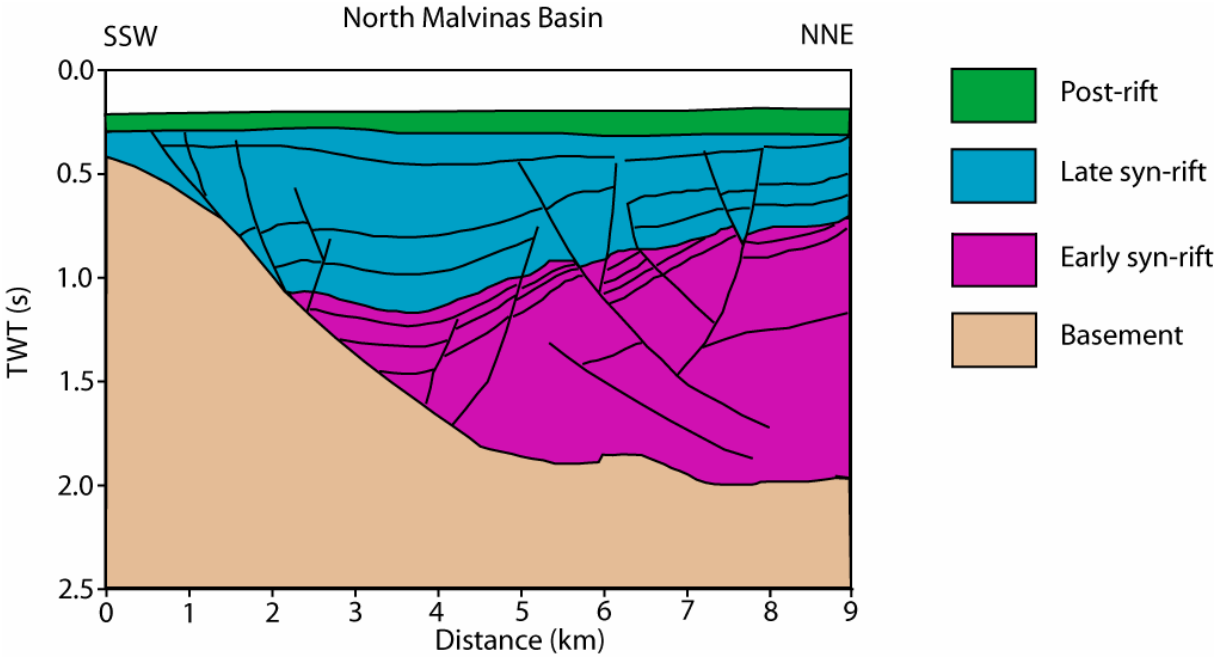

Fig. 2.9. Interpreted seismic profile across the North Malvinas Basin (see location of basin in Fig. 2.6). The two Mesozoic rift phases are indicated (modified after Ross et al., 1996).

2.5 Lithostratigraphy of the Argentine Margin

The tectonic and sedimentary evolution of rift-related basins can be characterized by three phases: pre-rift, syn-rift and post rift (sag phase). In fully developed passive margins, like the South Atlantic, a fourth phase (passive margin phase) takes place, corresponding to the period of relative tectonic quiescence with accumulation of sediments from the adjacent continent hinterland (Stoakes et al., 1991). This pattern of margin evolution is recorded by a set of sedimentary sequences, which were described in the northern part of the Argentine Margin by Stoakes et al. (1991) (Fig. 2.10), based on well data and seismic stratigraphy. These authors describe four main sequences overlying the pre-rift basement.

2.5.1 Pre-rift

This unit constitutes the basement to the syn-rift sequences across the continental margin. Its heterogeneous nature reflects the accretionary configuration of SW Gondwana, related to Pacific subduction during Phanerozoic times (Keeley et al., 1993) which resulted in a NW-SE trending tectonic array, with younger blocks to the south. Hence, the basement rocks along the

margin can be divided into three age groups: 1. Precambrian igneous and metamorphic basement: found in the Salado-Punta del Este and Colorado basins, has been correlated to exposed granitic and metamorphic rocks from the Tandilia Hills in the Buenos Aires province. 2. Permo-Carboniferous sedimentary rocks: consist of low grade metamorphic sediments described on the Ventana Hills. These sediments represent the exposed part of a larger Late-Paleozoic sedimentary basin, the Claromecó Basin, which lies buried under the area between the Tandilia Highs and the Ventana fold-belt (Fig. 2.7). They have been identified by wells in the Colorado basin, and seismically, by half-graben geometries on the rift-basin shoulders (Keeley et al., 1993). 3. Late Triassic and Jurassic volcanics and lacustrine sediments: known from Patagonia region (San Jorge Basin, Deseado and North Patagonian Massif). Sedimentary and volcanic rocks deposited in back-arc basins formed in response to extension caused by Pacific subduction from the SW (Keeley et al., 1993).

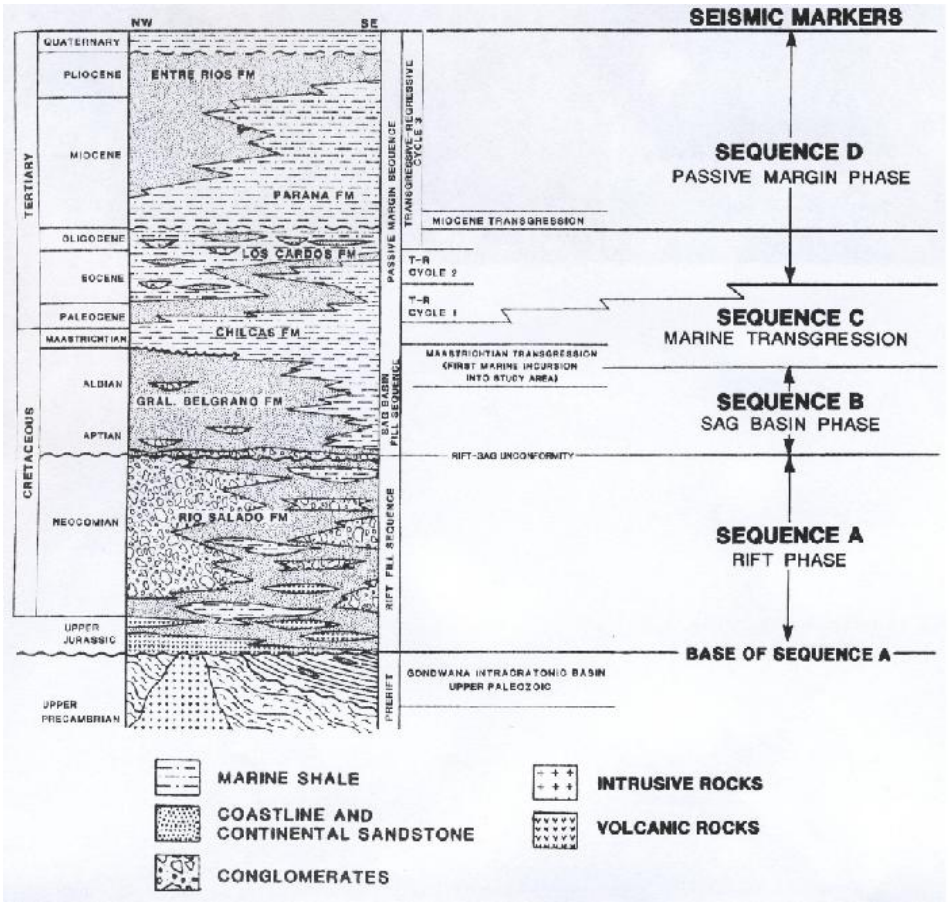

Fig. 2.10. Stratigraphic column and seismic markers of the Punta del Este Basin, in the northern Argentine margin (Stoakes et al., 1991).

2.5.2 Syn-rift

During this phase, sedimentation was controlled by extensional faulting and took place within graben-like structures in most of the pericratonic and aulacogenic basins of the Atlantic rifted margin (Stoakes et al., 1991). The infill of these depocentres consisted of a basal interval dominated by extrusive basaltic flows, followed by an upper interval of continental deposits exhibiting a fining-upwards sequence. The flow basalts have been attributed to the Serra Geral Formation in SE Brazil (Lesta, 1978), being part of the Paraná-Etendeka igneous province, and were assigned an ^{40}Ar-^{39}Ar age of 129 to 134 Ma (Peate, 1997).

The overlying sediments, known as the Río Salado Formation (Lower to middle Upper Cretaceous) (Fig. 2.10) consist of a thick package of conglomerates, sandstones, and reddish silty mudstones of alluvial fan to alluvial-plain origin. This formation has been correlated to the Fortín Formation in the Colorado Basin area, slightly younger than the latter (extending into Cenomanian). Important thickness have been documented in wells penetrating this sequence in the Salado Basin, reaching up to 1200 m in many cases (Tavella & Wright, 1996). Seismic data, however, suggest a maximum thickness of 4500 m in the Punta del Este Basin (Stoakes et al., 1991).

Further south, the San Jorge Basin underwent an earlier rift phase during the Late Triassic-Early Jurassic (Early rift phase), resulting in the accumulation of volcanic and volcaniclastic sediments in a continental envinronment, which are represented by the Lonco Trapial Group in the north, and the Bahía Laura Group in the south (Baldi & Nevistic, 1996). The so-called Late rift phase (Late Jurassic-Early Cretaceous) deposited the fluvio-deltaic and lacustrine sediments of the Pozo Anticlinal Aguada Bandera Formation and the Pozo Cerral Guadal Formation.

2.5.3 Sag basin phase

The existence of an external ridge along the Argentine margin from the Punta del Este Basin to the San Julián Basin area prevented its flooding until the mid-Tertiary, resulting in a not very pronounced thermal subsidence, tectonically stable conditions, and massive volcanic activity (Soares et al., 2000). Sediments deposited during a period of regional thermal subsidence, ranging in age from mid-Cretaceous to Paleocene times in the Salado and Colorado basins area. These deposits were grouped into two sequences: a lower sequence of

non-marine sediments (Sequence B) and an upper interval of shoreface to marine sediments (sequence C) (Fig. 2.10) (Stoakes et al., 1991).

Sequence B consists of continental sandstones and conglomerates associated to a proto-oceanic setting, represented by an interbedding of shallow marine with continental deposits (Tavella & Wright, 1996). In the Salado Basin, this interval is referred to the General Belgrano Formation, of Aptian-Cenomanian age, while further south, in the Colorado Basin area, it correlates with the Colorado Formation, of younger, Turonian to Paleocene age (Stoakes et al., 1991). It shows its maximum development in the Salado Basin, where it makes up an accumulation of over 2000 m.

Sequence C (upper sag basin interval) reflects the change to open marine conditions in Maastrichtian-Paleocene times (Maastrichtian Transgression) (Tavella & Wright, 1996). It is represented by the Chilcas Formation (Salado Basin) and the Pedro Luro Formation (Colorado Basin), consisting of dark-greenish claystones and burrowed glauconitic sandstones. The small thickness variation of this interval in the Salado and Punta del Este basins denotes connection between the two basins for the first time.

2.5.4 Passive margin phase

The continental margin evolved as seafloor spreading kept separating the continents. Cooler oceanic crust adjacent to the margin sank, and was progressively buried under a thick layer of continent-derived sediments. Subsidence was generally slow and strongly controlled by eustatic changes (Tavella & Wright, 1996). The stratigraphy is then, divided into three major transgressive-regressive sequences recognized in the northern part of the Argentine Margin, almost unaffected by faulting: a first sequence starting with the Maastrichtian transgression, is represented in the Salado area by the deltaic deposits of the Chilcas and los Cardos formations and their equivalents upper Pedro Luro and Elvira formations; a second sequence, less widespread, took place during the Eocene, during which were deposited fluvio-deltaic deposits of the General Paz Formation (Tavella & Wright, 1996). The third sequence began with the widespread Miocene transgression, generalized over the entire Atlantic margin.

2.6 Breakup-related volcanism

Continental extension and breakup leading to the opening of the South Atlantic was strongly influenced by magmatism, resulting in the development of common crustal units and structural features within the newly formed margins (Eldholm et al., 2000). In the South American and conjugate African margins, breakup related magmatism is represented by two widely extended geological features defining the so called South Atlantic Large Igneous Province (LIP): a voluminous wedge of seaward dipping reflectors sequences (SDRs) and the Continental Flood Basalts (CFB) of Paraná-Etendeka (Fig. 2.11).

The seaward-dipping reflectors are wedge-shaped bodies consisting of basaltic flows and volcani-clastic rocks extruded near or above sea-level immediate prior to and during the first stage of breakup (Hinz et al., 1999). In the Argentine Margin, the width of these feature ranges from 60 to 120 km, and they extend continuously along the entire length of the margin. Continuing northwards, it extends along the Uruguayan and Brazilian margins to 20ºS, totalling a length of 3500 km (Fig. 2.11) (Hinz et al., 1999, Eldholm et al., 2000). SDRs studied over the world are correlated to both high amplitude magnetic anomalies and free-air gravity highs (Direen & Crawford, 2003).

The lava fields of Paraná in South America and Etendeka in Southern Africa formed a single magmatic province associated with the opening of the South Atlantic during Early Cretaceous times (Peate, 1997). The exposures of the flood basalts at both sides of the Atlantic are connected through the fossil trace of the Tristan da Cunha mantle plume, represented by the Río Grande Rise and the Walvis Ridge (Fig. 3.1 and 2.11). The inferred age of the main volcanic episode that produced this large igneous province has been inferred to 129-134 Ma (Late Jurassic- Early Cretaceous) (Peate, 1997). The Paraná lava field, with an extension of at least 1.2 x 10^6 km^2, extends over southern Brazil, Uruguay and Paraguay. In northern Argentina, the presence of flow-basalts have been detected from well-cores at the bottom of the Salado-Punta del Este, and presumably also in the Colorado Basin (Lesta, 1978; Tavella & Wright, 1996; Stoakes et al., 1991), representing the southernmost expression of the volcanic province.

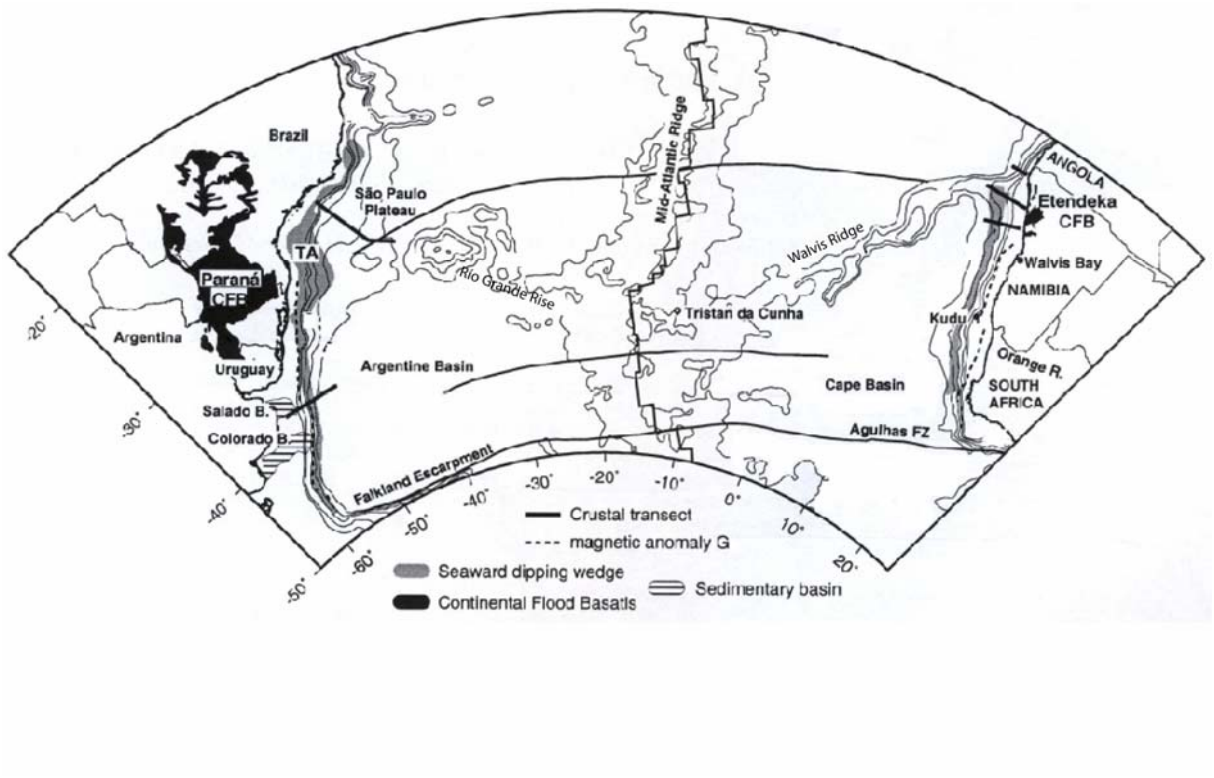

Fig. 2.11. Areal distribution of South Atlantic Large Igneous Provinces: Paraná-Etendeka Continental Flood Basalts (CFB) in black; Seaward-dipping reflector wedges, in dark gray. The major bathymetric features and marginal basins are indicated (modified after Gladczenko et al., 1997).

Further south in the Argentine Margin, the extrusives have a different character and age. South of the Colorado Basin, no basaltic flows are found. Instead, rhyolitic lavas and pyroclastic flows of Early and Middle Jurassic age extend widely in the Patagonia region, forming an extense "rhyolitic plateau" (Ramos, 1996). These volcanic rocks constitute a thick basal syn-rift sequence within the southern basins of the Argentine margin (Rawson-Valdés, San Jorge, San Julián and Northern Malvinas) that was associated to a Middle Jurassic early rift phase (165 to 155 Ma) related to the initial stages of Gondwana breakup (Ramos, 1996).

Chapter 3
Data

The following data have been used in the study: published multi-channel seismic (MCS) lines BGR87-01, -02, -04 and -05 from BGR (Bundesanstalt für Geowissenschaften und Rohstoffe) (Hinz et al., 1999); bathymetry, gravity and magnetic data from LDEO (Lamont-Doherty Earth Observatory, Columbia University, USA) academic ship tracks; 1x1´ elevation grid (GEBCO, General Bathymetric Chart of the Oceans, Jakobsson et al., 2000); 1x1´ gridded satellite-radar-altimeter free-air gravity (Sandwell & Smith, 1997 v.15.1); 2x2´ global marine free air gravity data based on ERS-1 and GEOSAT satellite altimetry (KMS; Andersen & Knudsen, 1998); Bouguer-corrected gravity anomalies; along-track single-channel seismic reflection profiles (LDEO); and 5x5´ grid of total sediment thickness of the World's Oceans & Marginal Seas (NOAA, National Oceanic & Atmospheric Administration, USA).

3.1 Margin setting

Available regional grids of the bathymetry, gravity, magnetic anomaly and sediment thickness are used to reveal and study the main structural features and elements of the continental margin offshore Argentina. These data sets are presented in different basemaps within the extent of the study area. The basemaps have been constructed utilizing the GMT (Generic Mapping Tools, v. 4.7) software package (Wessel & Smith, 1998). GMT has been also used in data editing, reduction, visualization and display. In particular, the grids described above have been used to extract data along the published MCS profiles used in this study.

3.1.1 Bathymetry

Bathymetry data used in the study are provided by two different sources: the General Bathymetric Chart of the Oceans (GEBCO, Jakobsson et al., 2000) and ship-borne LDEO tracks.

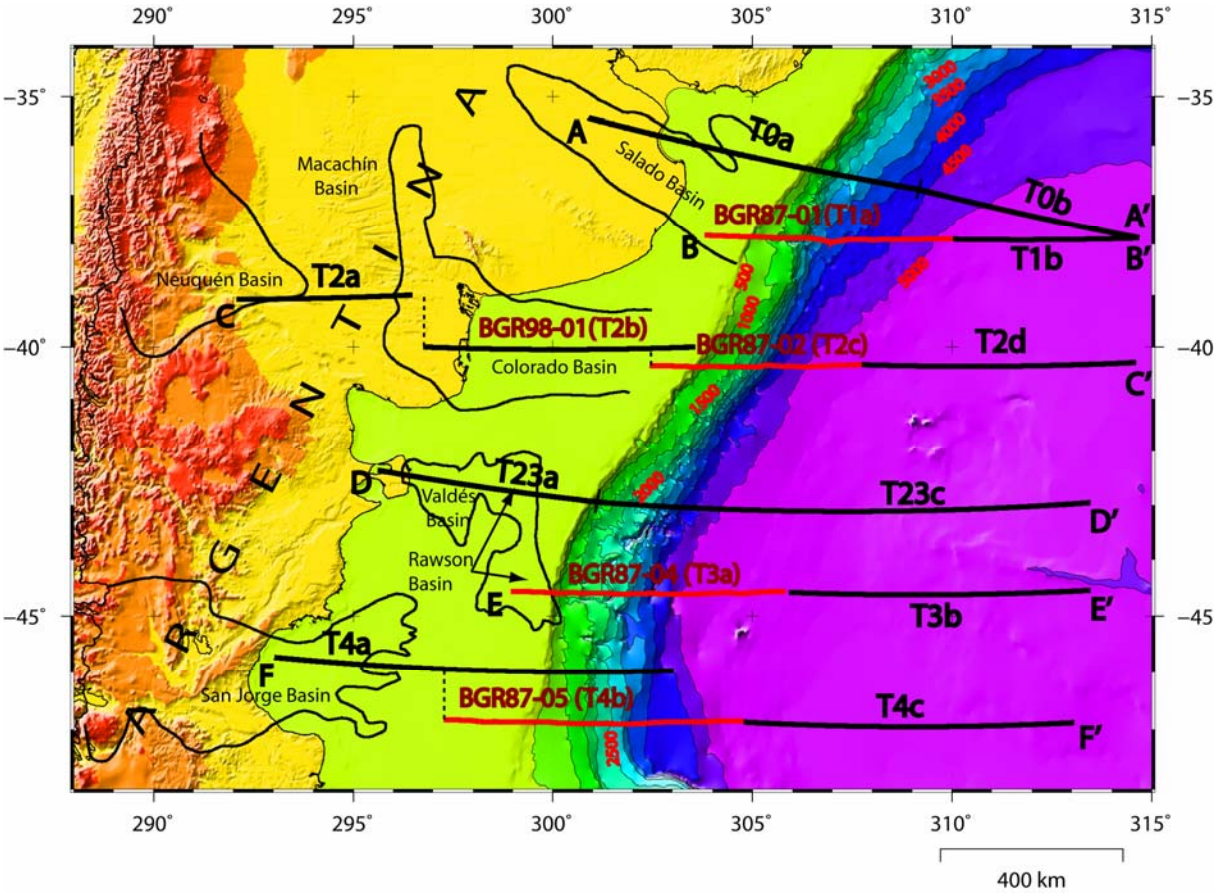

Fig. 3.1. 1x1' elevation grid (GEBCO, General Bathymetric Chart of the Oceans, Jakobsson et al., 2000). The outlines of the major basins are also indicated. Locations of composite transects are indicated (lines AA´-FF´).

The elevation grid plot is shown in Figure 3.1, and the general physiographical features of the Argentine margin are clearly displayed. These include the continental platform, that parallels the NE-SW coastline trend, and its boundary, the shelf break, that diverges from the coast towards the SW. In the same direction, the platform widens reaching a width of over 600 km, east of the Gulf of San Jorge (Fig. 3.1). The shelf-edge is sharp and well marked on the bathymetry map, following approximately the 200 m isobath. At the southernmost end of the study area, however, the shelf-break is slightly smoother (Fig. 3.1). Furthermore, the continental slope shows also a considerable variation in width along the margin, with a maximum width in the NE and the narrowest width in the central part at latitudes 39º-45ºS (Fig. 3.1). Between the shelf edge and the abyssal plain, two slope breaks can be identified: the first one at a depth between 1500 and 2000 m, and another one at the boundary between the slope and the rise (between 3500 and 4500 m). Several submarine canyons are recognized crossing the slope all the way down to the abyssal plain (Fig. 3.1). The abyssal plain, known

as the Argentine Basin, has a rather homogeneous depth between 5000 and 6000 m and there is a bathymetric rise of several hundred meters towards the centre of the plain in the east (Fig. 3.1)

3.1.2 Gravity

Similar to bathymetry data, the gravity data used in this study derive from several sources. By using and comparing the different data sources we can test their reliability. Two different grids of satellite-radar-altimeter free-air gravity anomalies were utilized: the 1x1' Sandwell & Smith (1997, v.15.1) (Fig. 3.2) and the KMS99 global marine free air gravity field (Andersen & Knudsen, 1998) (Fig. 3.3). It was realized that the KMS99 gravity field produces a slightly smoother image of the gravity anomaly field, eliminating the shortest wave-length variations displayed in the Sandwell & Smith (1997, v. 15.1) (Fig. 3.2), especially over the oceanic crust areas (Fig. 3.3).

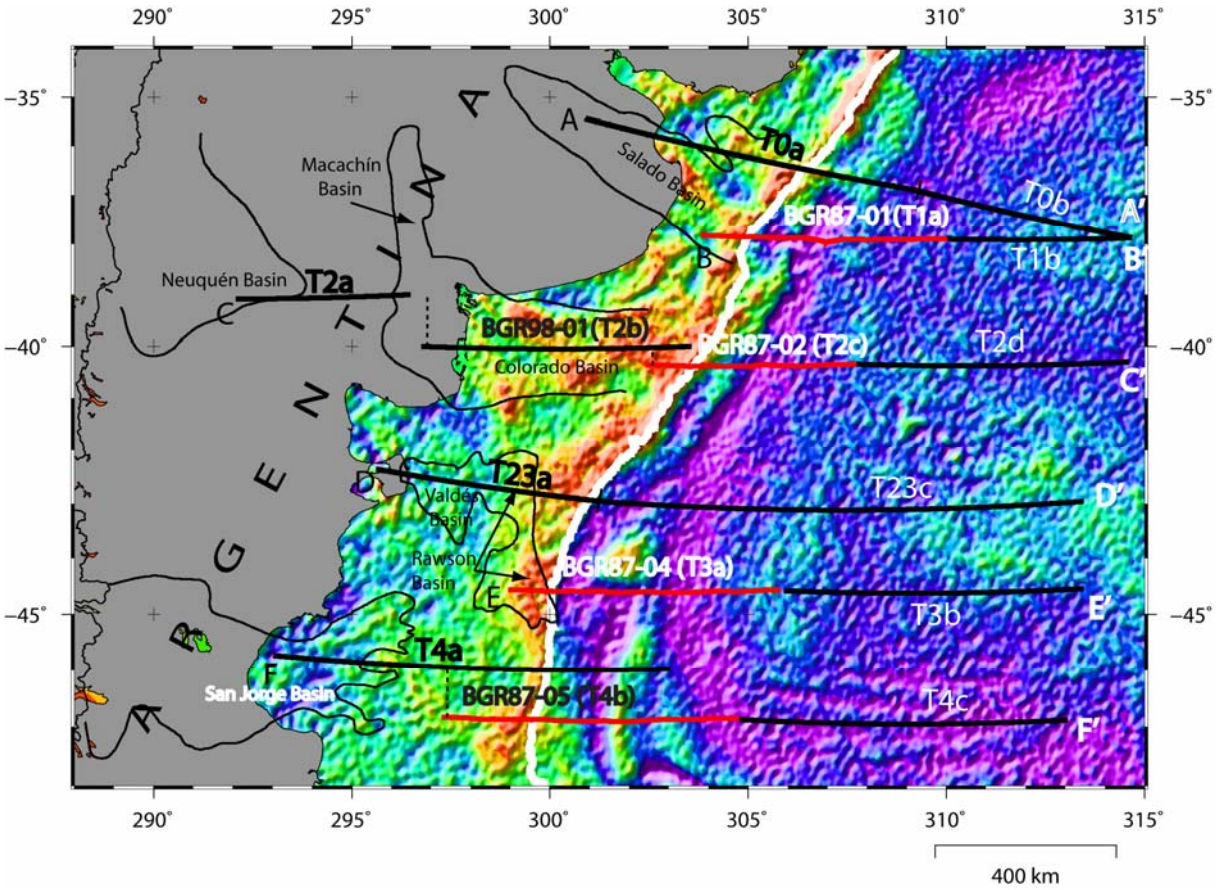

Fig. 3.2. 1x1' satellite-radar-altimeter free-air gravity anomaly grid (Sandwell & Smith, 1997 v.15.1). The 500 m bathymetric curve is indicated, contouring the shelf-edge. Outline of major basins as in Fig. 3.1. Locations of composite transects are indicated (lines AA´-FF´).

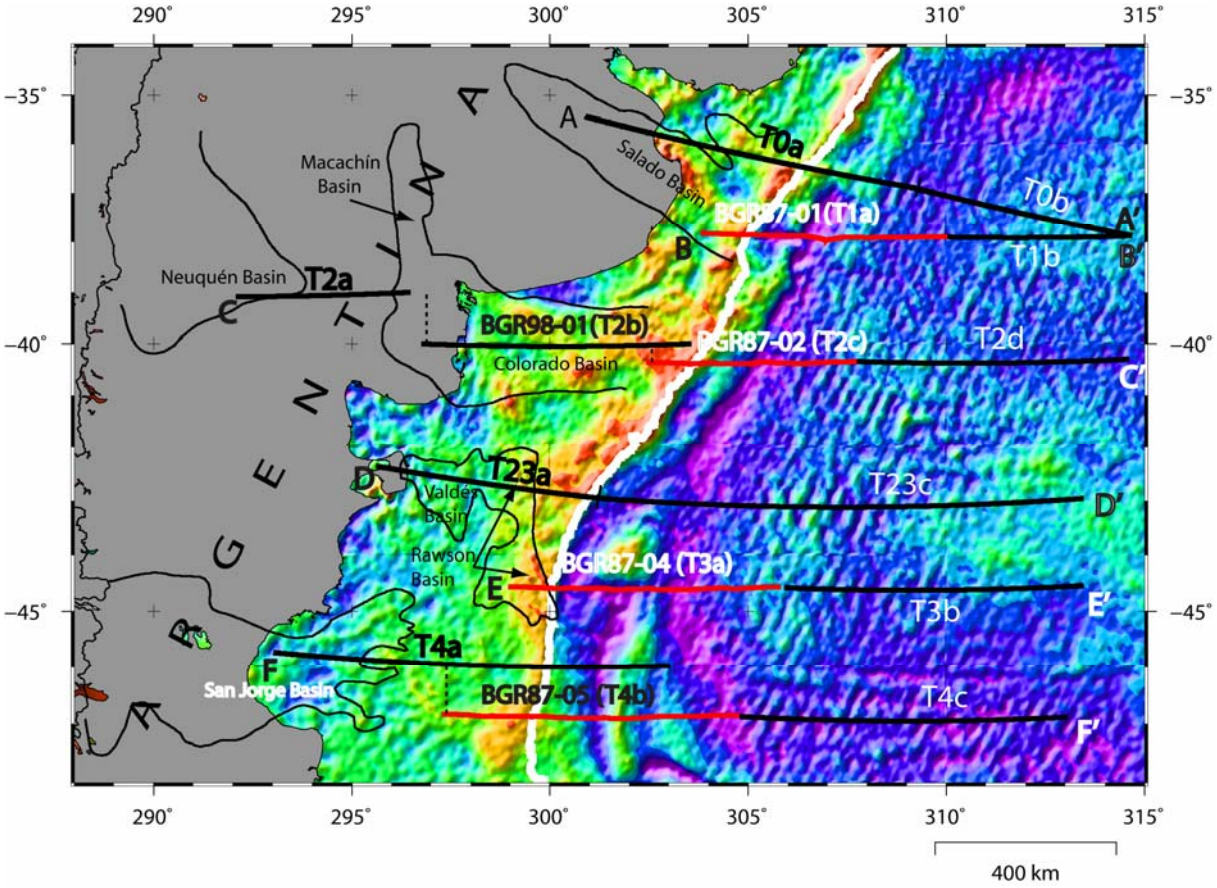

Fig. 3.3. 2x2' KMS99 global marine free air gravity grid (Andersen and Knutsen, 1998). The 500 m bathymetric curve is indicated, contouring the shelf-edge. Outline of major basins as in Fig. 3.1. Locations of composite transects are indicated (lines AA´-FF´).

On both free-air gravity basemaps (Figs. 3.2 and 3.3), the major anomaly trends reflect the main structural elements and features of the region. In particular, several prominent positive and negative anomalies are located on the continental shelf. The most striking gravity feature is an elongated NE-SW trending anomaly strip located along the shelf-edge. This anomaly strip has been described by Rabinowitz et al. (1979) and named as the G-anomaly, and was attributed to the transition from continental to oceanic crust. To the east of this lineation, the vast Argentine Basin is represented by a zone of rather homogeneous negative anomaly.

Ship-borne gravity data were also extracted along the BGR-lines, i.e. along transects T1a, T2c, T3a and T4b (Fig. 3.1). This higher resolution gravity measurements complement the

gravity extracted from the Sandwell & Smith (1997) grid on the four transects in the region between the shelf edge and the abyssal plain. The coincidence between the two curves is high, proving additional reliability for the gridded gravity anomaly data. LDEO (Lamont-Doherty Earth Observatory) gravity anomaly tracks are also an available source of data that has been used to complement the gravity profiles along the multichannel seismic transects when both tracks have a coincident position.

The Bouguer-corrected gravity anomaly grid (Fig. 3.4) was constructed utilizing the satellite-radar-altimeter grid (Sandwell & Smith, 1997, v.15.1) the GEBCO bathymetry (Jakobsson et al., 2000), and a Bouguer density of 2670 kg/m³. The gravity effect of the bathymetry relief is eliminated from the Bouguer gravity anomaly field which, thus, provides a better image of the Moho depth shallowing and the continent-ocean transition/boundary (COT/COB).

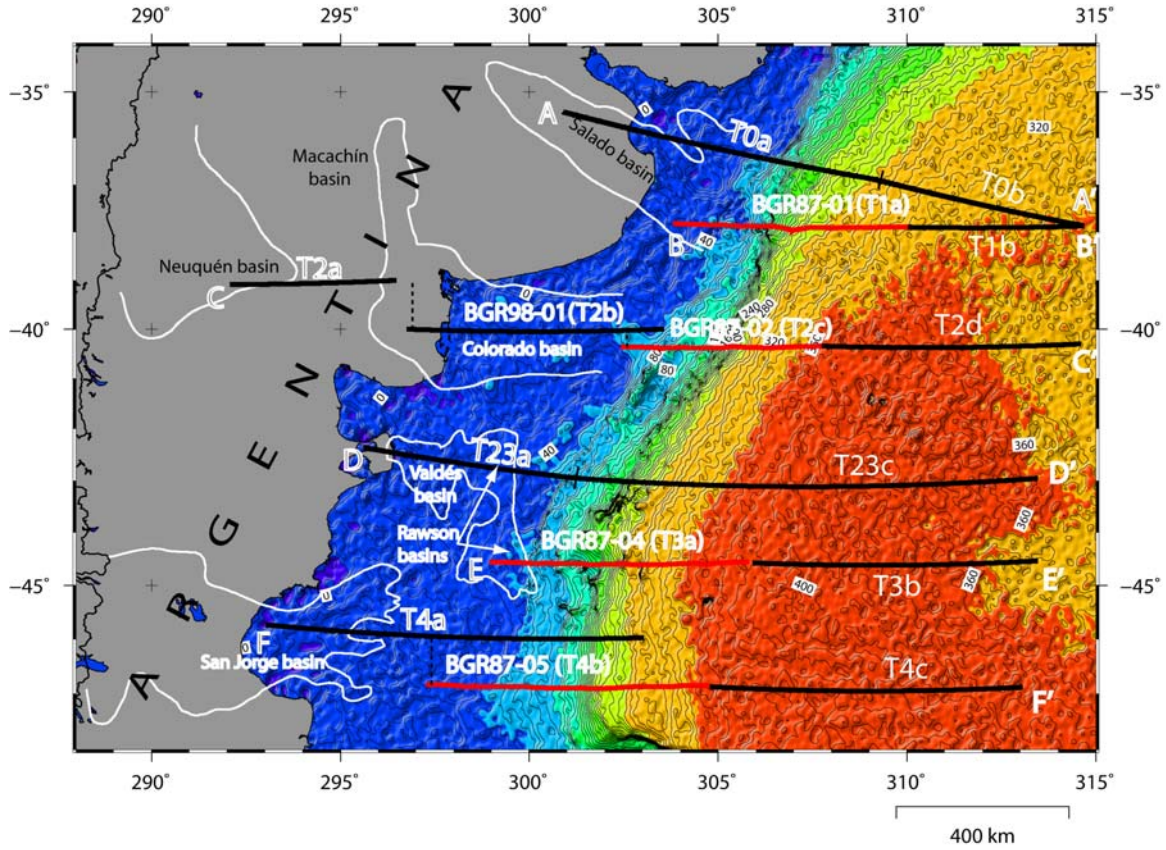

Fig. 3.4. Bouguer corrected gravity anomaly grid. Locations of composite transects are indicated (lines AA´-FF´).

In particular, having removed the local variations of gravity caused by the bathymetric relief, the gravity anomaly plot is dominated by the relative depth to the Moho discontinuity. Therefore, the highest values correspond to the oceanic crust, i.e. the abyssal plain of the Argentine Basin, and they are gradually decreasing towards the coastline, where Moho lies deeper under thick continental crust.

3.1.3 Magnetics

The magnetic anomaly map (Fig. 3.5) was constructed by utilising all LDEO academic ship-tracks available for the region. Gridding uses the nearest neighbour algorithm to assign an average value to each node with a certain radius. A grid spacing of 10x10' has been implemented in the computations. Extraction of magnetic anomalies can be performed both from the grid or directly from the available LDEO tracks which can be of interest due to the proximity to the multichannel seismic lines used in the study. The latter will be a better option since the LDEO lines bear the direct ship-borne magnetic measurements.

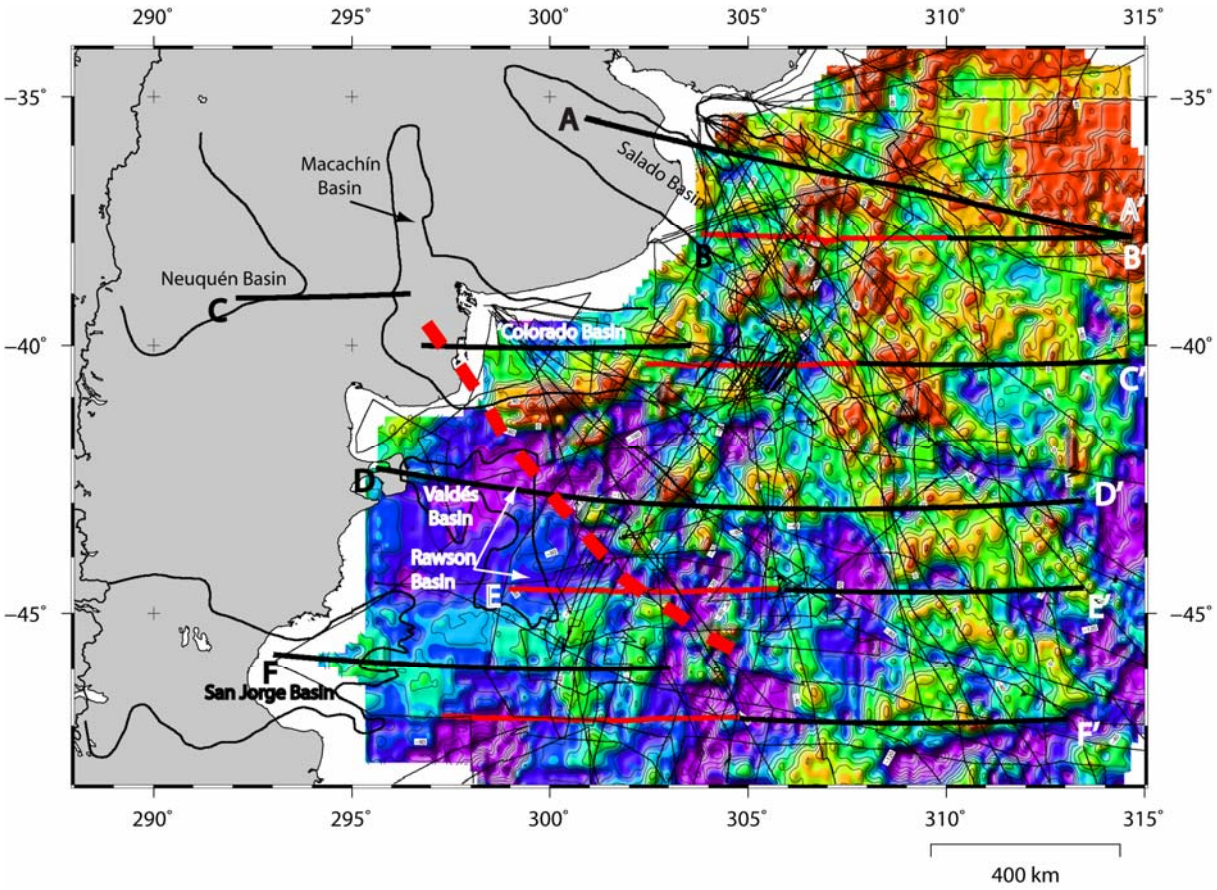

The magnetic anomaly map reflects an overall regional NE-SW anomaly trend, with the most prominent magnetic anomalies located in the NE of the study area (Fig. 3.5). Superimposed on this regional pattern, a short-wavelength setting of highs and lows dominates almost the entire region, with the exception of the SW part of the study area, which shows much more homogeneous, low-amplitude magnetic anomalies. The line separating these two differentiated sectors has been named as the "Colorado Discontinuity" (Fig. 3.5) (Ghidella et al., 1995). Finally, the G-anomaly of Rabinowitz & LaBrecque (1979) (Fig. 3.5) has its associated expression as an elongated positive magnetic anomaly, attributed to the transition from continental to oceanic crust and the corresponding COT/COB.

3.1.4 Sediment thickness

A sediment thickness map has been generated (Fig. 3.6) from the 5x5' grid of the total sediment thickness of the World's Oceans and Marginal Seas (NOAA, National Oceanic and Atmospheric Administration, USA). Since the measurements of the sediment thickness are based on the acoustic contrast at the contact between the upper sedimentary layer and the more rigid underlying basement, the sediment thickness grid has been used to position the inferred top of the oceanic crust along the seaward extensions of the transects. Over the continental crust, the acoustic boundary displayed by the gridded data is used with caution and is always compared with the available seismic reflection profiles when positioning the post-rift sedimentary cover.

The sediment thickness basemap displays a NE-SW trending elongated depocentre, coincident with the position of the continental slope (Fig. 3.6). This feature represents a continuous accumulation of sediments of more than 4000 m, reaching its maximum development at the NE of the study area. At both sides of this axial depocentre, the sediment thickness decreases drastically, with a minimum of 400 m in the Argentine Basin (Fig. 3.6).

Fig. 3.5 (opposite page). Magnetic anomaly grid derived from all available LDEO academic ship-tracks The traces of all tracks used for the construction of the grid are indicated. Locations of composite transects are also indicated (lines AA´-FF´). Thick, red dashed-line, Colorado Discontinuity (DC); continuous white line, G anomaly of Rabinowitz & LaBrecque (1979).

Over the continental shelf, the relatively small sediment thickness trend is interrupted by several depocentres, transversal to the direction of the coastline, the most prominent corresponding to the Salado and Colorado basins (Fig. 3.6).A minor relative high can be seen at the SW end of the shelf, coincident with the position of the offshore portion of the San Jorge Basin (Fig. 3.6). Between latitudes 39ºS and 43ºS, a narrow basement high paralleling the shelf edge, is bounding the Salado and Colorado basins to the SE. On the Argentine Basin, the sediment thickness shows a general increase towards the centre of the basin in the east (Fig. 3.6).

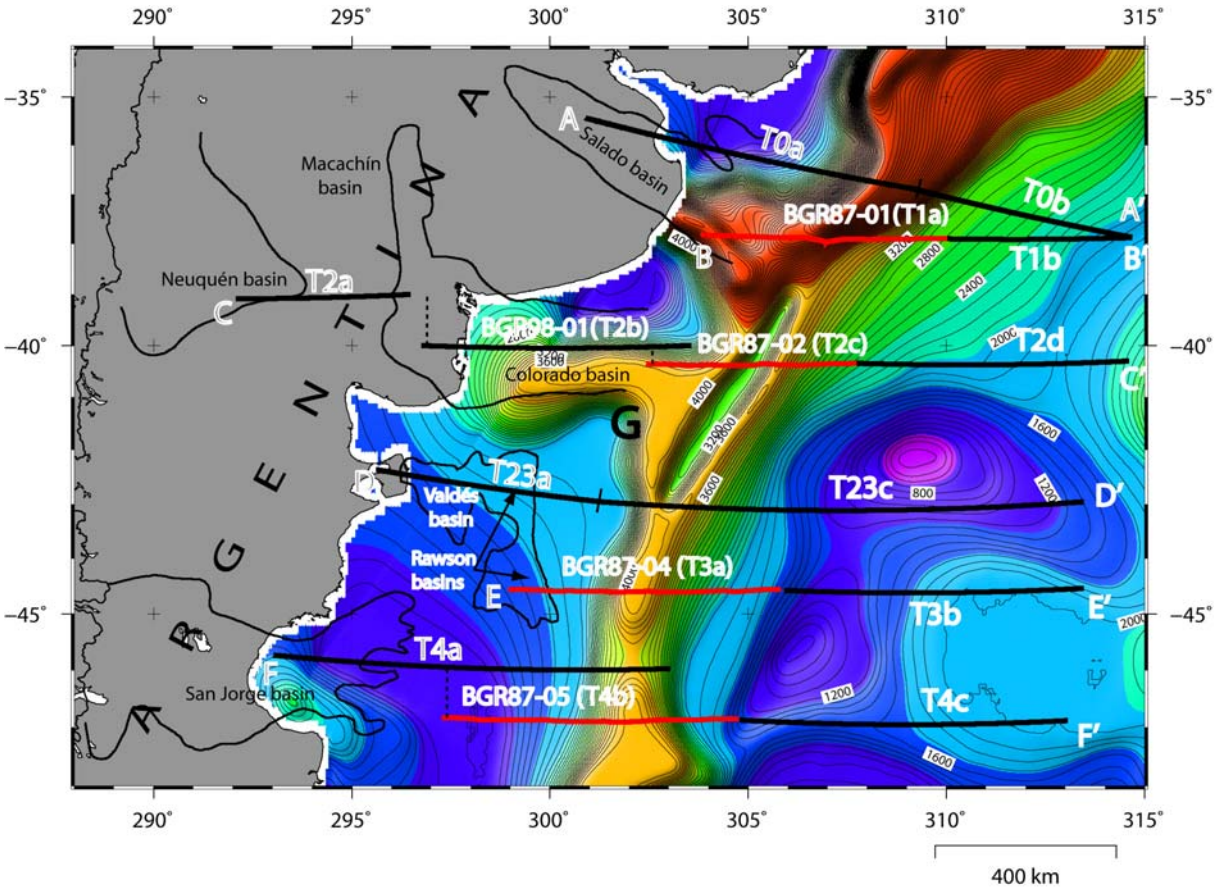

Fig 3.6. 5x5' grid of total sediment thickness of the World's Oceans and marginal seas (NOAA, National Oceanic and Atmospheric Administration, USA). Locations of composite transects are indicated (lines AA´-FF´).

3.2 Published seismic profiles

Published multichannel seismic (MCS) reflection profiles from BGR (Bundesanstalt für Geowissenschaften und Rohstoffe) have been used in this study (Hinz et al., 1999, Franke et al., 2004). Four of these profiles (Hinz et al., 1999), cover the outermost shelf, the slope and rise region, and they have been extended seaward and landward. The constructed transects extend from onshore or near onshore to the abyssal plain, mostly in a W-E direction (Fig. 3.1).

Four landward extensions have been added to the data set: a BGR multichannel seismic reflection profile (BGR 98-01) (Franke et al., 2004) and three geological sections based on proprietary seismic profiles (Urién & Zambrano,, 1996), thus providing a wider and denser data coverage within the study area (Fig. 3.1). All seismic profiles (Table 3.1) were digitized with the "in-house" software package SECTION (Planke, 1993).

Seismic profile	**Location in basemap**	**reference**
BGR87-01	Segment T1a of line B-B'	Hinz et al. (1999)
BGR87-02	Segment T2c of line C-C'	Hinz et al. (1999)
BGR87-04	Segment T3a of line E-E'	Hinz et al. (1999)
BGR87-05	Segment T4b of line F-F'	Hinz et al. (1999)
T0a	Landward portion of line A-A'	Urién & Zambrano (1996)
BGR98-01(T2b)	Landward portion of line C-C' (offshore)	Franke et al. (2004)
T23a	Landward segment of line D-D'	Urién & Zambrano (1996)
T4a	Landward segment of line F-F'	Urién & Zambrano (1996)

Table 3.1. Published seismic profiles used in this thesis.

3.2.1 BGR seismic profiles

The BGR multichannel seismic profiles from Hinz et al (1999) were acquired with a Sercel SN 358 DMX digital seismic recording system, using a 3000 m long, 60-trace streamer and a tuned airgun array with 32 guns, using a total airgun volume of 80.4 litres and an operating pressure of 140 bar. The seismic data were processed using conventional processing routines, including predictive deconvolution, that was implemented to attenuate the multiples, and

stacked CDP (common depth point) traces that were band-pass filtered and normalized. Only selected parts of the profiles were migrated. The four BGR profiles from Hinz et al. (1999) used in this study (BGR87-01, BGR87-02, BGR87-04, BGR87-05) extend to distances between 450 and 550 km in a general W-E direction (Fig. 3.1). The BGR98-01 profile represents a landward extension of the profile BGR87-02, with similar length and orientation (Fig. 3.1). Seismic interpretation of the BGR profiles was based on the interpretations by Hinz et al. (1999) and Franke et al. (2004).

BGR87-01 profile

The profile has a length of 550 km and extends from ~100 km off the coast, following the axis of the Salado Basin into the Argentine Basin (Fig. 3.1). The interpreted section extends to a depth of 12 s twt (two-way traveltime) (Fig. 3.7).

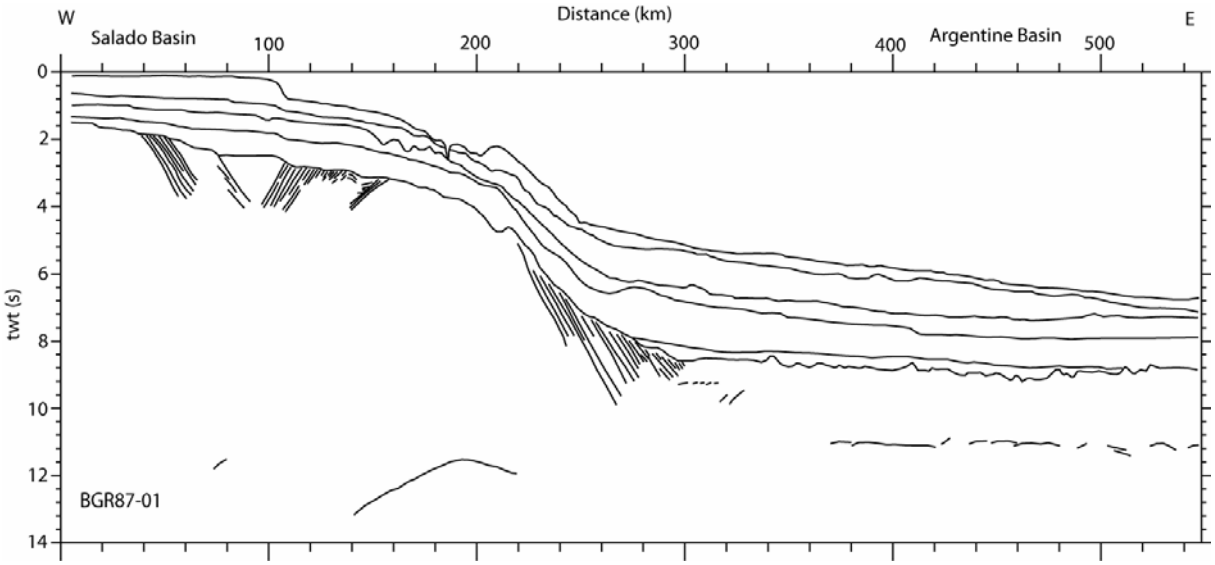

Fig. 3.7. Line-drawing interpretation of the BGR87-01 seismic profile (after Hinz et al., 1999). Location of profile in Fig. 3.1.

BGR87-02 profile

The profile runs parallel to the elongated Colorado Basin (along its easternmost part) and it extends 450 km towards the Argentine Basin (Fig. 3.8).

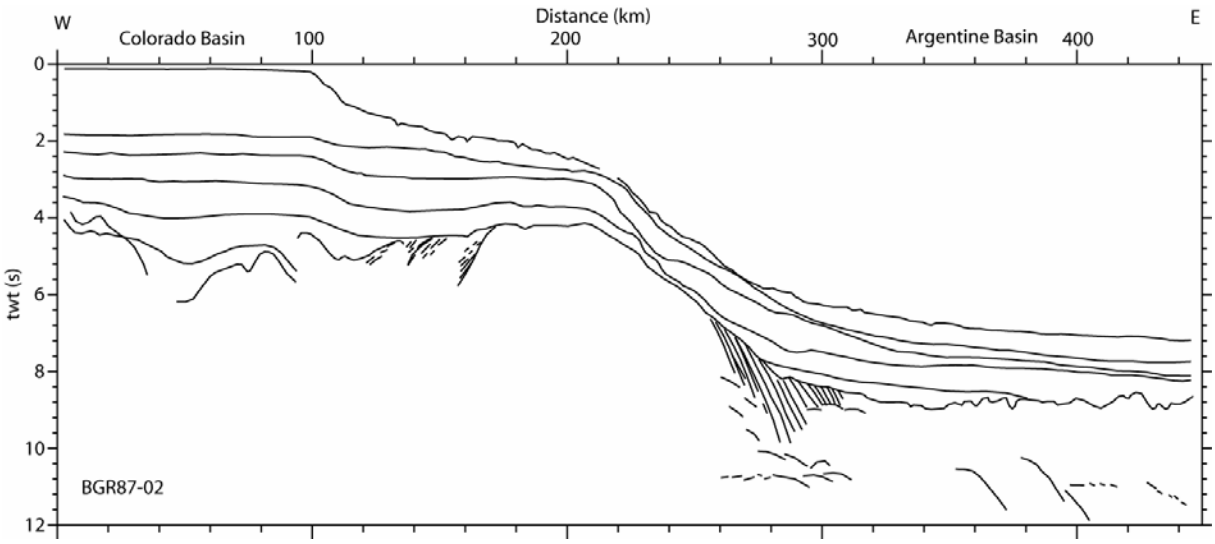

Fig. 3.8. Line-drawing interpretation of the BGR87-02 seismic profile (after Hinz et al. 1999). Location of profile in Fig. 3.1.

BGR87-04 profile

The profile has a length of 525 km and extends eastward across the southernmost part of the Valdés-Rawson basins (Fig. 3.9).

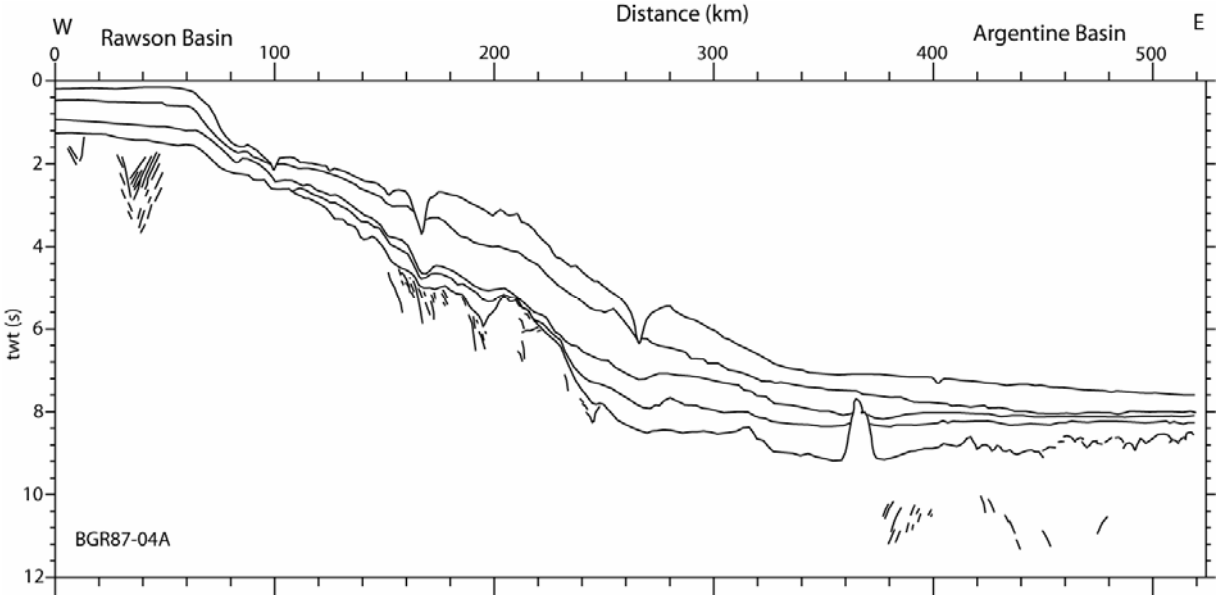

Fig. 3.9. Line-drawing interpretation of the BGR87-04 seismic profile (after Hinz et al., 1999). Location of profile in Fig. 3.1.

BGR87-05 profile

The profile has a length of 500 km across the continental slope east of the San Jorge basin (Fig. 3.10).

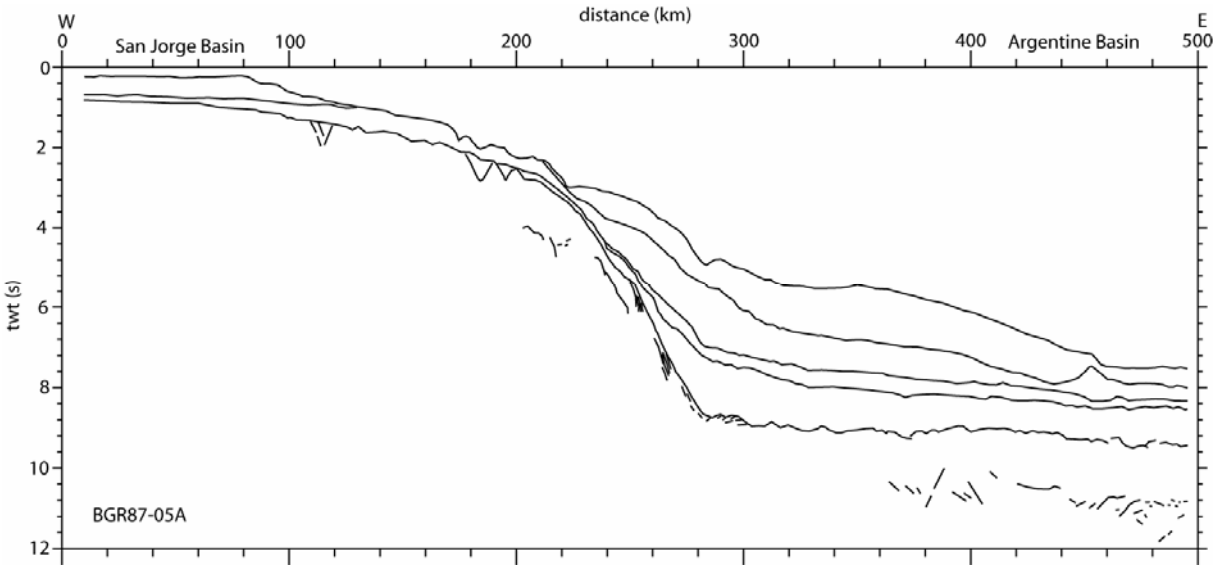

Fig. 3.10. Line-drawing interpretation of the BGR87-05 seismic profile (after Hinz et al., 1999). Location of profile in Fig. 3.1.

BGR98-01 (T2b) profile

This profile includes both reflection and wide-angle seismic refraction data along the offshore Colorado Basin extending from the coast to the shelf edge (Fig. 3.1) (Franke et al., 2004). The seismic source used for both seismic reflection and refraction data was a tuned set of four linear subarrays with 32 airguns with a volume between 0.62 and 3.28 litres, deployed 7.5 m below sea surface. For the MCS data acquisition, a 4500-m-long streamer with a group-length of 25 m was utilized. The shot distance was 50 m and the fold was 45. Predictive deconvolution was applied and the processing sequence completed with Kirchhoff-time migration (Franke et al., 2004). Fig. 3.11. is a composite seismic refraction/reflection section, where the boundaries from the refraction seismic model are superimposed, converted to two-way-traveltime.

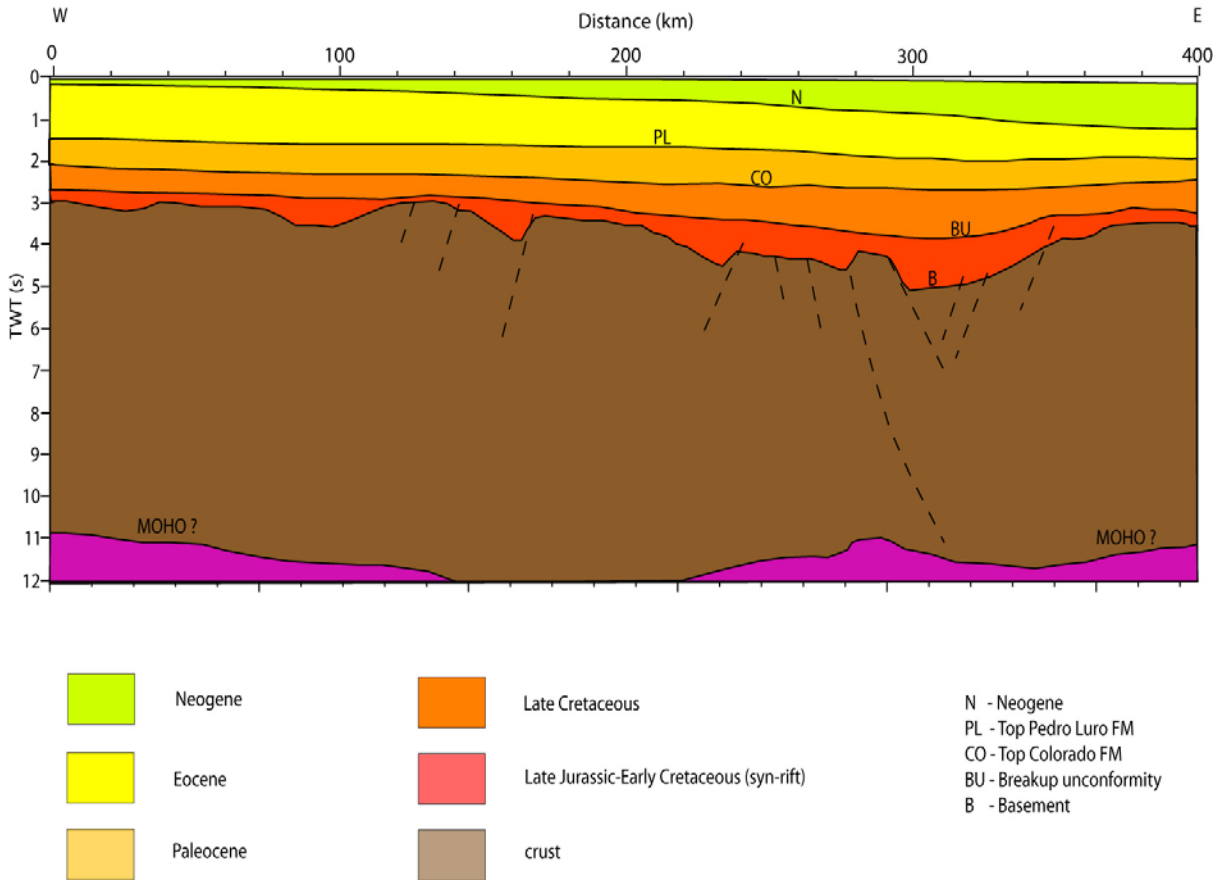

Fig. 3.11. Multichannel reflection seismic profile BGR98-01 along the landward part of the offshore Colorado basin (after Franke et al., 2004). Location of profile in Fig. 3.1.

3.2.2 Landward extension of seismic profiles

The continental shelf and onshore areas along the Argentine margin have been covered by several reflection and refraction profiles (Urién & Zambrano, 1996) that resolve the crustal structure down to 8-10 km. However, no technical information about their acquisition and processing is available, as these profiles are proprietary (industry) data.

Transect T0a

This section has a length of 800 km and extends in a direction closely orthogonal to the coastline, along the NE limb of the Salado basin (Fig. 3.1). It images well the unconformities within the Mesozoic-Cenozoic sedimentary cover and the relief of the basement, and it reaches depths of 9 km, down to the top of the oceanic crust (Fig. 3.12).

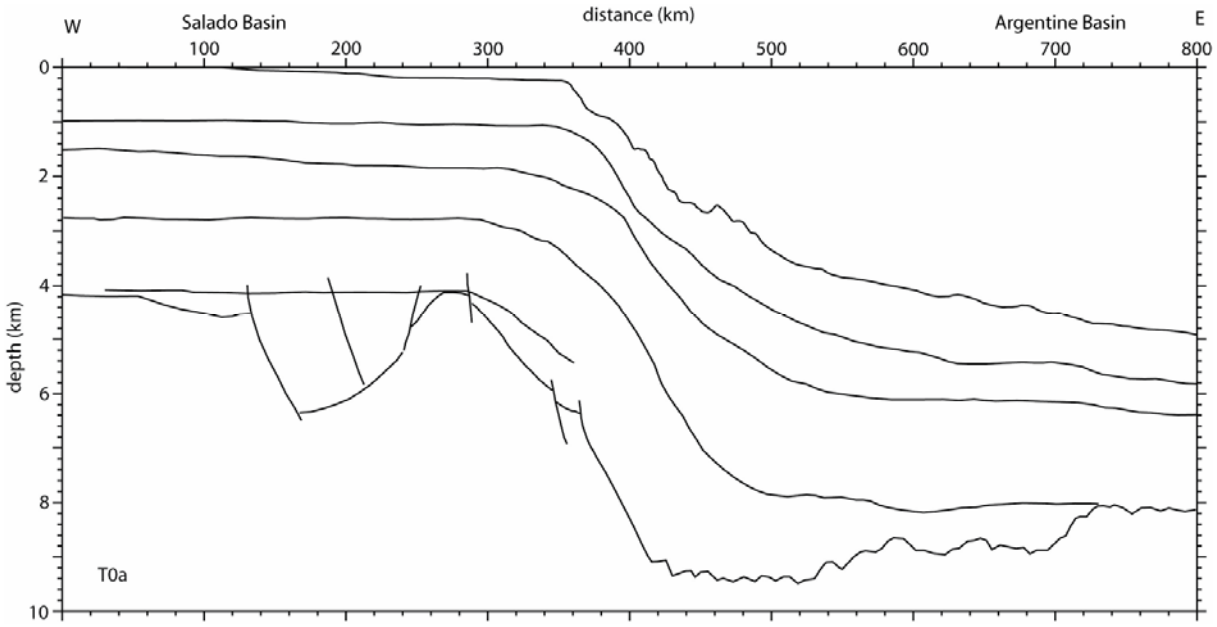

Fig. 3.12. Line-drawing interpretation of a proprietary seismic seismic profile along the Salado basin. (Modified after Urién & Zambrano, 1996). Location of profile in Fig. 3.1.

Transect T23a

The transect is an approximately 600 km long section extending from the Valdés peninsula in a W-E direction towards the shelf-edge (Fig. 3.1). It traverses perpendicularly the N-S elongated Valdés and Rawson basins, imaging the basement relief under a Mesozoic-Cenozoic sedimentary cover (Fig. 3.13).

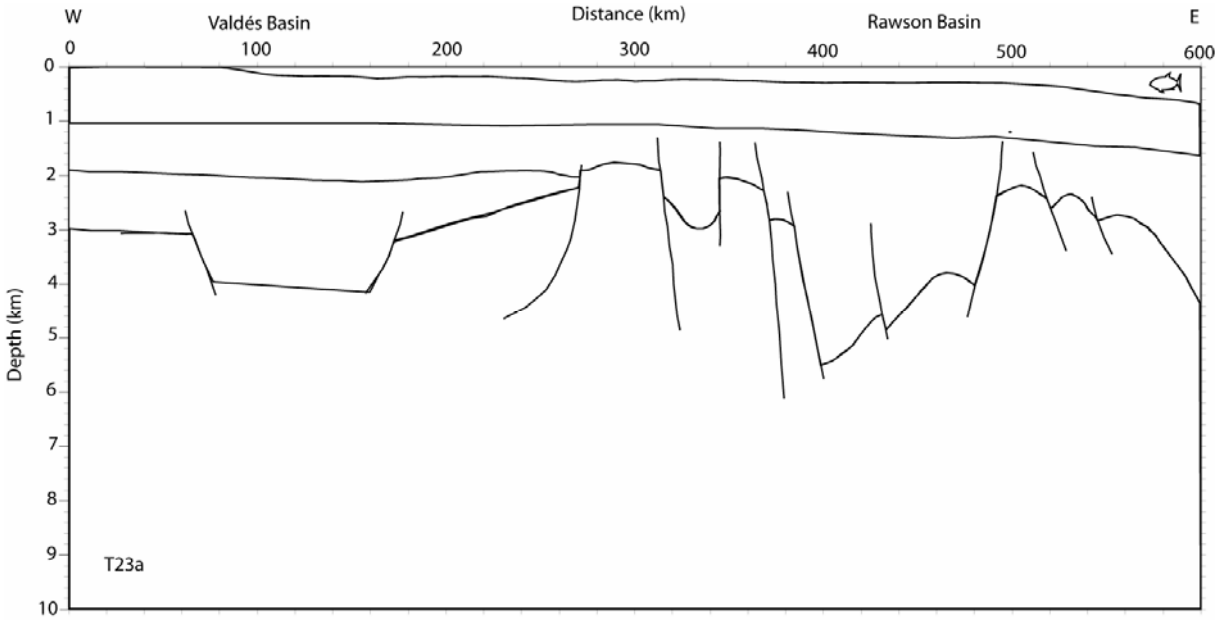

Transect T4a

The transect stretches more than 1000 km over the offshore part of the San Jorge Basin and into the Argentine Basin (Fig. 3.1), where it reaches depths of 8 km to the top of the oceanic crust (Fig. 3.14). The landward part of this section was used in the extension of BGR87-05 profile, towards the coastline, resulting in the composite section F-F' (Fig. 3.1).

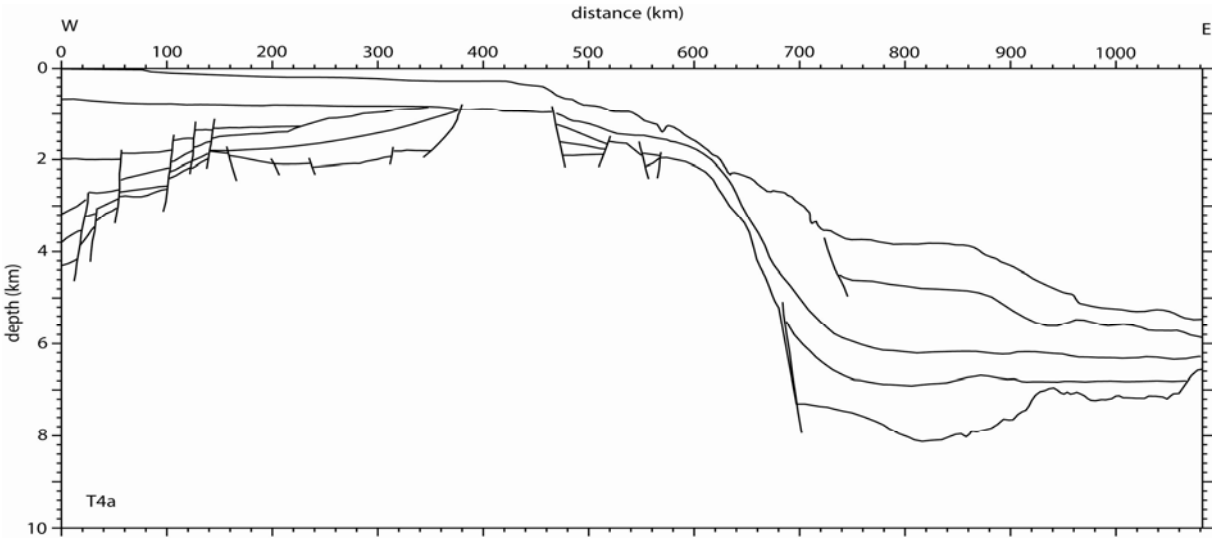

Fig. 3.14. Line-drawing interpretation of a proprietary seismic profile (transect T4a, Fig. 3.1) along the offshore part of the San Jorge Basin (modified after Urién & Zambrano, 1996). Location of profile in Fig. 3.1.

Fig. 3.13 (opposite page). Line-drawing interpretation of a proprietary seismic profile (transect T23a, Fig. 3.1) across the Valdés-Rawson Basins (modified after Urién & Zambrano, 1996). Location of profile in Fig. 3.1.

Chapter 4
Transect construction

A total of six composite transects across the Argentinian margin have been constructed, based on published seismic profiles and their landward and oceanward extensions. The names and locations of these transects, from north to south, are shown in Table 4.1 and Fig .3.1. Ship-born magnetics and gridded satellite-radar-altimeter gravity have been extracted along all sections, the latter being used as input gravity in TAMP modelling.

Transect name	Seismic profiles	Extensions	Location on Fig. 3.1
T0	T0a	T0b	Line A-A'
T1	T1a	T1b	Line B-A'
T2	T2b, T2c	T2a, T2d	Line C-C'
T23	T23a	T23b, T23c	Line D-D'
T3	T3a	T3b	Line E-E'
T4	T4b	T4a, T4c	Line F-F'

Table 4.1. Names and locations of the composite transects used in gravity modelling. For locations see Fig. 3.1.

4.1 Seismic interpretation and depth conversion

Seismic interpretation is based on existing publications including line-drawings of seismic profiles. The regional setting of the study area as a typical passive margin confers a characteristic pattern of basin evolution which is recorded in the sedimentary infill. Thus, basin infill should be characterized through the identification of the main tectono-sedimentary phases of rifted margins, that is, pre-rift, syn-rift, and post-rift sequences. Moreover, the volcanic character of the South Atlantic margin provides an additional insight to the seismic reflection interpretation. The four BGR seismic profiles all bear poor identification of the rift phase unconformity that correlates with the main rift event of Late Jurassic-Early Cretaceous (Hinz et al., 1999). This may be due to the presence of a very reflective Paleozoic basement

beneath the shelf, obscuring the interpretation. Therefore, the upper crustal unit appears to be entirely formed by a continuous accumulation of the post-rift and passive margin phase sediments in a margin setting regionally dipping towards the Atlantic deep oceanic basin to the east (Fig. 3.1). The absence of faults penetrating these sediments is also a common observation in the seismic sections. Most of the seismic profiles are oriented parallel to the opening axis of the basins, like in the Salado and Colorado basins, meaning that the main extensional faults are not intersected (Fig. 3.1). This makes difficult the identification of the spatial relation between the different seismic sequences. The top oceanic basement reflector produces two different seismic images according to the zonation proposed by Hinz et al. (1999). A rather smooth zone from beneath the foot of the slope to magnetic anomaly M0, and a more irregular relief zone with poorer reflectivity, related to the Cretaceous Magnetic Quiet Zone (CMQZ).

Unit	**Average interval velocity (km/s)**
Water	1.48
Plio-Pleistocene	1.90
Eocene-Miocene	2.1
Paleocene-Eocene	2.3
Late Cretaceous	3.0
Early Cretaceous	3.5
Paleozoic sediments	4.75
Seaward dipping reflectors	4.25
Crystalline basement	6.30
Oceanic crust	6.50

Table 4.2. Velocity model utilized in depth conversion of transects T1a, T2c, T3a and T4b (BGR seismic profiles). For locations see Fig. 3.1.

The four seismic profiles from BGR (Hinz et al. 1999) have been depth converted utilizing a simplified seismic velocity-depth function (Table 4.3). The velocity model incorporated velocity-depth functions derived from OBS studies (Franke et al., 2006) and regional considerations. In addition, published velocity-depth fuctions from similar margin settings

have been incorporated (e.g. NE Atlantic margins, Mjelde et al. 1997; Tsikalas et al., 2005). The latter were applied to the crystalline basement and the seaward-dipping reflector wedge, since these crustal layers exhibit a rather uniform density at a regional scale. Velocity stations for all profiles were constructed at intervals of 20 km, reducing that distance to 10 and 5 km over the zones of complex relief in the bathymetry and/or the main reflectors. The number of velocity stations range from 32 to 56, at the individual seismic profiles.

4.1.1 Transect T0

Seismic profile T0a

The interpretation of this proprietary profile is based on Urien & Zambrano, (1996). The profile resolves the upper crust down to a depth of 10 km, thus depicting the Mesozoic-Cenozoic rift sediments and imaging the top of the pre-rift basement within both continental and oceanic crust (Fig. 4.1). Syn-rift deposits are recognized filling a graben-shaped structure to the west of the Martín García- La Plata High, a large horst block that separates the Punta del Este Basin from the Salado Basin (Fig. 2.6 and Fig. 4.1) The sediment infill is bounded by listric faults and shows increased thickness towards the footwalls. Seismic interpretation of similar grabens in neighbouring lines suggested the presence of Late Paleozoic sediments at the bottom of the structure, based on the presence of zones of contrasted reflection strength (Urién & Zambrano, 1996). Furthermore, the post-rift and passive margin sequences constitute a thick homogeneous cover which overlies the pre-rift and syn-rift sequences, extending from the continental shelf to the deep marine basin (Fig. 4.1). Based on well-data and onshore outcrop stratigraphy, several internal reflectors have been attributed to regional Cretaceous and Cenozoic unconformities within this package: the base of the passive margin sequence (Mid-Cretaceous unconformity); Upper Cretaceous unconformity (Maastrichtian Transgression); Mid Cenozoic unconformity (Urien & Zambrano, 1996).

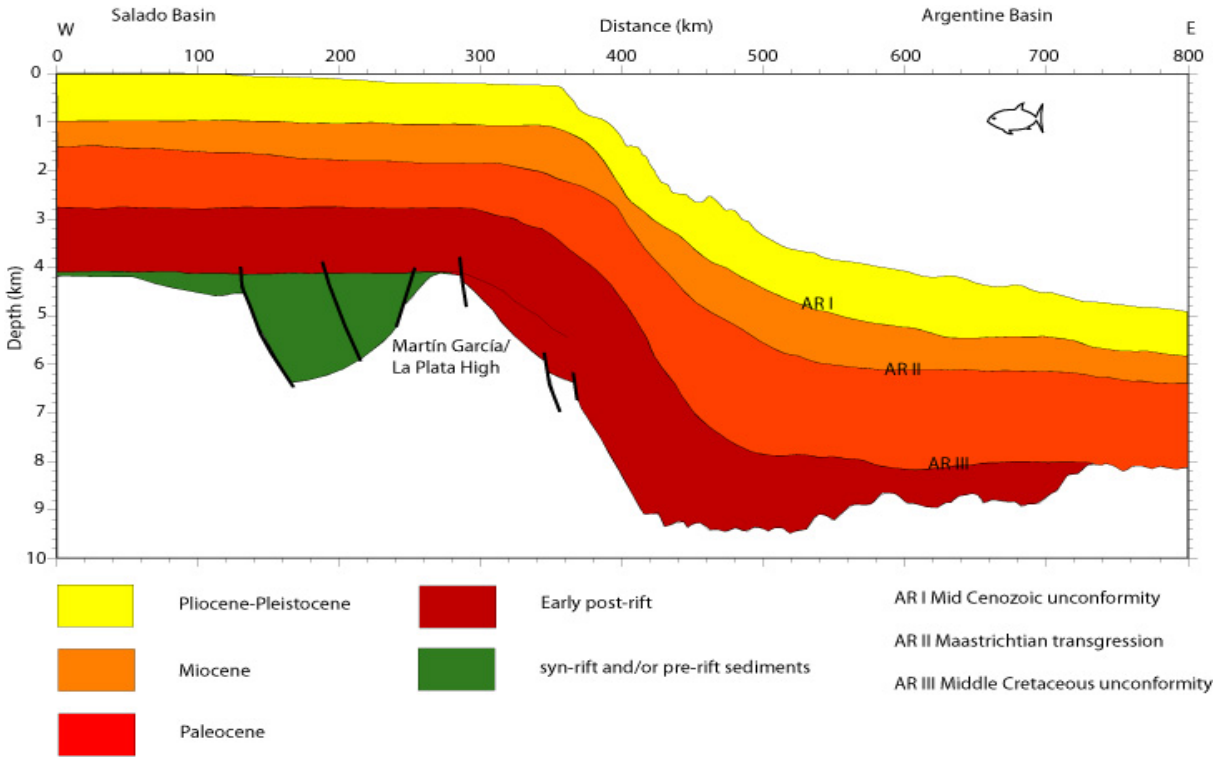

Fig. 4.1. Interpretation of seismic profile T0a (modified from Urién & Zambrano (1996). For locations see Fig. 3.1.

4.1.2 Transect T1

Seismic profile BGR87-01A (section T1a)

The seismic profile is located on the outer (eastern) portion of the Salado Basin and its E-W continuation into the Argentine Basin, through the continental slope (Fig. 3.1). It is a highly penetrative seismic profile, imaging a clear Moho candidate reflector under continental crust at profile distance between 120 and 220 km (Fig. 4.2). A horizontal linear set of upper mantle reflectors is also recorded under the oceanic crust domain, east of the 350 km distance (Fig. 4.2). A main angular unconformity, represented by the most prominent and extended horizon (AR1) separates two very different seismic domains (Fig. 4.2) (Hinz et al., 1999):

1) An upper crustal domain consisting of a homogeneous set of subparallel continuous reflectors, extending over the total length of the profile, attributed to sediments of Cretaceous and Cenozoic age. There have been identified five regional seismic marker horizons within these sediments, AR1-AR5 (Fig. 4.2), although the level of uncertainty about their age and origin remains high due to scarcity of published data. The inferred age and name of these

seismic markers are presented in Table 4.3 and apply for all four BGR seismic profiles (sections T1a, T2c, T3a and T4b) (Fig. 3.1).

Marker	Inferred age (Hinz et al. 1999)
AR1	Hauterivian (c.130 Ma)
AR2	Late Aptian (115-112 Ma)
AR3	Early Campanian (81 Ma)
AR4	Late Eocene (37-33 Ma)
AR5	Middle Miocene (c. 15 Ma)

Table 4.3. Nomenclature and inferred ages of the seismic markers used in the interpretation of the BGR seismic profiles (after Hinz et al., 1999).

2) A lower crustal domain, beneath the continental shelf, the slope and the oceanic basement. This unit has been divided into four regional structural zones (Hinz et al. 1999). Zone 1 comprising the outer shelf and upper slope, contains a sequence of antithetic reflectors that are interpreted as narrow half grabens of unknown age and nature, observed in the seaward extension of the Salado and Colorado basins (Hinz et al. 1999). Under these deposits, a unit of imbricate thrust sheets or asymmetrical folds was observed following the trend of the Ventana Hills and Tandilia High (Fig. 2.6) (Hinz et al., 1999). South of the 41ºS there are few indications of the presence of such syn-rift basins. Zone 2, occupying most of the slope, contains a remarkable and characteristic structural feature of the Argentine continental margin, namely a voluminous set of seaward dipping reflectors, recognized down to approximately 10 seconds (c. 12 km) depth (Fig. 4.2). Zones 3 and 4 extend over the oceanic crust, and differ from each other in the character of the surface of the oceanic crust, the latter being smoother in Zone 3. In this zone, this surface is represented by a strong reflector with several offsets representing fault-displacements and/or west-facing edges of basaltic flows (Hinz et al., 1999).

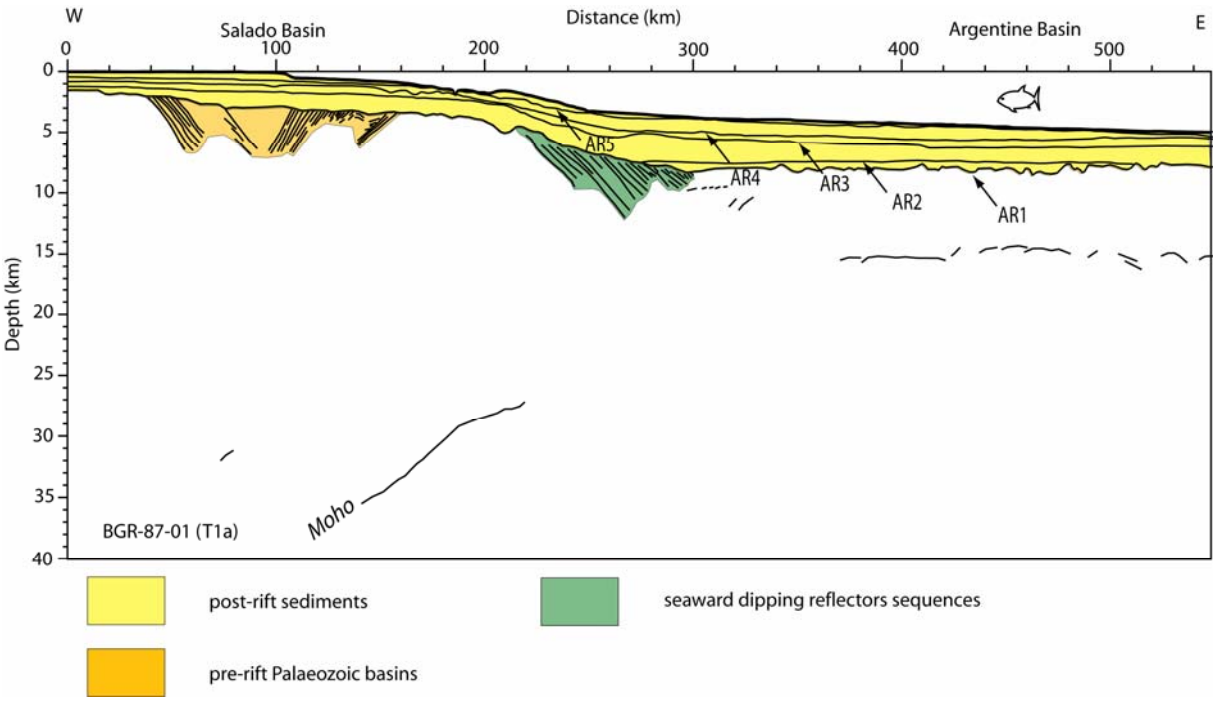

Fig. 4.2. Depth-converted seismic profile BGR87-01 (T1a). For locations see Fig. 3.1.

4.1.3 Transect T2

The onshore extension (Transect T2a) of this section, consists of a Bouguer-corrected gravity section (Kostadinoff et al., 2005), later used in the gravity modelling. Field gravity measurements were obtained with a Worden gravimeter, within a 6x6 km grid over an area of 35000 km², and geographic positions were verified with a Legend type Garmin GPS. Line BGR98-01 (transect T2b) (Franke et al., 2004) provides also shipboard free-air gravity data, acquired using a LaCoste & Romberg air/sea gravimeter system.

Seismic profile T2b

This seismic profile, extending entirely within the Colorado Basin, was interpreted based on Franke et al., (2004). The pre-rift basement reveals a relief geometry of highs and lows that in some cases has been attributed to rift-related fault geometries, thus allowing to the recognition of the syn-rift sequences (Fig. 4.3). Syn-rift sediments can be identified in the deepest part of the basin, at a distance between 350 and 400 km, where a graben structure appears to be controlled by extensional faults. Some high-reflectivity reflectors within this unit suggest the presence of basaltic flows and pyroclastic rocks similar to those encountered in the Salado Basin (Lesta et al., 1978). Other possible small syn-rift troughs may be located

within relative lows of the basement surface but identification is difficult, in part due to the orientation of the section, i.e. perpendicular to the opening direction caused by the Late Jurassic-Early Cretaceous extension. The breakup unconformity (BU) bounds the top of the syn-rift sequences, above which, the sag phase develops. The latter is illustrated by the sedimentary unit between Top Colorado Fm (reflector CO) and the break-up unconformity (BU), reaching its maximum thickness over the above mentioned depocentre (Fig. 4.3). The successions above the sag sequence show little or no thickness variation, corresponding to the passive margin formation. Franke et al. (2006) interpreted the hummocky relief of the basement surface as an offshore continuation of the Ventana and Tandil highs, and accounted for magmatic intrusives/extrusives in a region of low amplitude reflectivity with no internal structuring, at distance of around 540 km (Fig. 4.3).

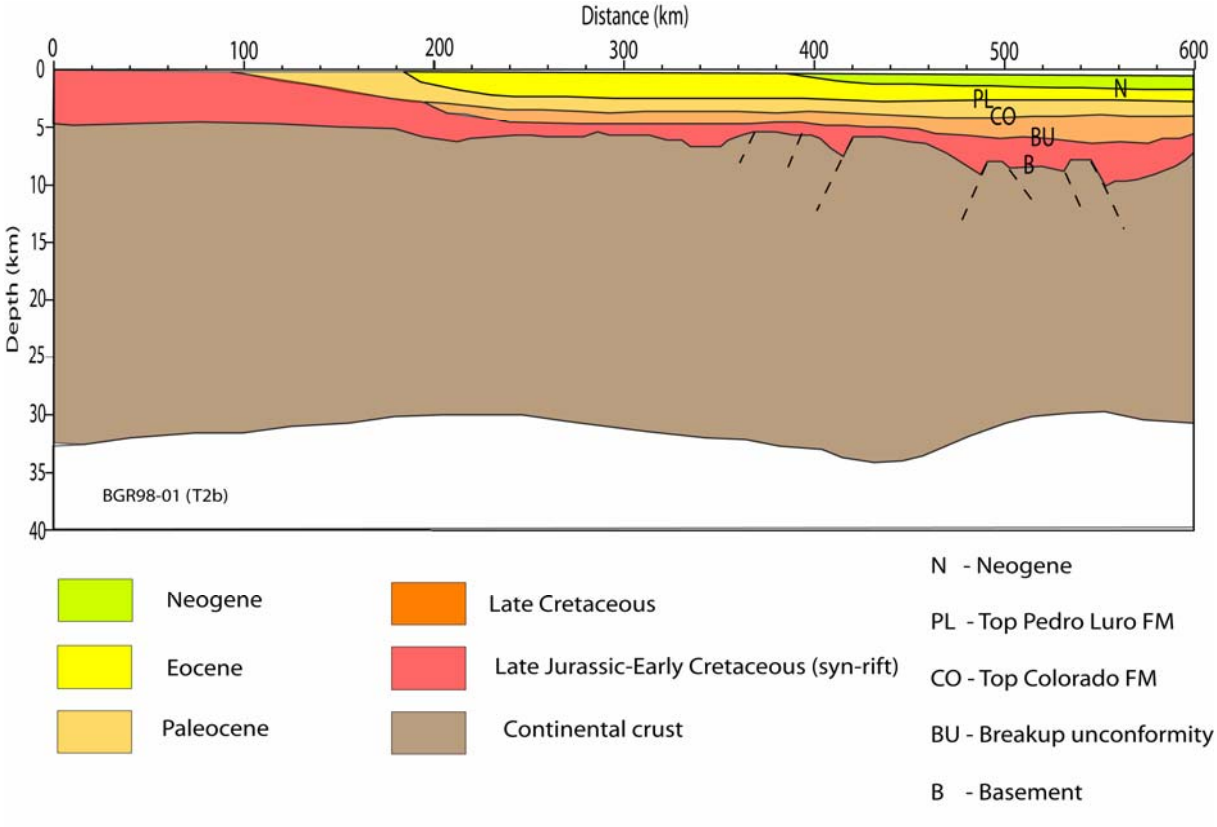

Fig. 4.3. Interpretation of seismic profile BGR98-01 (T2b), (after Franke et al., 2006).
For locations see Fig. 3.1.

Seismic profile BGR87-02 (transect T2c)

The section bears many similarities with respect to transect T1a. The two main crustal units separated by reflector AR1 are recognized. The lower continental crust exhibits a more

transparent seismic reflectivity unit and a Moho candidate is only observed beneath the continental slope (Fig. 4.4). In the oceanic domain there are several dipping reflectors of uncertain origin within the upper mantle. In the shelf area, the deepest observed reflectivity may be related to similar features as those observed in transect T1a, and may be attributed to deeply buried Permo-Carboniferous sedimentary units like the ones exposed in the Tandil Hills (Franke et al., 2006). Seaward-dipping reflectors sequences of similar proportions to that of transect T1a are observed beneath the continental slope (Fig. 4.4). The thickest accumulations of rift-related sediments are found under the landward sector of the shelf, and it appears that a basement high separates the Colorado Basin from the Argentine Basin. To the west in the seismic profile, between the 0 and 100 km distance, strong curvilinear reflectors appears to correspond to the imbricate thrust sheets described by Franke et al. (2006) (Fig. 4.4). The top of these reflectors outline a depocentre of 7 to 10 km. The age of the deepest rocks in this depocentre, and subsequently, the position of the horizon AR1 in this region are unclear.

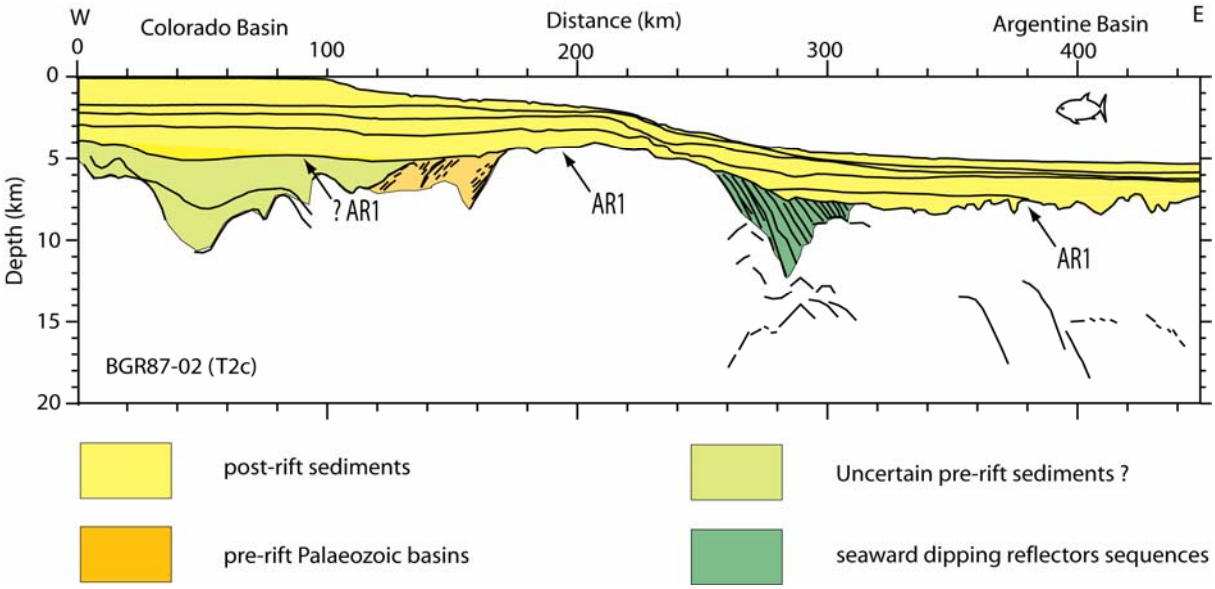

Fig. 4.4. Depth-converted seismic profile BGR87-02 (T2c). For locations see Fig. 3.1.

4.1.4 Transect T23

Seismic profile T23a

This profile is a schematic line-drawing of a proprietary seismic reflection profile, imaging the upper crustal levels to a depth of 6 km (Fig. 4.5). Seismic interpretation was based on

Marinelli & Franzi (1996). In this area, the main extensional faults that formed the Valdés and Rawson basins, strike roughly N-S, i.e. perpendicular to the section, hence enhancing the fault geometry (Fig. 4.5). The Valdés and Rawson basins are separated by a basement high and their evolution is controlled by extensional faults. At the bottom of the narrow grabens of these basins, two wells penetrated sedimentary rocks of Paleozoic age (Marinelli & Franzin, 1996).

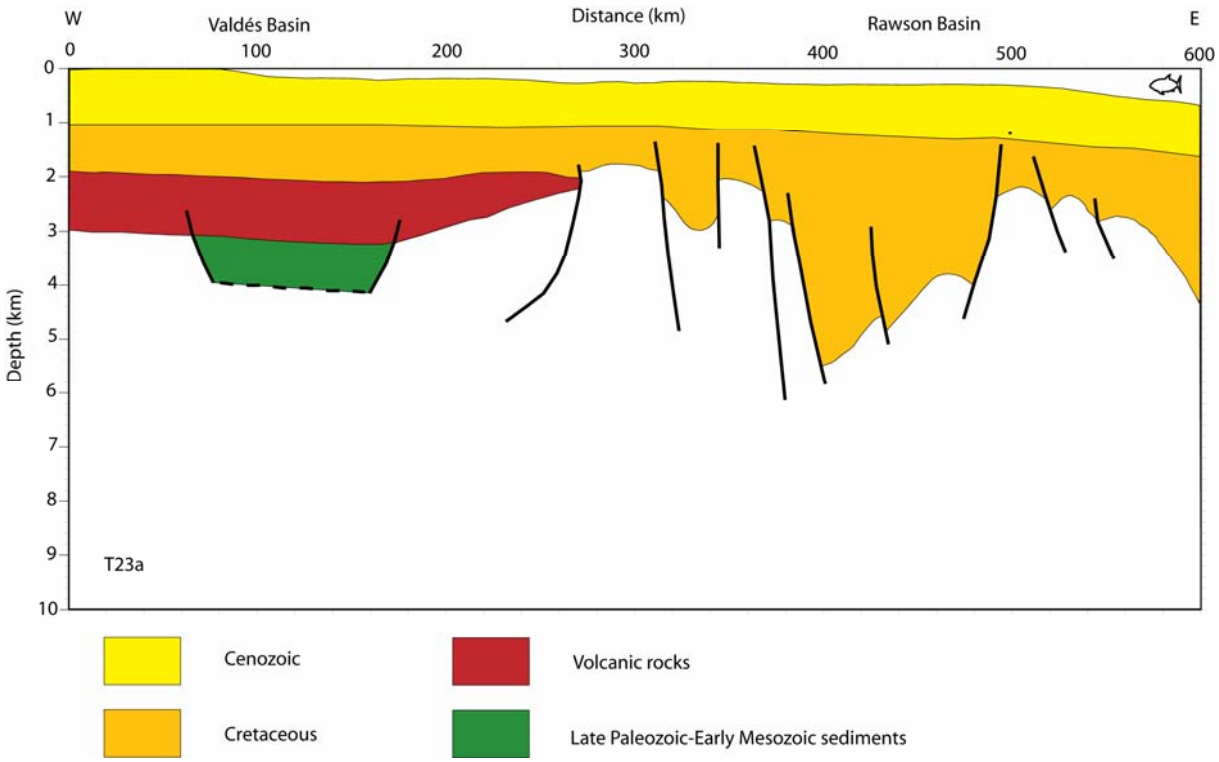

Fig. 4.5. Interpretation of seismic profile T23 (modified after Marinelli & Franzin, 1996). For locations see Fig. 3.1.

4.1.5 Transect T3

Seismic profile BGR87-04 (T3a)

This section, intersecting the southern edge of the smaller Rawson Basin, is characterized by a thinner (~1.2 s) post-rift veneer of sediments on the shelf and upper slope (Fig. 4.6), compared to the northern sections across the Colorado and Salado basins. Seaward dipping reflector sequences (SDRs) at the lower slope are also observed in this part of the margin, but they consist of smaller, individual wedge shaped bodies, compared to the larger massive bodies observed farther north (Fig. 4.6). Observations from drilling cores showed that these

wedges are composed of basaltic flows and interlayered volcaniclastic sedimentary layers (Hinz et al. 1999). Seaward of the SDRs, magnetic anomaly M4 has been recognized (Hinz et al. 1999), compared to the M3 at equivalent position at 35.5ºS. In this seismic profile, the two different characters of the top oceanic basement are clearly imaged: a smooth surface landward of the 400 km distance, and a more irregular seaward of that distance, away from the Cretaceous Main Quiet Zone (CMQZ) (Fig. 4.6). A set of peculiar reflectors within the oceanic basement are observed in the seismic profile. These reflectors dip steeply at different directions, and are of unknown origin, but they may be considered as fault events, since they lie beneath important offsets in the surface of the top oceanic basement above (Fig. 4.6) (Hinz et al., 1999).

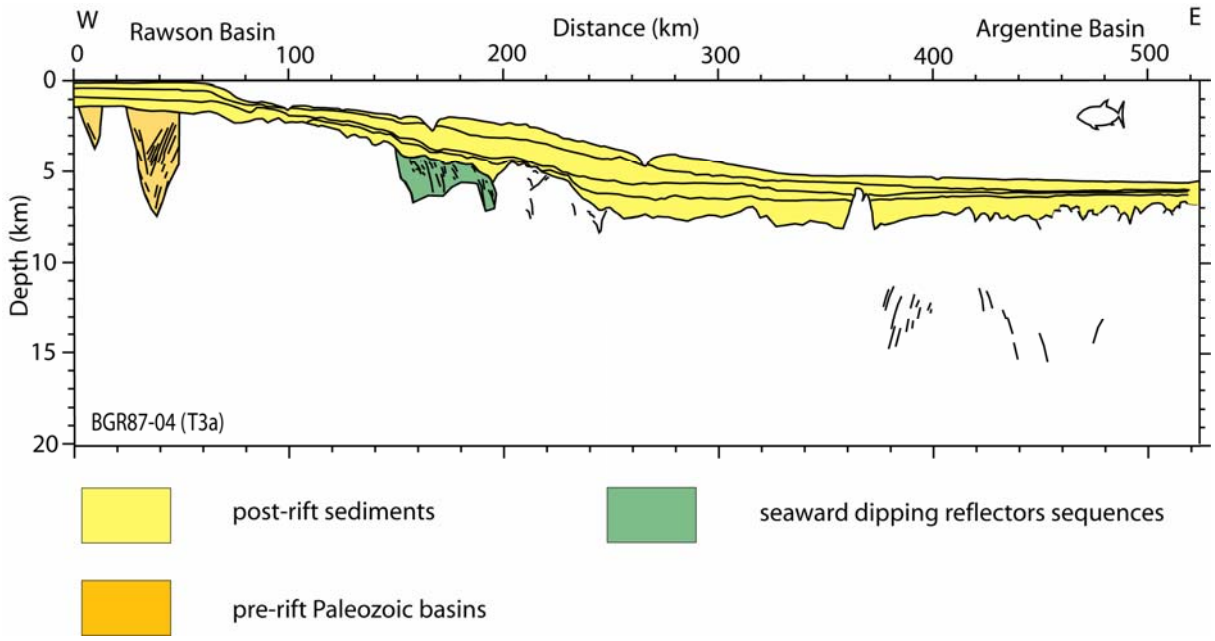

Fig. 4.6. Depth-converted seismic profile BGR87-04 (T3a). For locations see Fig. 3.1.

4.1.6 Transect T4

Seismic profile BGR87-05 (T4b)

The main feature imaged in this seismic profile is the Eastern Deseado High (Fig. 2.6), which separates the San Jorge Basin from the Argentine Basin (Fig. 4.7). Unlike the Salado and Colorado basins, the San Jorge Basin does not continue down the slope into the abyssal plain. This explains the poor sediment infill over the shelf and upper slope (Fig. 4.7). Instead, a comparatively thick pile (up to 4 s; ~4.5 km) of post-rift sediments occupies the lower slope and rise and the edge of the Argentine Basin. This thick sediment accumulation may be

related to erosion of the basement high during uplift caused by the Andean Orogeny. Following the trend observed in transect T3a, the SDRs consist of shallower individual wedges along the slope (Fig. 4.7). The continental crust appears almost featureless, with only small reflections at the top of the basement.

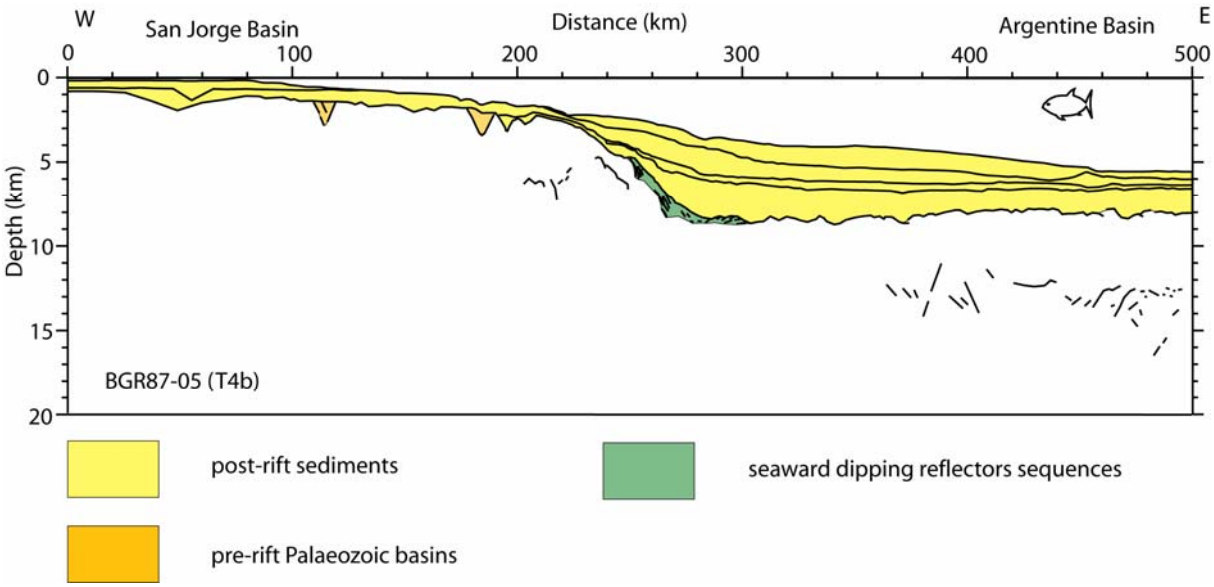

Fig. 4.7. Depth-converted seismic profile BGR87-05 (T4b). For locations see Fig. 3.1.

Seismic section T4a (based on Urien & Zambrano, 1996)

This profile is a schematic line-drawing of a proprietary seismic profile showing the seaward termination of the San Jorge Basin against the Eastern Patagonian High, as well as the thick accumulation of post-rift sediments on the continental slope and rise (Fig. 4.8). The margin of the San Jorge Basin is densely faulted by extensional faults. Late Paleozoic and early Mesozoic sediments accumulated in wide depocentres like the one at the top of the basement high, at 150-400 km distance. They are unconformably overlain by the Late Jurassic-Early Cretaceous rift sediments, onlapping the eastern edge of the basin. The high-velocity layer detected by refraction seismic within the depocentres mentioned above were attributed to extrusives and pyroclastic flows of the Middle Jurassic Chon Aike formation (Urién & Zambrano, 1996).

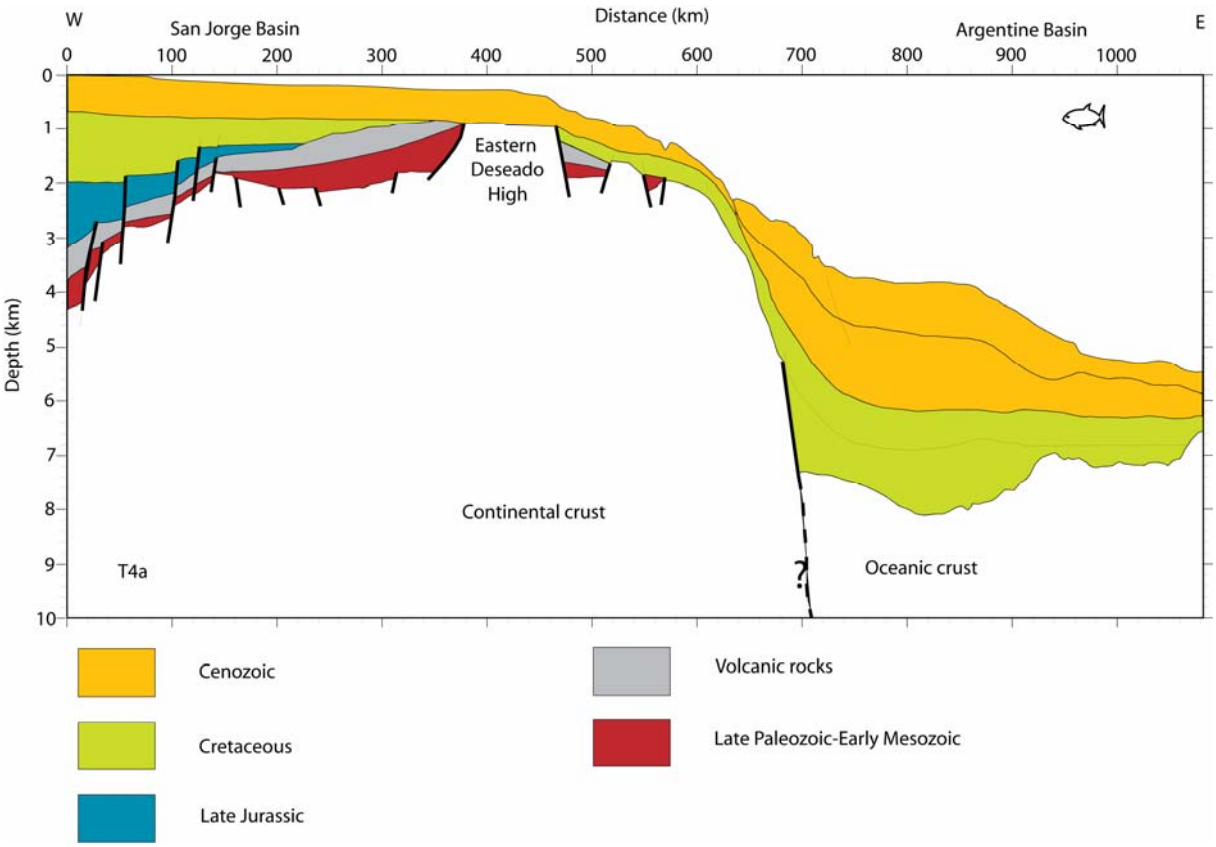

Fig. 4.8. Interpretation of seismic profile T4a (modified after Urién & Zambrano, 1996). For locations see Fig. 3.1.

4.2 Initial Moho relief estimates

The Moho discontinuity is recognized seismically by an abrupt increase in P-velocity, from less than 7.6 km/sec to at least 8 km/s (Condie, 2005), accompanied also by a prominent change in density corresponding to the abrupt transition between the lower crust and the upper mantle (Allen, 1990). The seismic velocity and density contrasts at the Moho level can be explained either by a compositional change or by a phase change from a low to a high pressure mineral assemblage (Condie, 1989). The depth to Moho along the transects has been estimated by forward isostatic balancing and inverse modelling, utilizing the in-house software TAMP (Breivik et al., 1990). Three different values of crustal mean density have been tested for each transect, in both modalities of modelling, and finally, an averaged integration of the two methods is presented. Calculations are based on a simplified three-polygon crustal model, each polygon having a specific density value: the upper water layer

with density ρ=1.03 g/cm³; a polygon representing the crust, with densities ρ=2.70 g/cm³, 2.80 g/cm³ and 2.90 g/cm³; and finally, a lower polygon representing the upper mantle, with ρ=3.20 g/cm³. The digitized bathymetry along the seismic profiles, as well as grid extracted bathymetric data for the seaward extended profiles, was the input to define the boundary between the water and the crustal polygons. The "observed" grid-extracted gravity along the sections is displayed over the gravity models for comparison. The Moho geometry has been estimated for six composite transects that will later be used in 2D forward crustal-scale gravity modelling. In Table 4.4, the modelled transects are presented, with the total length and the position of the anchor points.

Transect name	position in Fig. 3.1	Total length (km)	Position of anchor point
T0	A-A'	1260	1250
T1	B-A'	959	950
T2	C-C'	1917	1907
T23	D-D'	1461	1450
T3	E-E'	1147	1140
T4	F-F'	1560	1575

Table 4.4 Composite transects modelled with TAMP. For locations see Fig. 3.1. For locations see Fig. 3.1.

4.2.1 Forward isostatic balancing

This method is based upon the assumption of an isostatically balanced crust, according to the Airy model, by which the balance between crust and mantle is achieved by changes in crustal thickness, with constant density. TAMP calculates the geometry of an isostatically balanced Moho from an initial simplified crustal model, in which bathymetry is the only variable. Thus, the Moho relief can be directly correlated to bathymetric changes. Finally, the "calculated" gravity response of the modelled crust is plotted together with the "observed", grid-extracted gravity along the section (Fig. 4.9). The areas of misfit between the two curves will be eventually matched through 2D forward crustal-scale gravity modelling. As a constraint to the modelling process, we introduce an "anchor point", i.e. a point in which the depth to Moho is known, usually in the oceanic crust domain. This position can be inferred either with the help

of single-channel ship-track seismic profiles and grid-extracted sediment thickness, as well as by adding the world average thickness of the oceanic crust (6.5 km) to the water depth on a point of interest. The latter was implemented, since no single-channel seismic profiles with a clear image of the oceanic basement crossed any of the transects.

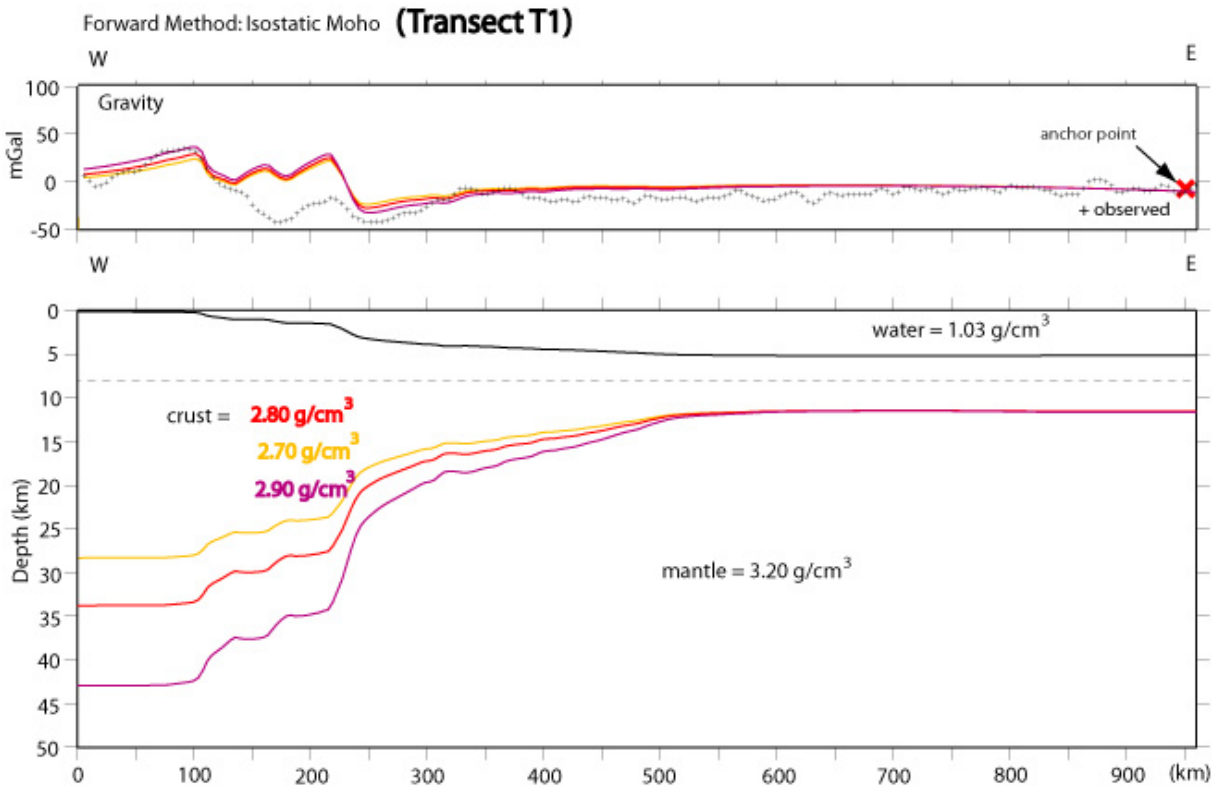

Fig.4.9. Example of Moho relief along transect T1, using forward isostatic balancing and three alternative density values for a uniform crystalline crust.

4.2.2 Inverse modelling

This method, developed by Cordell & Henderson (1968), estimates the Moho geometry that would result from the "observed", grid-extracted gravity along the section. Thus, a hypothetical Moho-derived "calculated" gravity curve is adjusted to the "observed" gravity curve, and the corresponding Moho relief is then inferred (Fig. 4.10). This is done in TAMP by iterative calculation of Moho depth along a segmented section (in columns) until the adjustment of the two curves is satisfactory. The input to the model is the bathymetry along the profile and an initially flat Moho. Anchor points of fixed Moho depths are also used to constrain the modelling, as it was done in forward isostatic balancing.

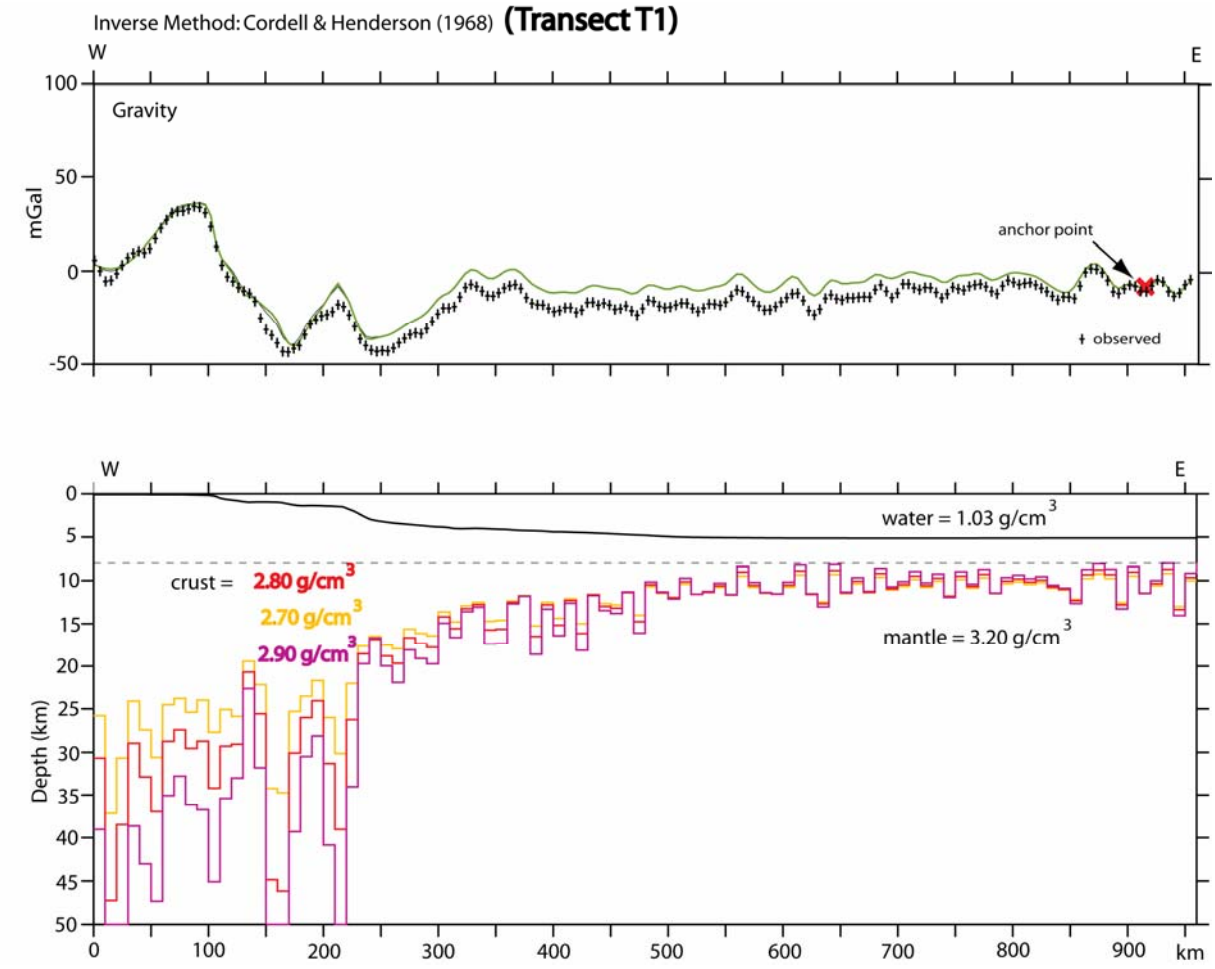

Fig. 4.10. Example of estimated Moho relief along transect T1, using inverse modelling (three coloured curves corresponding to three different crust density values).

The Moho relief along all transects, estimated with TAMP with forward isostatic balancing and inverse modelling, and their computed gravity anomalies is presented in Fig. 4.11. On the forward isostatic balancing model, calculated gravity response fits well to the general trend of the observed gravity along the section. A conspicuous positive anomaly over the 100-200 km position is the main discrepancy along the transect T1.

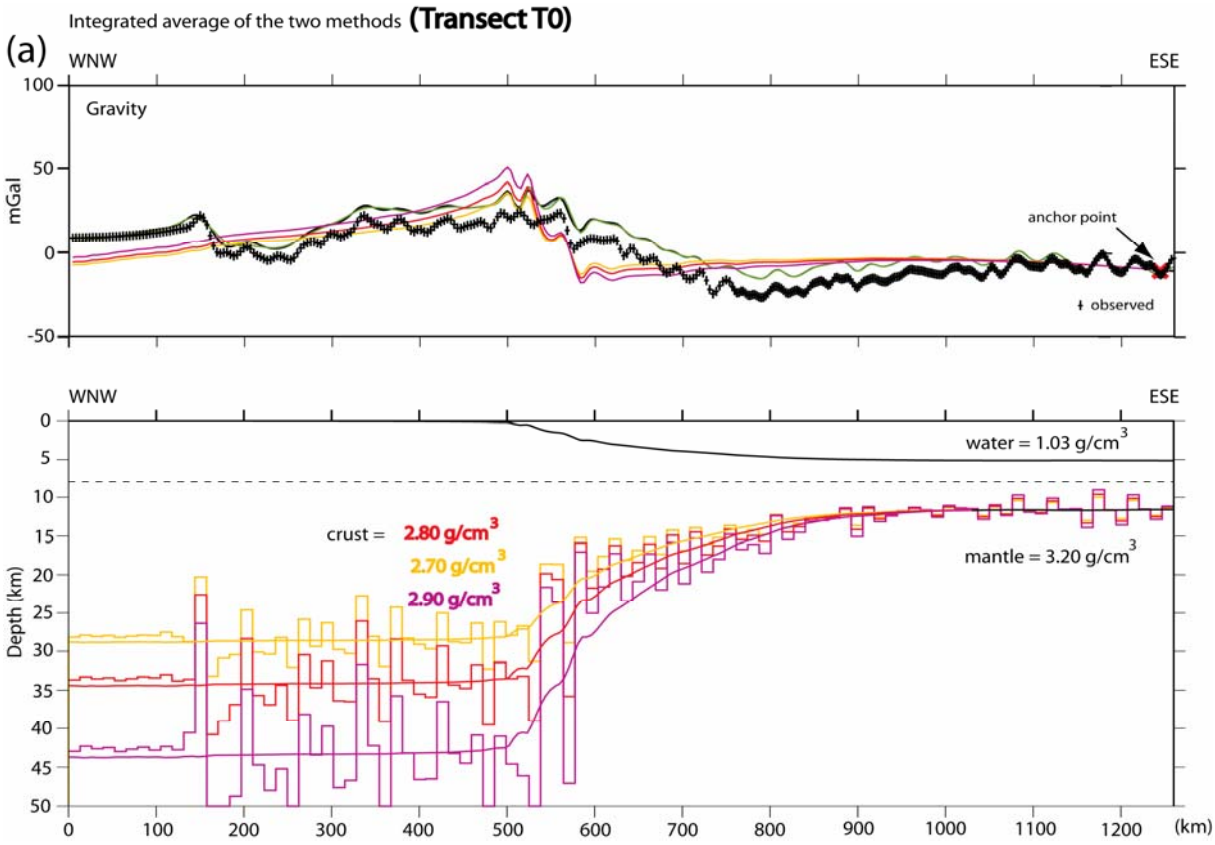
Integrated average of the two methods (Transect T0)
(a)
WNW
ESE
Gravity
mGal
anchor point
observed
water = 1.03 g/cm3
crust = 2.80 g/cm3
2.70 g/cm3
2.90 g/cm3
mantle = 3.20 g/cm3
Depth (km)
(km)

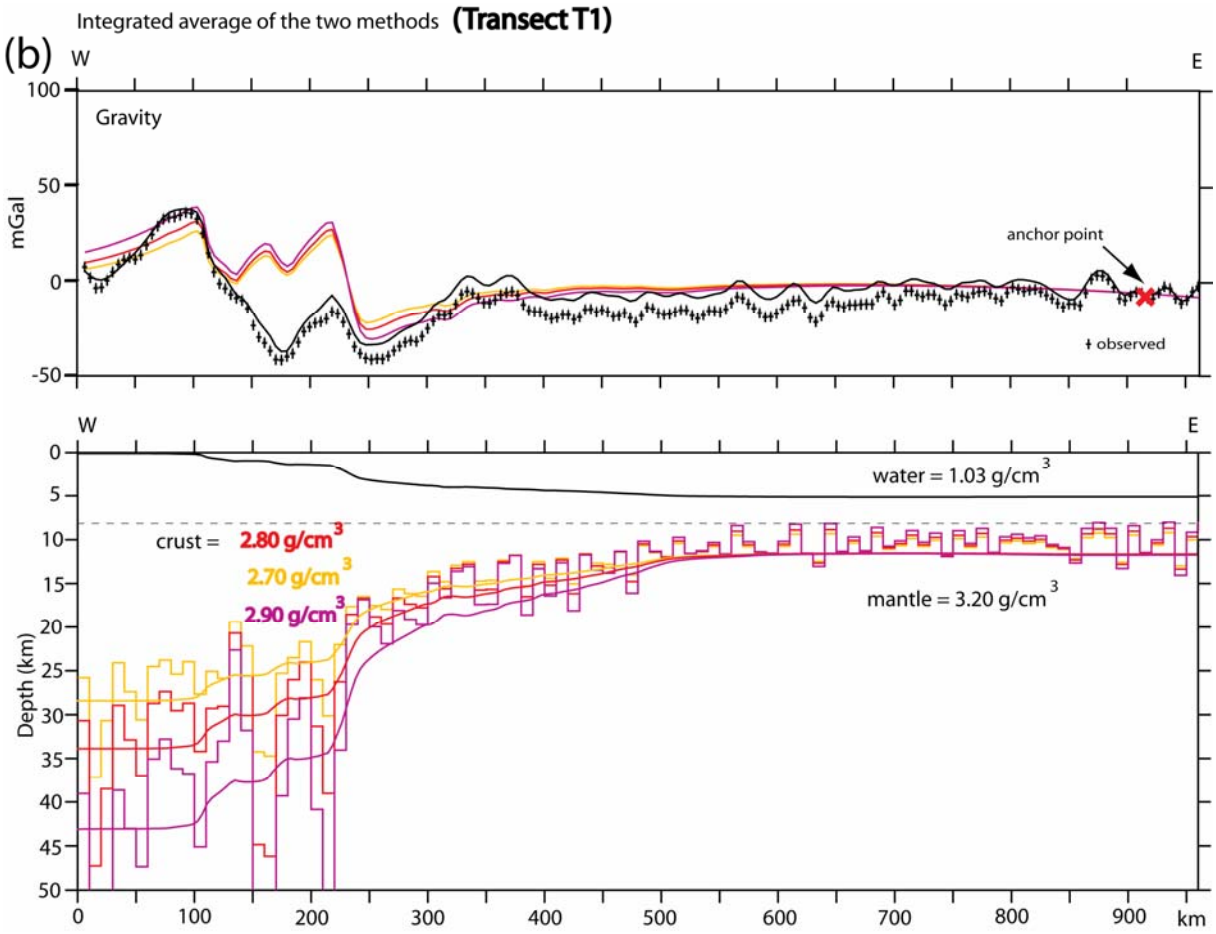
Integrated average of the two methods (Transect T1)
(b)
W
E
Gravity
mGal
anchor point
observed
water = 1.03 g/cm3
crust = 2.80 g/cm3
2.70 g/cm3
2.90 g/cm3
mantle = 3.20 g/cm3
Depth (km)
km

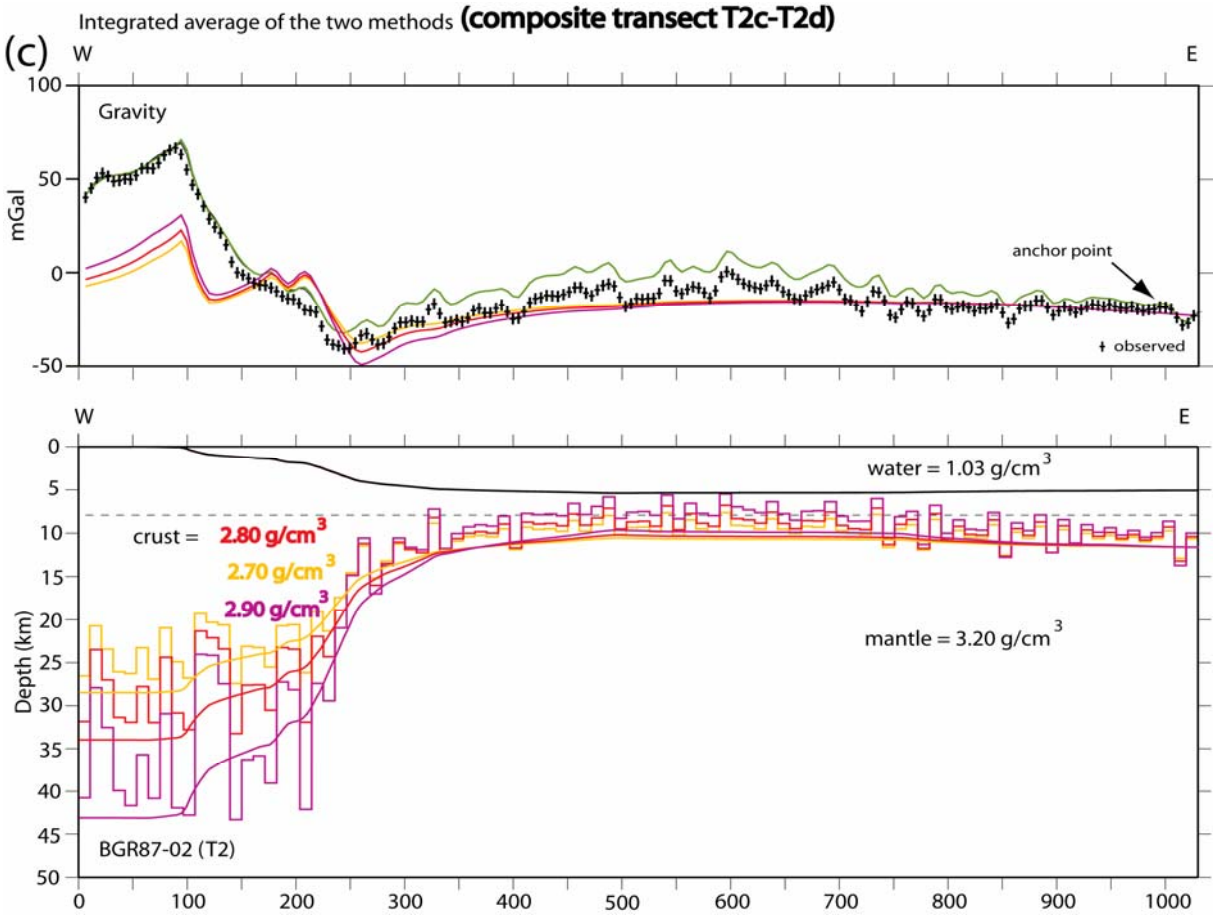
Integrated average of the two methods (composite transect T2c-T2d)
(c)
W
E
Gravity
mGal
anchor point
observed
water = 1.03 g/cm3
crust = 2.80 g/cm3
2.70 g/cm3
2.90 g/cm3
mantle = 3.20 g/cm3
Depth (km)
BGR87-02 (T2)

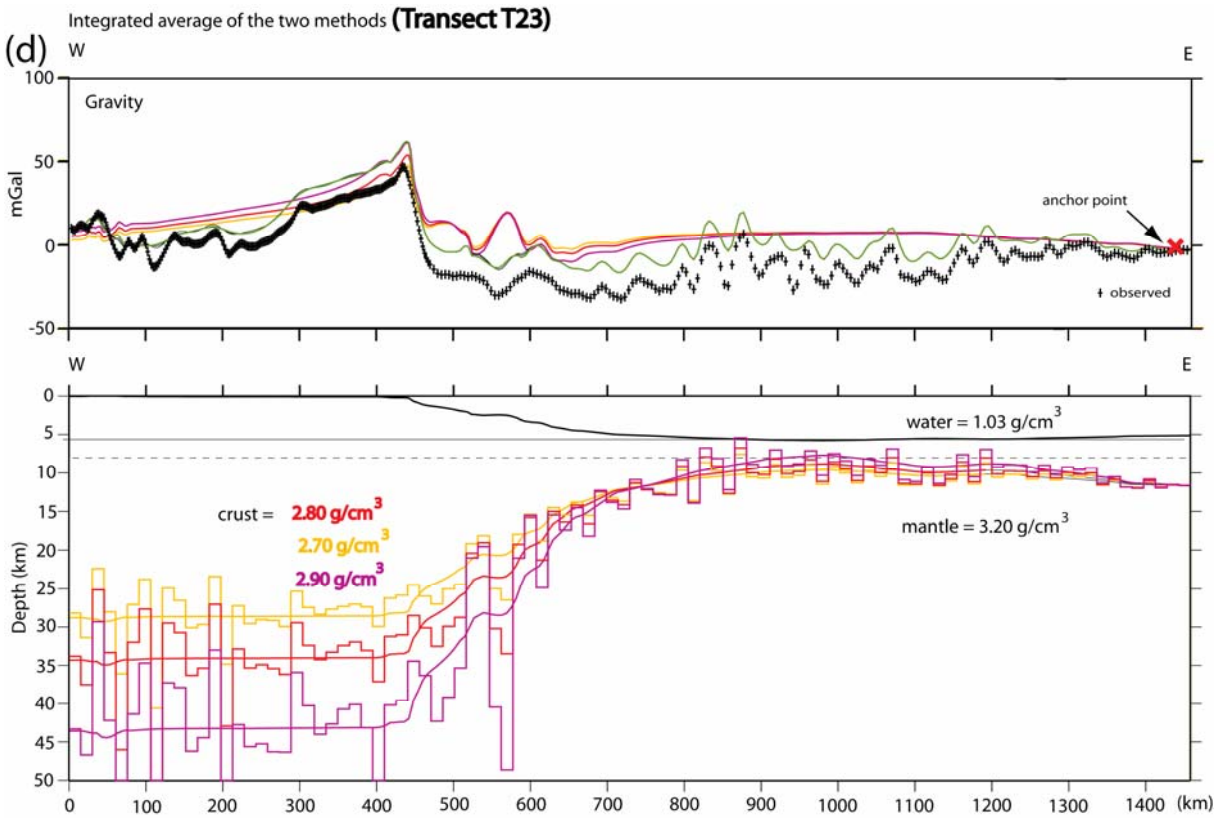
Integrated average of the two methods (Transect T23)
(d)
W
E
Gravity
mGal
anchor point
observed
water = 1.03 g/cm3
crust = 2.80 g/cm3
2.70 g/cm3
2.90 g/cm3
mantle = 3.20 g/cm3
Depth (km)
(km)

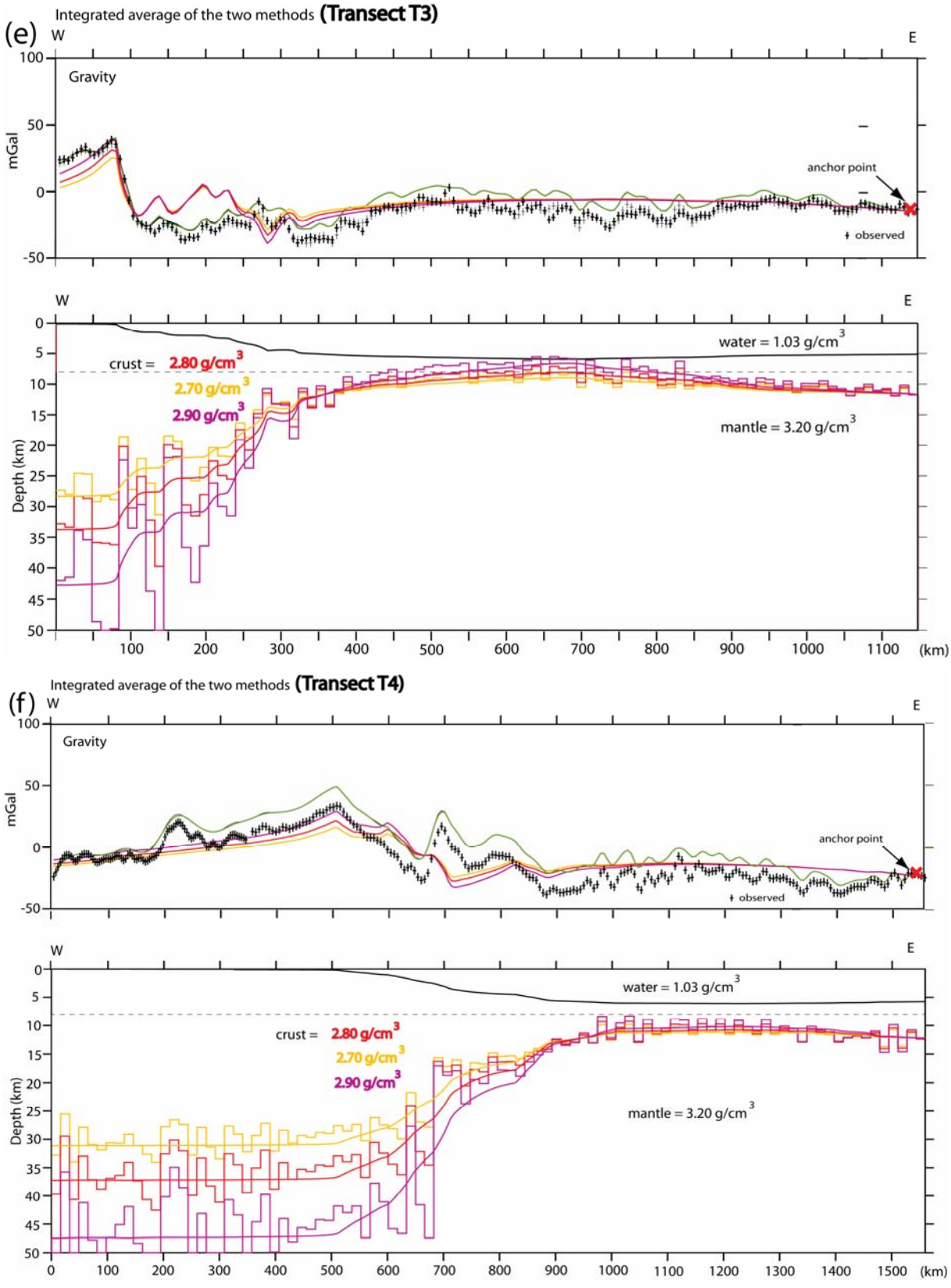

Fig. 4.11. Estimated Moho relief and calculated gravity anomalies utilizing both forward isostatic balancing and inverse modelling along all constructed transects, T0(a)-T4(f) (from north to south).

4.3 Potential-field gradient and continent ocean transition/boundary

Continental passive margins are the result of plate tectonic evolution involving rifting, breakup and continent drift. A variety of margin configurations result from the complexity of the processes involved in their formation, which are still not fully understood, and are object of extensive debate. Seismic reflection and refraction data have proved to be insufficient to characterize in detail the style of rifting at margins, or to confirm the presence or absence of detachment surfaces (Watts et al., 1998), in part, because of reduced penetration due to the presence of volcanic rocks, or to multiple generation within the sedimentary column. Characterization of the continent-ocean boundary /transition (COB/COT) between continental and oceanic crust can be tackled by a different approach, which implies the use of potential field data and modelling. Talwani & Eldholm (1973) related topographic features to gravity and magnetic anomalies to differentiate oceanic and continental domains. A major change in basement elevation at the boundary between oceanic and continental crusts is expected, due to the isostatic response caused by two materials of different density. These changes in basement elevation are associated to steep gradient in the gravity anomaly curves and often define contrasted magnetic anomaly fields at either side.

Rabinowitz & LaBrecque (1979) have defined the COB based on correlated lineaments of magnetic and gravity anomalies bordering the conjugate continental margins of southern South America and southern Africa. On the South American margin, a continuous magnetic anomaly, (magnetic "G" anomaly) was identified and was correlated to the shelf-edge isostatic gravity anomaly, the latter interpreted as a manifestation of thickened, elevated oceanic crust adjacent to the continent (Rabinowitz & LaBrecque, 1979). The G anomaly is very pronounced to the north of the Salado Basin and was modelled as an edge-effect separating oceanic from continental basement, and correlated to its counterpart anomaly on the conjugate margin, north of the Orange River. The magnetic G-anomaly appears to be associated with a prominent gradient in the gravity anomaly field. In contrast, south of the Salado Basin and in its conjugate African margin, the magnetic G-anomaly is associated with a very much attenuated gravity anomaly. Further south, between the Colorado Basin and the Falkland Escarpment, the magnetic anomaly G is poorly defined, yet coincident with an isostatic gravity anomaly.

The Bouguer-corrected gravity anomaly was used to obtain a first approximation of the COB/COT. Bouguer reduction removes the gravity attraction effect over a station caused by topography relative to a reference level. The simplest approach assumes a simplified topography consisting of an infinite slab of thickness equal to the height of the station over the reference level, and a standard, constant density (average crust density) (Milsom, 2003). Thus, the Bouguer effect increases the gravity in areas of positive topography, and a negative correction is needed. Over the sea-surface, the assumption of replacing the water layer by a rock-slab of crustal density increases the values of the residual gravity anomaly, and a positive-negative landward gradient is expected.

However, the very pronounced gradient observed in the Bouguer-corrected gravity anomaly between oceanic and continental areas, mostly reflects the lateral density contrast between lithospheric mantle and crystalline crust, that takes place beneath the continent-ocean transition zone (COT). In this zone, the relatively steeply-dipping Moho relief between oceanic and continental domains is the cause of the pronounced regional Bouguer-corrected gravity gradient, separating two main regional gravity levels (Figs. 3.4 and 4.12).

Sections of the Bouguer anomaly across the continental margin, display this gradient as a rather wide and pronounced slope (Fig. 4.12). The steepest portion of the curve, when clearly identified, can tentatively be attributed to a sudden lateral change of density within the basement, i.e. the COB/COT (Fig. 4.12). This assessment will be supported with additional constraints from the 2D forward crustal-scale gravity modelling.

Fig. 4.12 (opposite page). Bouguer-corrected gravity anomaly, free-air gravity anomaly (Sandwell & Smith, 1997 and KMS99 grids), and magnetic anomaly along all constructed transects T0(a)-T4(f) (from north to south). The inferred continent-ocean boundary (COB)/transition (COT) is indicated along each transect.

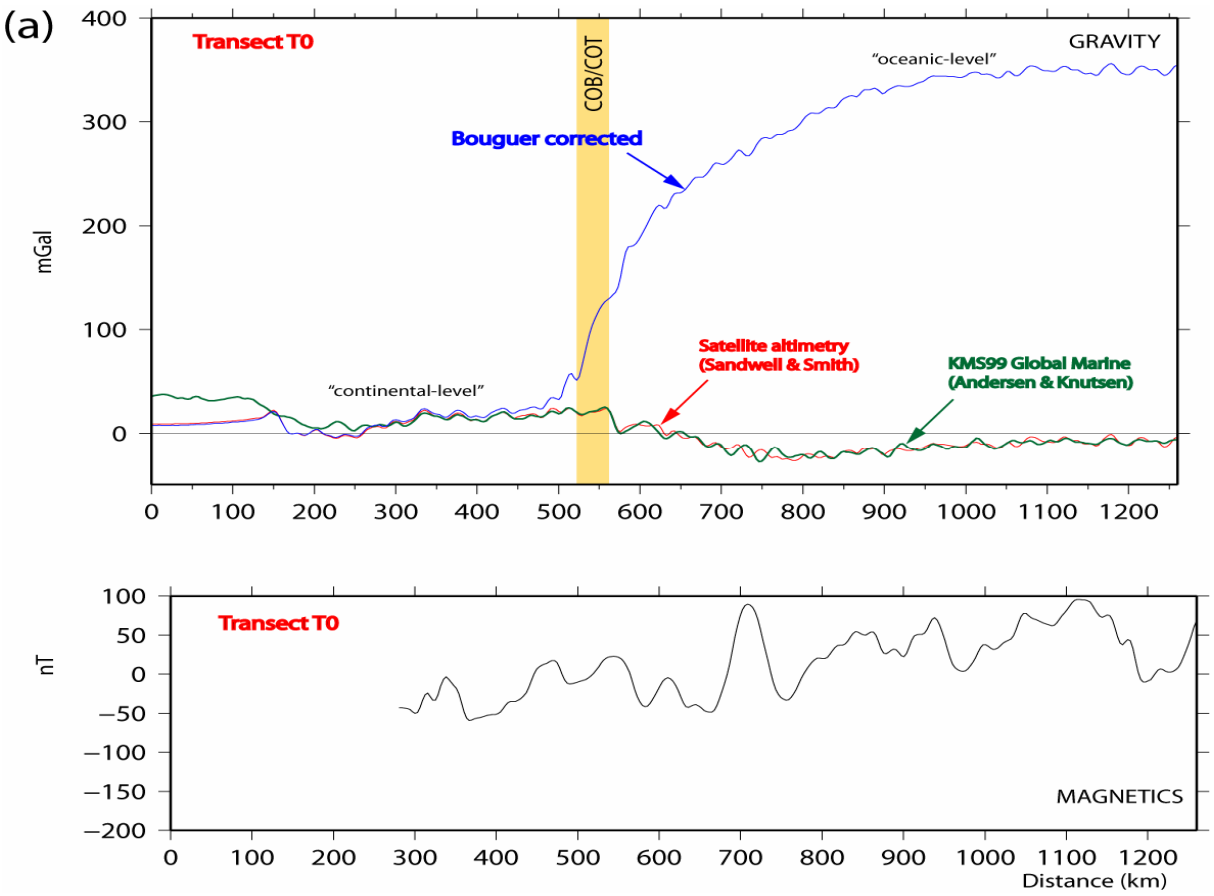
(a)
Transect T0
GRAVITY
"oceanic-level"
COB/COT
Bouguer corrected
Satellite altimetry
(Sandwell & Smith)
KMS99 Global Marine
(Andersen & Knutsen)
"continental-level"
mGal
400
300
200
100
0
0 100 200 300 400 500 600 700 800 900 1000 1100 1200
Transect T0
MAGNETICS
nT
100
50
0
−50
−100
−150
−200
0 100 200 300 400 500 600 700 800 900 1000 1100 1200
Distance (km)

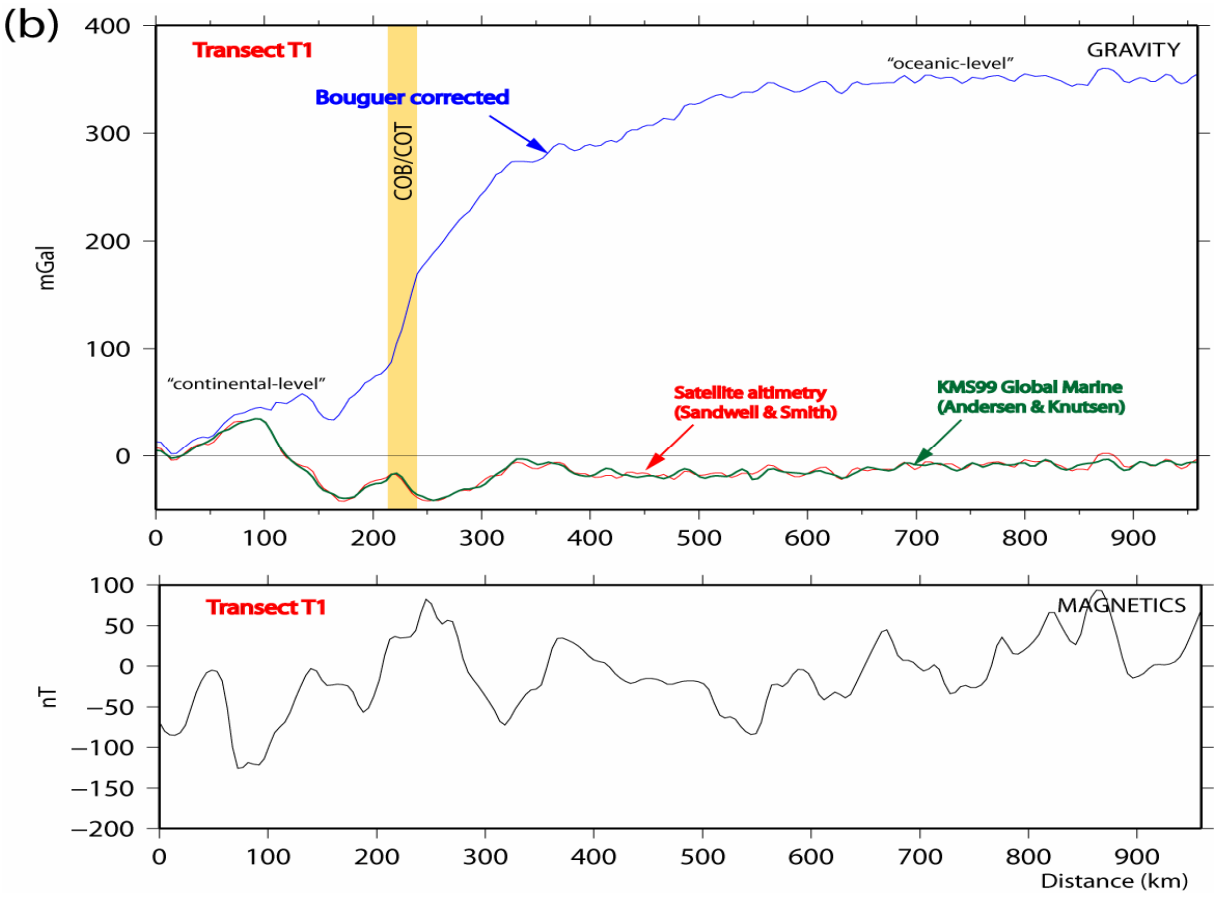
(b)
Transect T1
GRAVITY
"oceanic-level"
Bouguer corrected
COB/COT
"continental-level"
Satellite altimetry
(Sandwell & Smith)
KMS99 Global Marine
(Andersen & Knutsen)
mGal
400
300
200
100
0
0 100 200 300 400 500 600 700 800 900
Transect T1
MAGNETICS
nT
100
50
0
−50
−100
−150
−200
0 100 200 300 400 500 600 700 800 900
Distance (km)

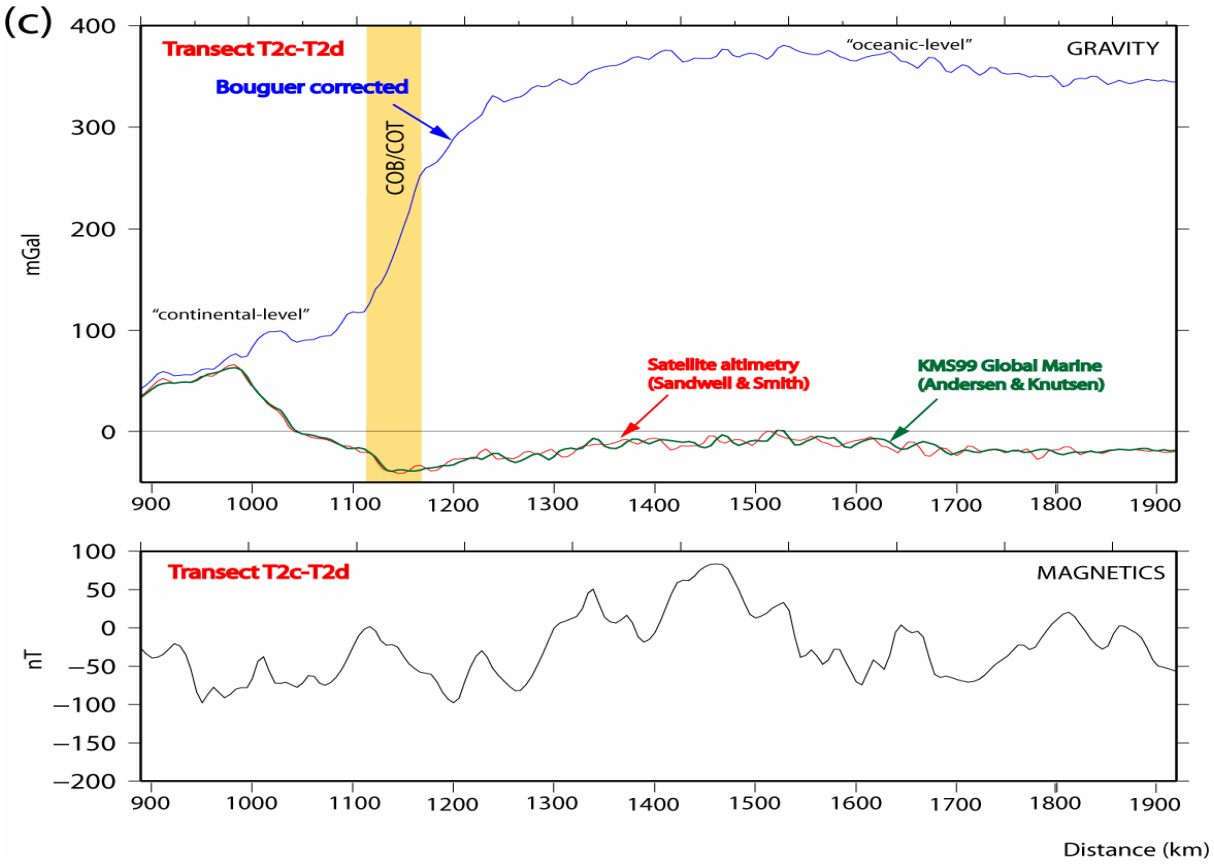
(c)
Transect T2c-T2d
Bouguer corrected
COB/COT
"oceanic-level"
GRAVITY
mGal
"continental-level"
Satellite altimetry
(Sandwell & Smith)
KMS99 Global Marine
(Andersen & Knutsen)
Transect T2c-T2d
MAGNETICS
nT
Distance (km)

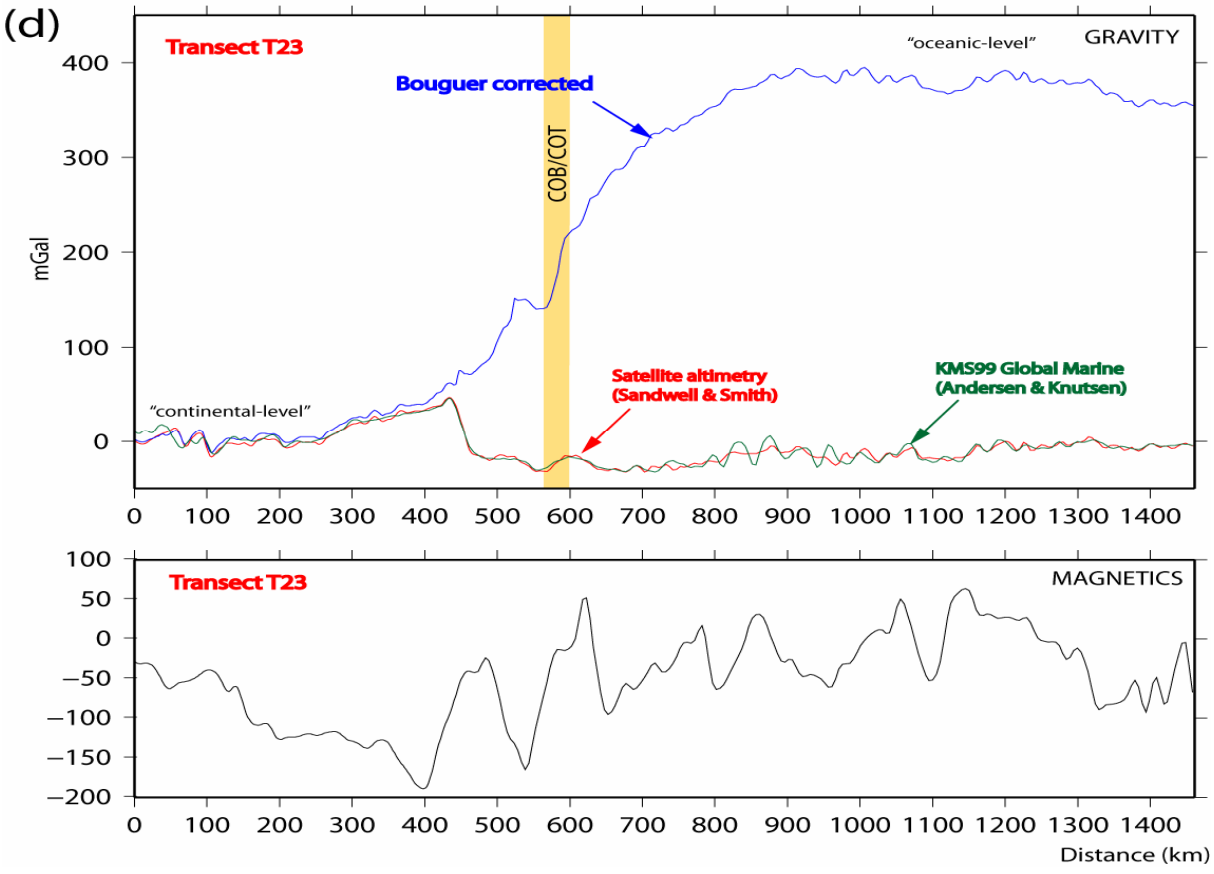
(d)
Transect T23
Bouguer corrected
COB/COT
"oceanic-level"
GRAVITY
mGal
"continental-level"
Satellite altimetry
(Sandwell & Smith)
KMS99 Global Marine
(Andersen & Knutsen)
Transect T23
MAGNETICS
Distance (km)

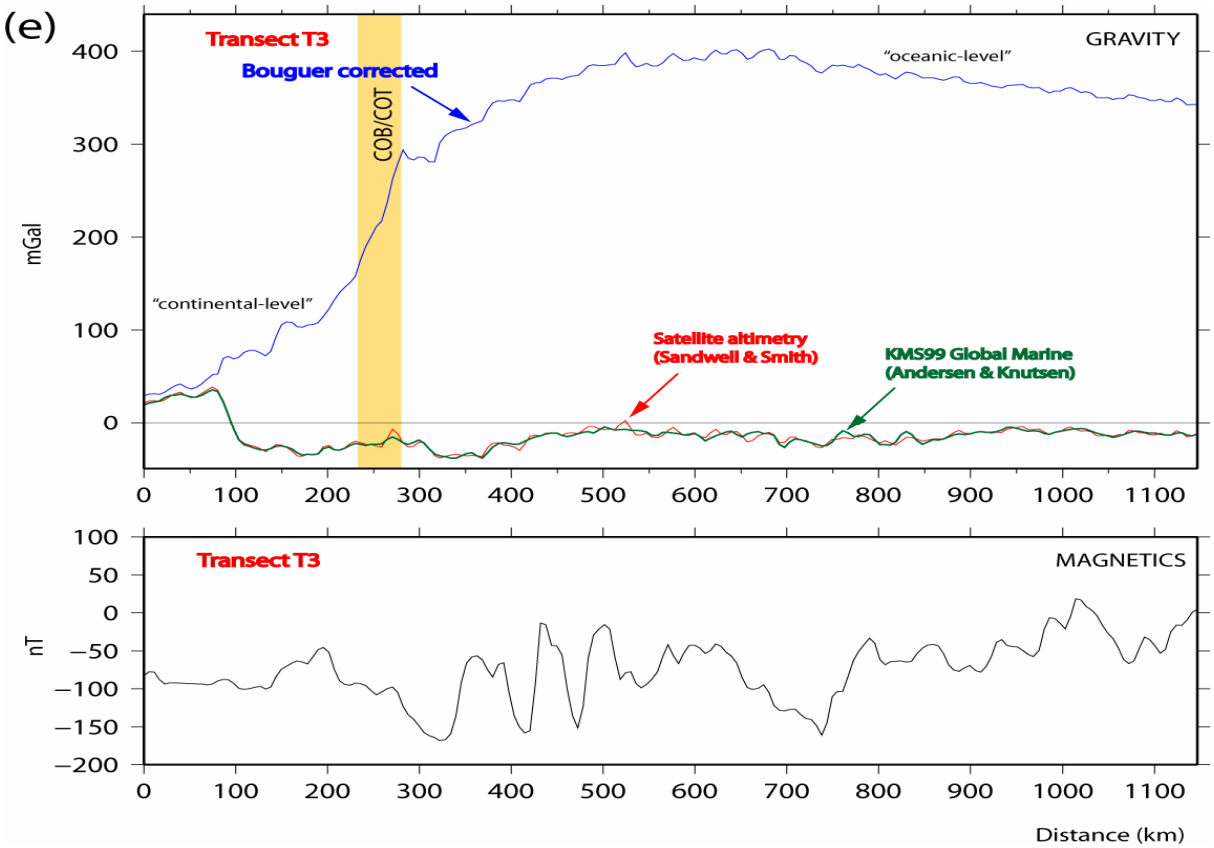
(e)
Transect T3
Bouguer corrected
COB/COT
GRAVITY
"oceanic-level"
"continental-level"
Satellite altimetry
(Sandwell & Smith)
KMS99 Global Marine
(Andersen & Knutsen)
mGal
Transect T3
MAGNETICS
nT
Distance (km)

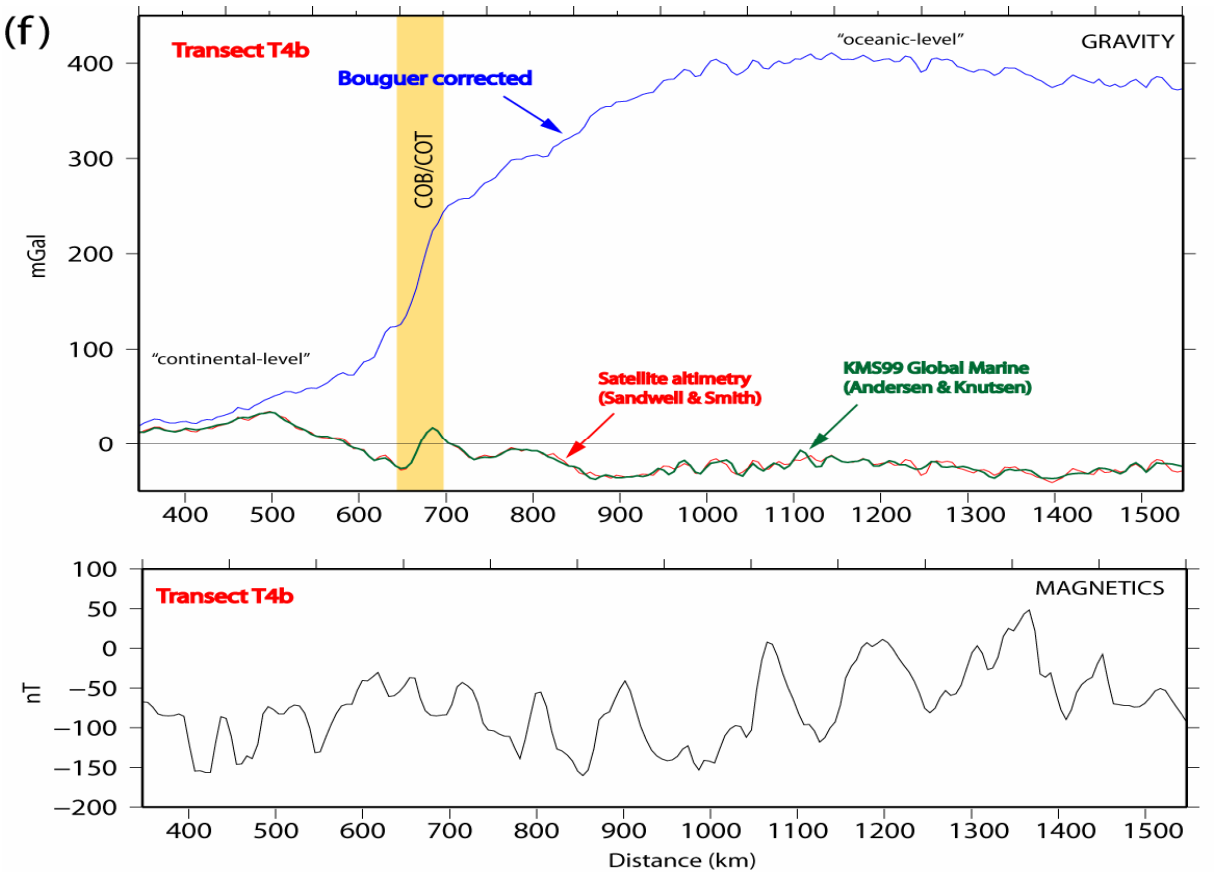
(f)
Transect T4b
Bouguer corrected
COB/COT
GRAVITY
"oceanic-level"
"continental-level"
Satellite altimetry
(Sandwell & Smith)
KMS99 Global Marine
(Andersen & Knutsen)
mGal
Transect T4b
MAGNETICS
nT
Distance (km)

Chapter 5
Gravity modelling

The purpose of gravity modelling is to provide additional and robust constraints to the seismic interpretation, as the latter may have poor resolution at deep crustal levels. Gravity modelling has been implemented to all the constructed composite transects. A two-dimensional, forward gravity modelling approach was applied in this study, using GMSYS v.4.7 software (NGA Northwest Geophysical Associates, www.nga.com). GMSYS is an interactive gravity and magnetic modelling software that enables generation of geological models that are verifiable by comparing their gravity and/or magnetic responses with the observed measured values along a particular section. The MCS profiles and the estimated Moho relief calculated with TAMP constitute the initial constraints to the modelling sections. Further geological input, such as grid-extracted bathymetry and sediment thickness is added to the seaward extension parts of the constructed transects. In GMSYS modelling, the constructed transects are divided into polygons characterized by a representative density value. To avoid edge-effects in the gravity response, the polygons which extend beyond the modelling area are extrapolated to a distance of 30,000 km. Density values have been inferred from seismic velocity-density conversion tables that utilize the empirical relationship of Nafe & Drake (1957). In addition, velocity-density relationships used on similar rifted continental margin settings were taken into consideration (e.g. NE Atlantic margins: Mjelde et al., 2002; Tsikalas et al., 2005).

The GMSYS workflow consists of iteratively improving the model, i.e. altering the geometry and/or the density of the polygons, until the residual gravity response (the difference between the calculated and the observed values) is reduced to acceptable values (generally below 10 mGal of mean residual error). In addition, the long-wavelength variations of the gravity field during gravity modelling of the constructed transects are attributed to lower crust features and to the Moho relief, while the short-wavelength anomalies are related to upper crust origins, and mostly to the basement relief. Initially, very simplified models for all constructed transects were gradually improved by adding new crustal elements and/or modifying pre-existing ones. An important remark about gravity modelling is its non-uniqueness, meaning that different geological models and solutions can satisfactorily fit the observed gravity anomalies. A main aim in the modelling process is, therefore, to generate solutions that are geologically realistic, in accordance with the available constraints, and to reduce the

uncertainty to a minimum. The observed gravity anomalies along each transect have been extracted from the 2x2´ KMS99 global marine free-air gravity anomaly grid (Andersen & Knutsen, 1998). As mentioned earlier, this grid is equivalent with the Sandwell & Smith (1997, v. 15.1) grid and was chosen because of the higher signal to noise ratio, resulting in the smoothing of the unwanted high-frequency oscillations.

A series of common steps were followed during gravity modelling of the constructed transects. In particular, the initial models were constructed based on a very simplified crustal structure, constrained by the main seismic reflection features and the Moho relief derived from the TAMP-models. Average estimated density values were assigned to the different blocks: water (1.03 g/cm³); post-rift sediments (2.30 g/cm³); continental basement (2.70-2.90 g/cm³); oceanic crust (2.80-2.90 g/cm³); upper mantle (3.20 g/cm³). The Moho relief along each transect calculated with TAMP for a homogeneous crustal density of 2.80 g/cm³ was used as input to the initial gravity model. This geometry had to be smoothed under the regions of high bathymetric relief, i.e. the outer shelf and slope, since the Moho geometry modelled with TAMP was highly dependant on the bathymetry. Below oceanic crust, Moho depth was fixed at a point of known oceanic crust, to an average depth of 6.5 km below the sedimentary layer, approximating the estimated oceanic crust global average thickness (White et al., 1992). The crystalline crust was divided into two polygons, continental and oceanic crust, separated by the continent-ocean boundary COB. This boundary was placed at the position of the maximum negative-positive gradient in the Bouguer anomaly (Fig. 4.12).

The mean residual error value exhibited by the models in this preliminary stage ranged between 25-50 mGal. In general, all the initial models constructed in this study reflect roughly the regional gravity anomaly trend, with the best match on the zones of pure oceanic crust, and the most remarkable discrepancies over the outer continental shelf, slope and rise zones. Modifications have been systematically applied to all transects, following a common pattern of routines in order to achieve coherent results between the models. Corrections have then been applied, in order to adjust the discrepancies in a hierarchical way, fitting the long-wavelength, lower crust and Moho-relief related anomalies and continuing with the smaller, short-wavelength anomalies related to basement-relief geometry, until a mean residual error of less than 10 mGal was achieved. Anchor points have been placed over positions of known oceanic crust. The modelled gravity anomaly over oceanic domains was matched to the observed gravity curve at an early stage of the modelling process, due to the relative

uniformity in its gravity response. Only high frequency gravity oscillations caused by oceanic basement relief had to be accounted for.

The followed systematic steps of gravity model improvement showed a higher degree of complexity, and in some cases, uncertainties within the continental crust. Nevertheless, gravity modelling is a robust method that has validated alternative crustal-scale models, and has tested interpretation uncertainties present due to resolution limitations of seismic reflection/refraction profiling. Based on reliable regional-scale understanding, gravity modelling has been further utilized to extrapolate geological information existing along seismic profiles, to areas uncovered by seismic data. In order to help visualize and understand the approach utilized in GMSYS modelling, the initial and final models of all six transects are presented (Fig.5.1-5.6). The modelling results consist of a plot of the 2D crustal-scale forward gravity modelling, together with the "calculated" and "observed" gravity anomaly curves along the transects. The representative density values (in g/cm^3) of the individual crustal blocks and the upper mantle are indicated. The 2D approach implemented in the gravity modelling process is subjected to a certain degree of uncertainty when ignoring the 3D distribution of the gravity sources. The gravity effect of an anomalous intracrustal mass of relatively high density may extend beyond its two-dimensional transect model. Hence, sections close to the edge of such high-density bodies may reveal an unrealistic subsurface relief. This can explain the difficulties found in fully eliminating local gravity discrepancies between the observed and calculated anomalies. An example of this effect was found in transect T23, where there is a local residual anomaly at a distance of 300 km (Fig. 5.4b). At that position, the transect T23 intersects the southern edge of a relative gravity high, situated landward of the G anomaly (Fig. 3.3).

5.1. Transects T0

The gravity anomalies observed along this transect reflect very clearly a regional gradient, exhibiting stepwise dip from the continental to ocean domains. In particular, three base-levels can be defined, corresponding respectively to the emerged areas, the continental shelf and the oceanic basin (Fig. 5.1). The initial model, anchored to oceanic crust, showed important discrepancies between calculated and observed gravity anomalies over the continental shelf and slope areas. The residual error was reduced considerably after applying corrections based

on the available constraints, like: (a) repositioning of the continent-ocean boundary (COB), based on Bouguer-corrected anomaly gradients, as earlier mentioned; and (b) introduction of a layered post-rift sedimentary cover, with assigned density values based on the velocity-model utilized to depth convert the sections. The representative density of the new created polygons exhibit decreasing density values for both shallower and more distal sediments (Fig. 5.1). Nevertheless, additional steps had to be incorporated to come with a better fit, including: (a) introduction of a lower crustal body (LCB) with high density (3.00 g/cm³) at the continent-ocean transition zone; and (b) the stepwise transition of the observed gravity between continental and oceanic domains has been successively fitted by extensional faulting of the margin basement, not adequately resolved in the seismic interpretation.

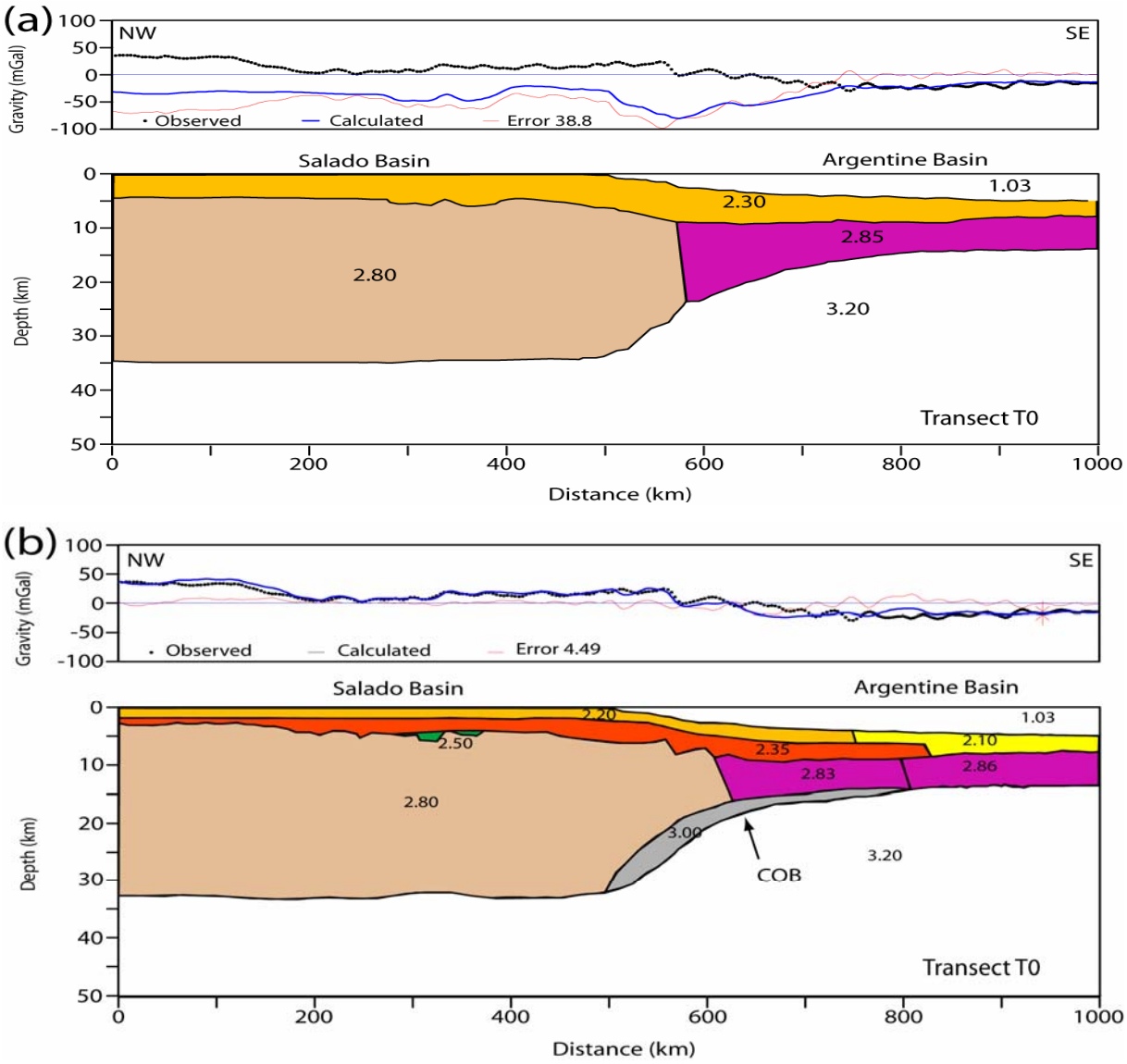

Fig. 5.1. Initial **(a)** and final **(b)** crustal-scale 2D forward gravity modelling for transect T0. Transect location in Fig. 3.1.

5.2 Transect T1

The BGR seismic reflection profiles (modified from Hinz et al., 1999) provide more robust constraints to the modelling, compared to the line-drawings from the other transects that are based on more schematic line-drawings (Urién & Zambrano, 1996). In particular, Transect T1 images a well defined Moho candidate reflector beneath the continental crust, which is in agreement with the Moho-relief estimates calculated in TAMP with a crustal density of 2.80 g/cm³. In this seismic profile, SDRs and pre-rift sedimentary basins within the basement are also well imaged. The general trend of the observed gravity anomaly exhibits a regional seaward gradient, interrupted by a wide negative anomaly centered over the shelf edge, with a secondary high in its central part. The major discrepancy along the transect, expressed as a conspicuous mass deficiency of the calculated gravity at the position of the continental shelf gravity high (Fig. 5.2a), was corrected by shallowing the Moho beneath the interpreted pre-rift sediments (Fig. 5.2b). The remaining regional discrepancy was satisfactorily corrected by introducing a high-density (3.00 g/cm³) lower crustal body (LCB) at the position of the continent-ocean transition (Fig. 5.2b). Magmatic underplating is thus spatially associated with the wedge of seaward-dipping reflectors (SDRs) present above the LCB (Fig. 5.2b). Shorter-wavelength discrepancies over the continental shelf were compensated by lowering the density at the uppermost basement levels, within the value-range of crystalline crust. Such solution could be interpreted by the assumption that the upper basement consists mostly of Paleozoic highly compacted sedimentary rocks displaying an array of ancient highs and depocentres that explain the lateral density variations within it. The final crustal geometry reveals a spatial coincidence between the local shallowing of Moho and the position of the inferred Paleozoic pre-rift depocentres (2.67 g/cm³, in Fig. 5.2b). This location appears to be coincident with the major depocentre axis of the Salado Basin, possibly indicating a pure-shear mode of deformation (stretching mechanism) in this part of the margin.

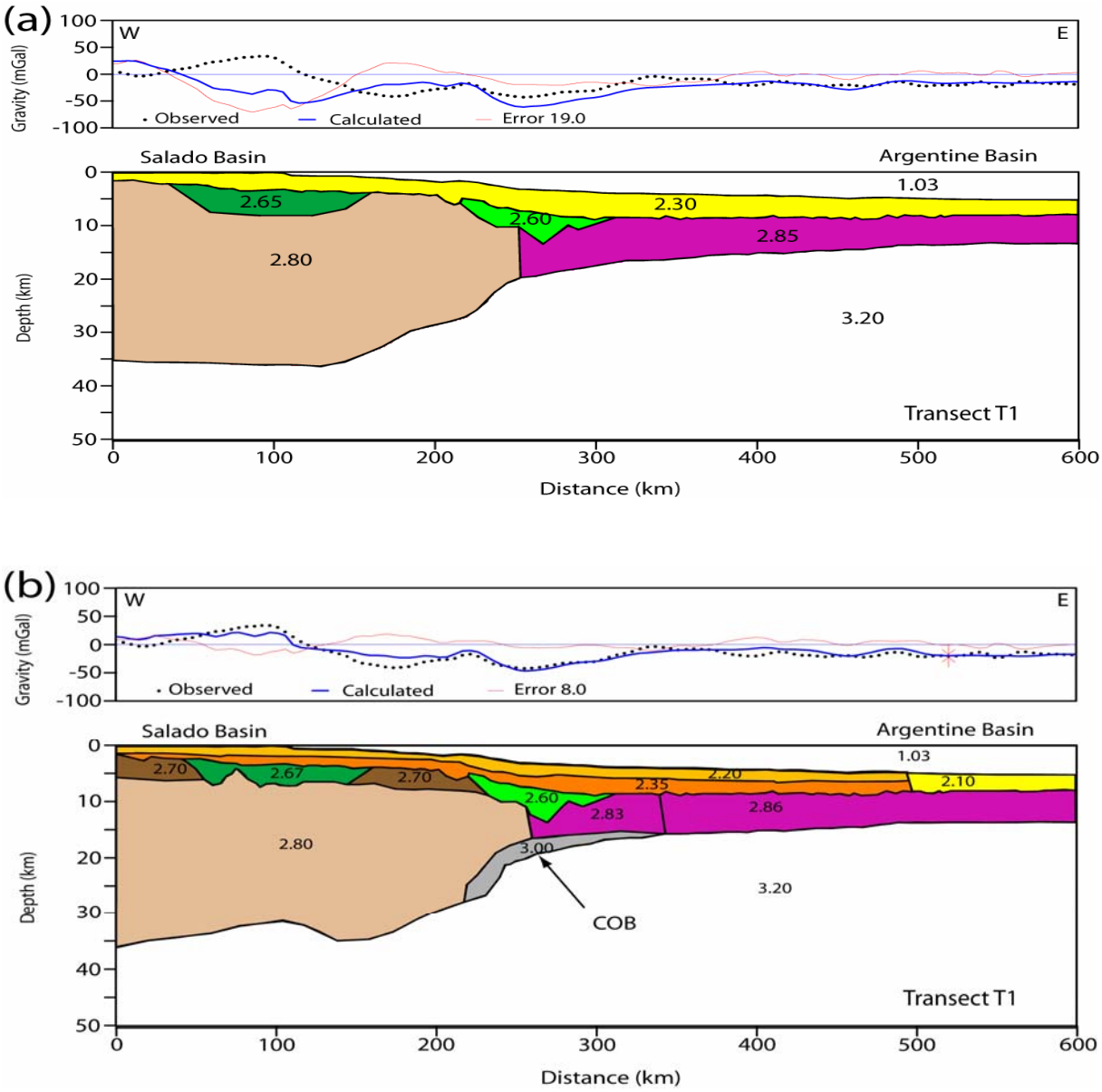

Fig. 5.2. Initial **(a)** and final **(b)** crustal-scale 2D forward gravity modelling for transect T1. Transect location in Fig. 3.1.

5.3 Transect T2

This long, composite transect has an onshore extension reaching the Neuquén Basin (Fig. 3.1) and is constrained by a Bouguer-anomaly profile (Kostadinoff et al., 2005). Although there is a gap of 200 km in the gravity profile, between the onshore and offshore portions of the transect, a regional gradient from the shelf edge towards the mainland can be recognized. The Moho relief has been constrained by the crustal model of Franke et al. (2006), which extends to the east of the 500 km distance (Fig. 5.3). West of that position, well into the mainland, Moho was best fitted as displaying a very gentle dip landwards, towards a region of thick

continental crust. A more complex crustal structure is needed to match the prominent discrepancies between observed and modelled gravity over the outer shelf and continental slope areas (Fig. 5.3). This includes the presence of a SDRs wedge interpreted from seismic reflection profiles, and a differentiated crust showing a locally layered density distribution: a lower crust with elevated density (2.87 g/cm³) and a low-density (~2.70 g/cm³) shallow basement, similar to that of transect T1.

The latter could be consistent with the widespread presence of Paleozoic pre-rift sedimentary strata, showing slightly lower density values than purely igneous or metamorphic basement. The relatively poorly constrained western part of the modelled section was matched by introducing a faulted basement relief, reflecting the extensional geometry of the eastern part of the Neuquén Basin (Fig. 3.1). The regional gravity level in this area was fitted by introducing a landward density gradient for the total crustal thickness, as well as by lowering the density to the uppermost basement, which, in this region constitutes a relatively prominent basement high, separating the Colorado and Neuquén basins (Fig. 5.3b).

The modelled deep crustal geometry shows a rapid thinning of the continental crust, resulting in a narrow transitional zone between continental and oceanic domains. Furthermore, a local shallowing of Moho at ~800 km distance, coincides with the position of the major depocentre of the Colorado Basin.

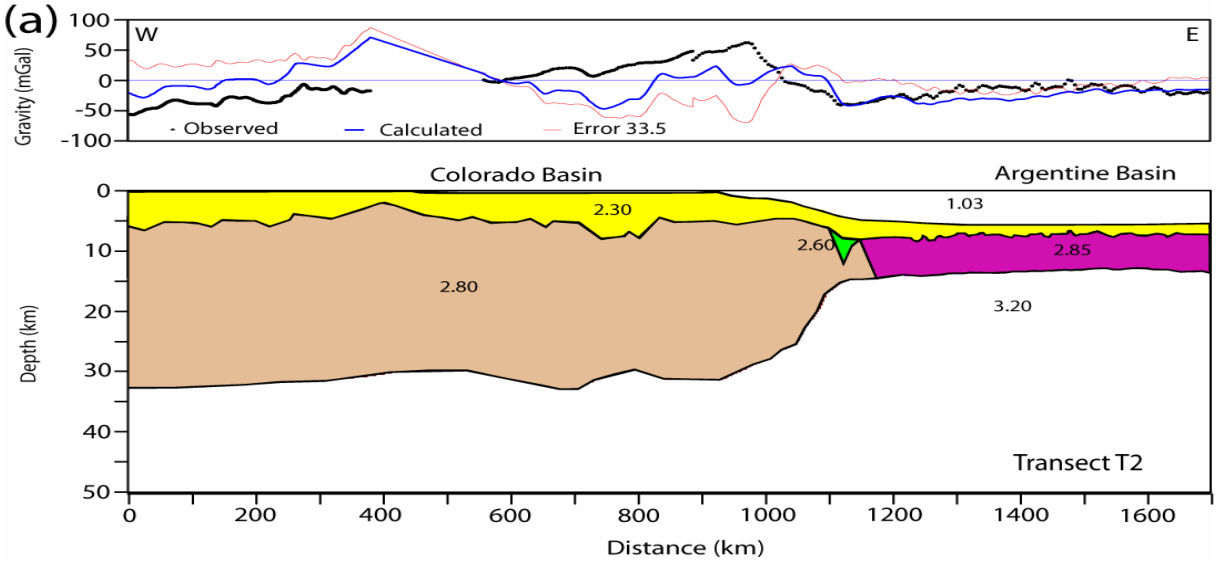

Fig. 5.3 (continues next page)

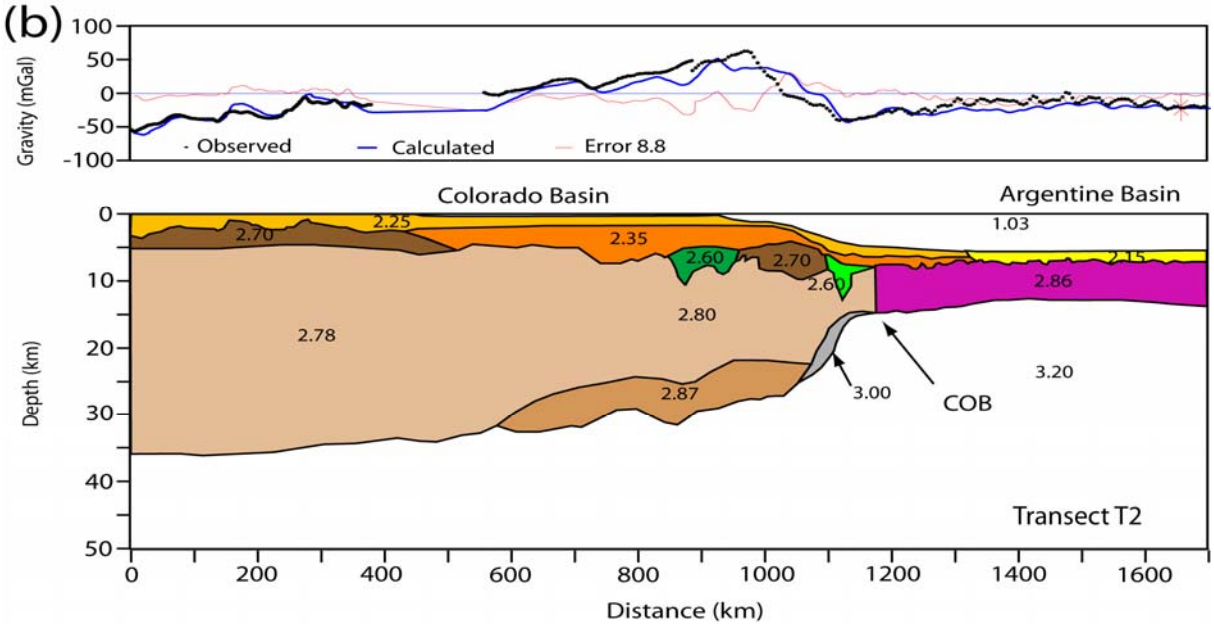

Fig. 5.3. Initial **(a)** and final **(b)** crustal-scale 2D forward gravity modelling for transect T2. Transect location in Fig. 3.1.

5.4 Transect T23

This transect extends perpendicularly to the main extensional structures related to the Mesozoic-Cenozoic rifting phase, which are oriented parallel to the margin in this area. This is shown as a short-wavelength anomaly in the observed gravity field over the shelf, presumably reflecting the faulted relief of the Valdés and Rawson basins (Fig. 5.4). The observed high-frequency component/variation of the observed gravity field suggests a more complex, undulating basement relief compared to that of the reflection seismic profile T23a used as the background constraint in this transect. The depocentres of the main basins over the continental shelf required higher density values to locally correct the gravity anomaly (Fig. 5.4 b). A rather prominent faulted relief at the top of the basement under the continental slope was introduced, in response to the relative gravity high above it. Since this faulted geometry is attributed to take place within continental crust, the COB, initially placed at the distance of 600 km in the transect (based on Bouguer-corrected gravity gradient), was shifted by 100 km eastward, resulting in a more consistent model (Fig. 5.4b).

At a more regional scale, the Moho relief at this transect shows a gradual transition between continental and oceanic crust (Fig. 5.4b), compared to the previous transects, indicating a

different regime of crustal extension. Moreover, the overall flat Moho relief under the continental crust, at a depth of 35 km, is consistent with estimates made with TAMP for a mean crustal density of 2.80 g/cm³, and produces a good fit of the regional gravity level over the continental crust. On the oceanic crust, however, the short-wavelength and high-amplitude oscillations of the observed gravity field are remarkable. These were matched with a rather exaggerated relief of the top oceanic basement surface.

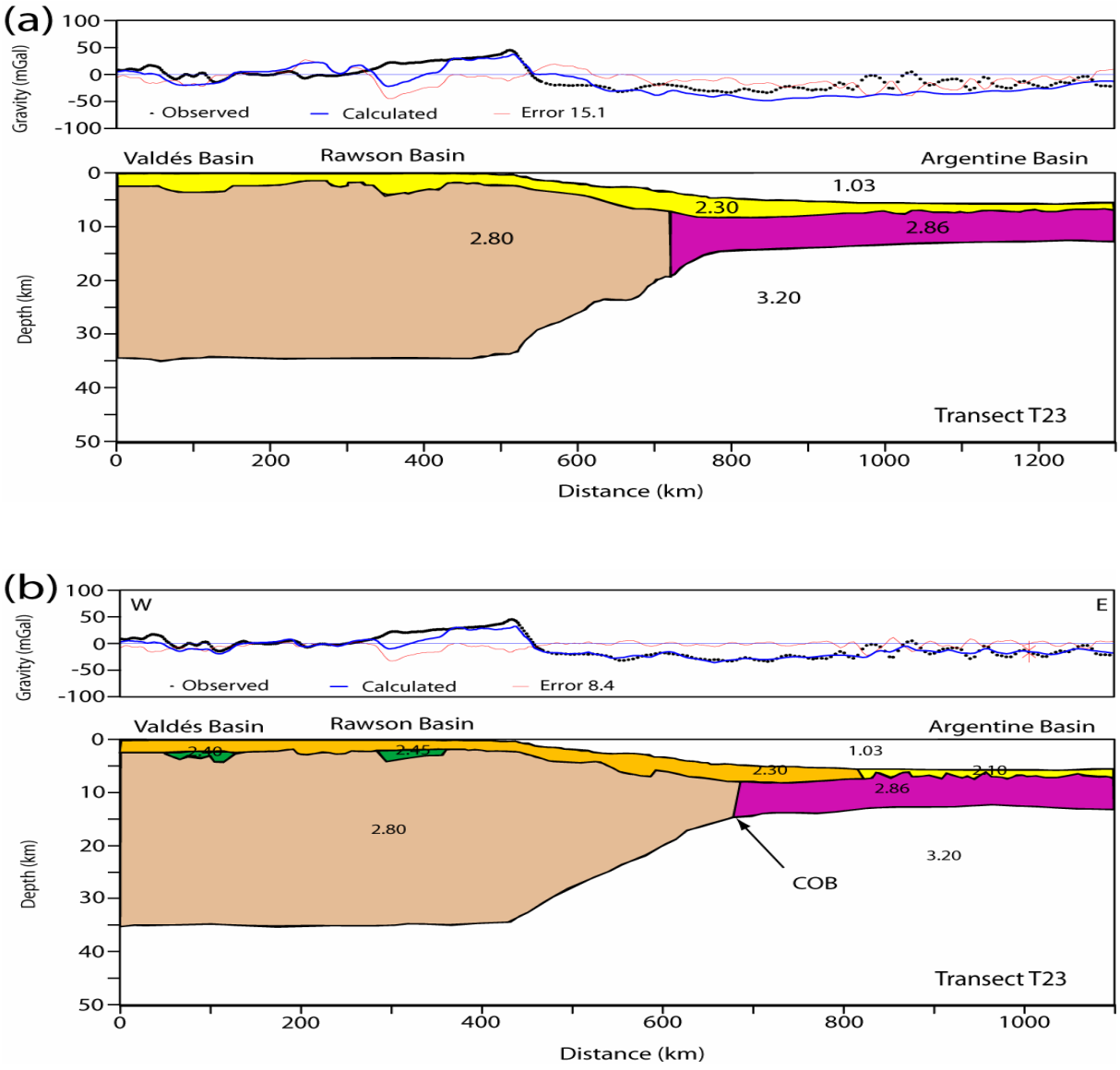

Fig. 5.4. Initial **(a)** and final **(b)** crustal-scale 2D forward gravity modelling for transect T23. Transect location in Fig. 3.1.

5.5 Transect T3

This model exhibits a comparatively simple gravity profile, consisting of a single prominent gravity high coincident with the continental shelf edge, and a rather constant base level over the oceanic domain (Fig. 5.5). Between the two, there is a broad, very attenuated and relatively low-amplitude gravity anomaly with a central elevation region (Fig. 5.5). The modelled Moho level under the continental crust, at about 33 km of depth, passes into the shallow oceanic level through a gentle slope (Fig. 5.5b). Similarly to transects T0 and T1, the density values of the upper basement under the upper slope were lowered, consistent with the position of the regional outer basement ridge mentioned above. The observed gravity over oceanic crust is relatively smooth, with few short-wavelength oscillations. A transitional crust zone between continental and oceanic domains, as well as a high-density lower crustal body (LCB) beneath the position of the seaward-dipping reflectors wedge were introduced in the modelling with satisfactory results (Fig. 5.5). Furthermore, several pre-rift sedimentary basins on the western part of the transect was inferred based on the seismic reflection interpretation. The presence of an upper basement layer displaying relatively lower density values (~2.70 g/cm³) suggest a more widespread presence of highly-compacted pre-rift sedimentary strata, as mentioned above (Fig. 5.5). The steeply-dipping reflections seen around the Moho level on the oceanic lithosphere (Fig. 4.6) does not seem to be relevant for gravity modelling.

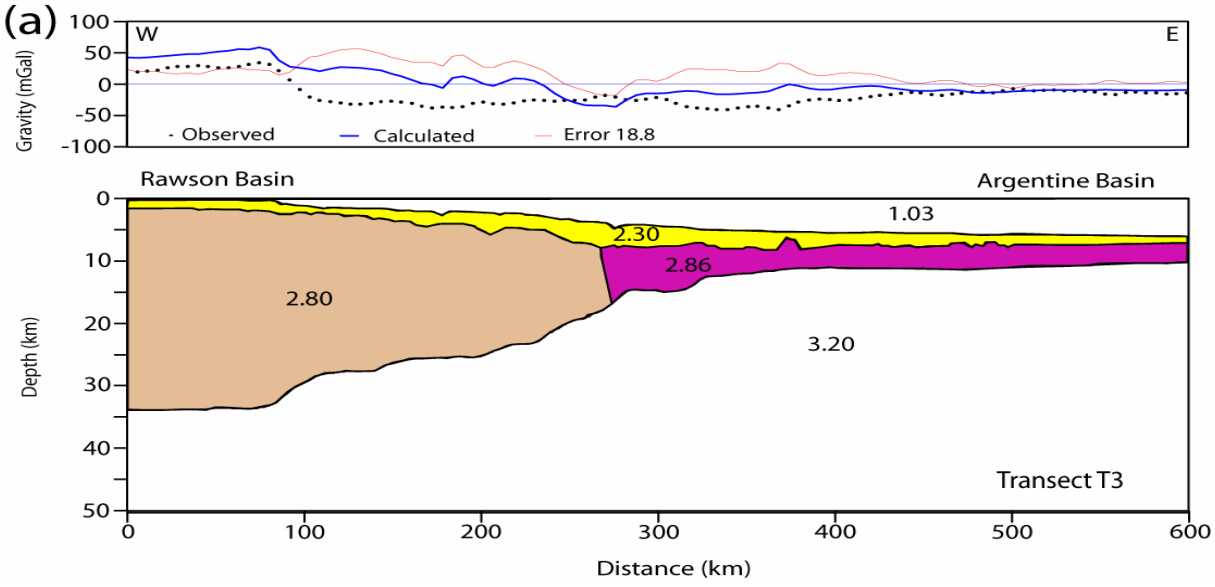

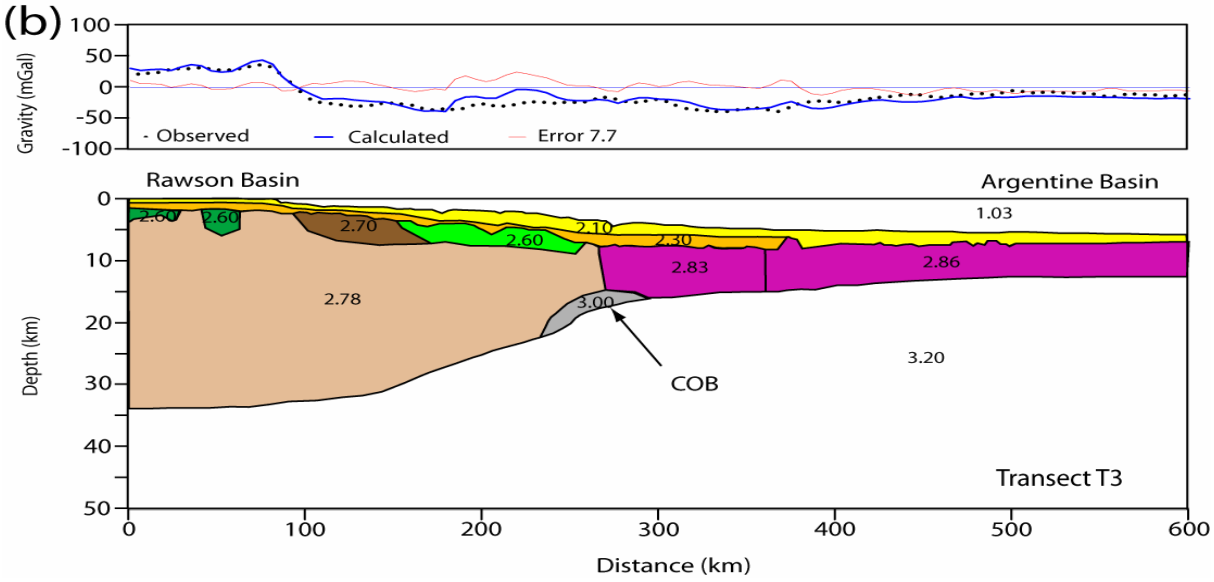

Fig. 5.5. Initial **(a)** and final **(b)** crustal-scale 2D forward gravity modelling for transect T3. Transect location in Fig. 3.1.

5.6 Transect T4

The observed gravity anomaly/field along this transect shows a regional symmetry, displaying landward and seaward gradients extending from a gravity maximum over the shelf edge. The landward gravity gradient is configured in a stepwise manner, suggesting extensional faulting within the crystalline basement. To the west, the transect extends over the San Jorge basin, where normal faulting has been documented (Baldi & Nevistic, 1996), constraining well the model in that part. The density of the eastern edge of the outer rise, seaward of the Eastern Deseado High (Fig. 5.6b) at a distance of 600-700 km, was lowered to 2.68 g/cm^3, corresponding with presumed pre-rift sedimentary strata within the basement. A prominent local gravity high at a distance of 720 km, over the COB position, could not be matched by faulted basement relief (Fig. 5.6b). Alternatively, a high-density body of extrusives was proposed, although not resolved in the BGR seismic reflection profile (Hinz et al., 1999). This volcanic rock unit could be associated with a somewhat leaky character of the neighbouring Falkland/Malvinas Fracture Zone (Fig. 1.1), south of the transect, resulting in preferential magma conduits (Fig. 3.1, 2.6). A thickened, transitional crust block of considerable dimensions have been proposed, in the zone that contains strong intra-basement reflectors of

unknown origin (Fig. 4.7). Such crustal configuration correlates with a steep Moho separating the two main crustal domains (Fig. 5.6b).

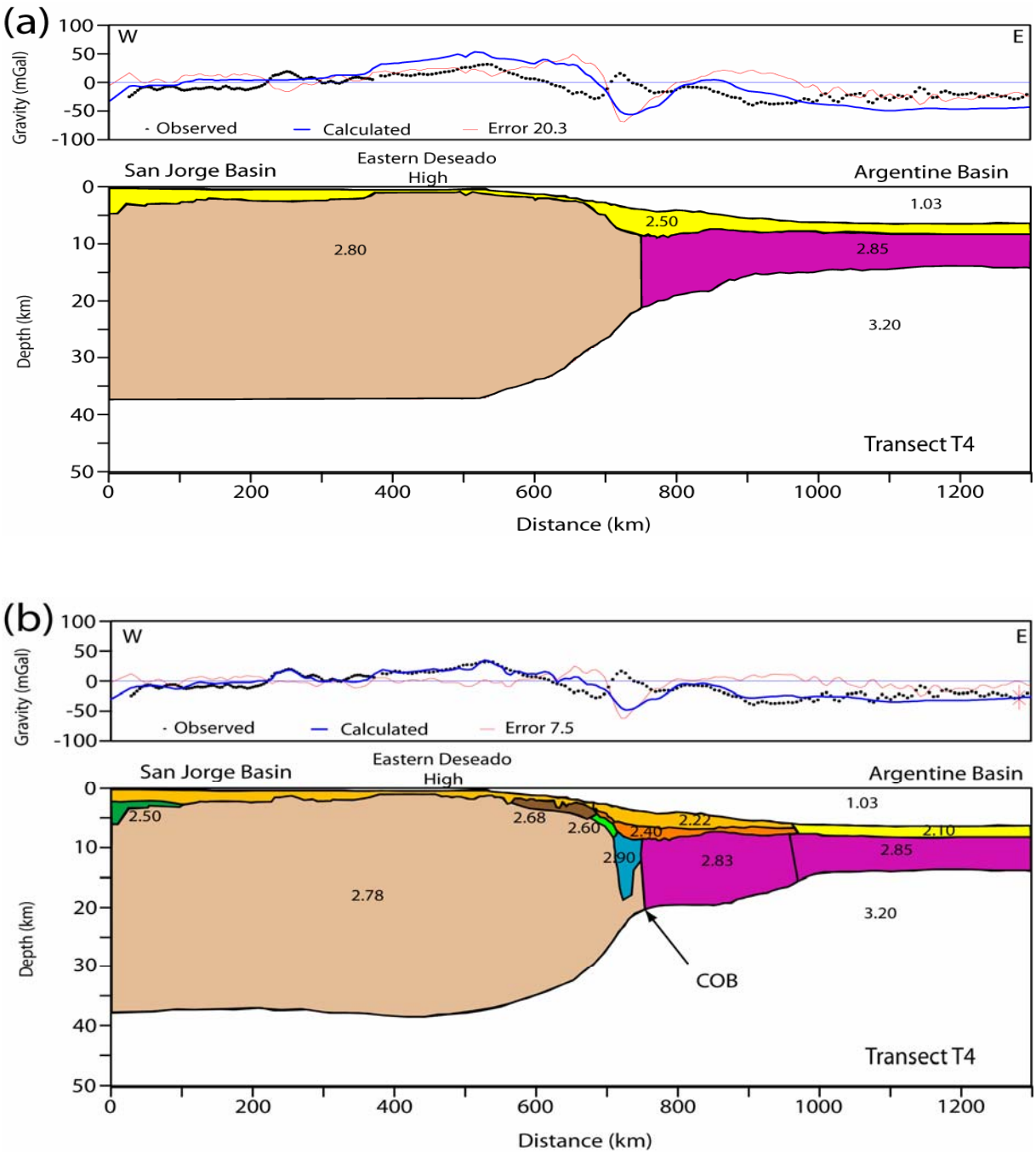

Fig. 5.6. Initial **(a)** and final **(b)** crustal-scale 2D forward gravity modelling for transect T4. Transect location in Fig. 3.1.

Chapter 6
Discussion

Understanding the complexity and variety of mechanisms involved in crustal/lithospheric extension that leads to the formation of passive margins is best achieved through a multidisciplinary approach. The integrated method used in this study, including reflection/refraction seismic profiles, potential field data and modelling has been satisfactorily used to elucidate the crustal structure beneath the Argentine margin. The constructed geological models were evaluated and compared both in along-margin and conjugate margin settings, to verify or add new insights on the crustal architecture and margin development. A particular focus in this study was made in constraining the margin geometry, by inferring the position of the continent-ocean boundary (COB) along the margin.

6.1 Onshore-offshore correlations

Inherited Paleozoic and Precambrian structural grains and lithological anisotropy exerted a strong control on the pattern of breakup of Gondwana supercontinent and, subsequently, on the development of the South Atlantic passive margins (Keeley et al., 1993; Ramos, 1996; Hinz et al., 1999; Macdonald et al., 2003). Suture zones associated with accretion of terranes into Gondwana during Paleozoic times were inherited in several orientations in the Mesozoic and Cenozoic structures and were related to weakness zones that controlled the extensional faults of the early rift phase related to the breakup of Gondwana.

Based on the subdivision of the Sub-Andean region along South America into tectonostratigraphic domains, Jacques (2003) proposed the presence of large-scale transverse zones of structural accommodation across the continent. These zones of weakness resulted from basement anisotropy and occur, in the study area, as a set of lineaments trending NW-SE. This direction coincides with that of the elongated fold belts that resulted from the multiple terrane accretion in SW Gondwana during the Precambrian and Phanerozoic orogenies (Ramos, 1996). The most prominent of these lineaments on the Argentine margin are, from north to south: the

Martín García Tectonic Lineament (southern limit of the Pelotas terrane); the Valle Fértil Tectonic Lineament; the San Rafael Tectonic Lineament; the Gastré-Agulhas Megashear; the South Malvinas Tectonic Lineament; and the North Scotia Ridge Lineament (Fig. 6.1). These zones of weakness played an important role in continental breakup from the earliest stage of rifting (from 180 to 130 Ma in southern South America) and have been correlated with failed arms of triple-junction rifts (Jacques, 2003). Lithospheric plate movements were accommodated by combined intracratonic extension and strike-slip movement, as suggested by Nürnberg & Müller (1991). Subsequently, several major crustal megashears or diffuse zones of intraplate deformation were originated, and some of them can be recognized in the southern South America (Jacques, 2003). The most conspicuous of these deformation zones within the Argentinian margin are represented by the Salado and Colorado basins and the Gastré-Agulhas Megashear (Fig. 6.1).

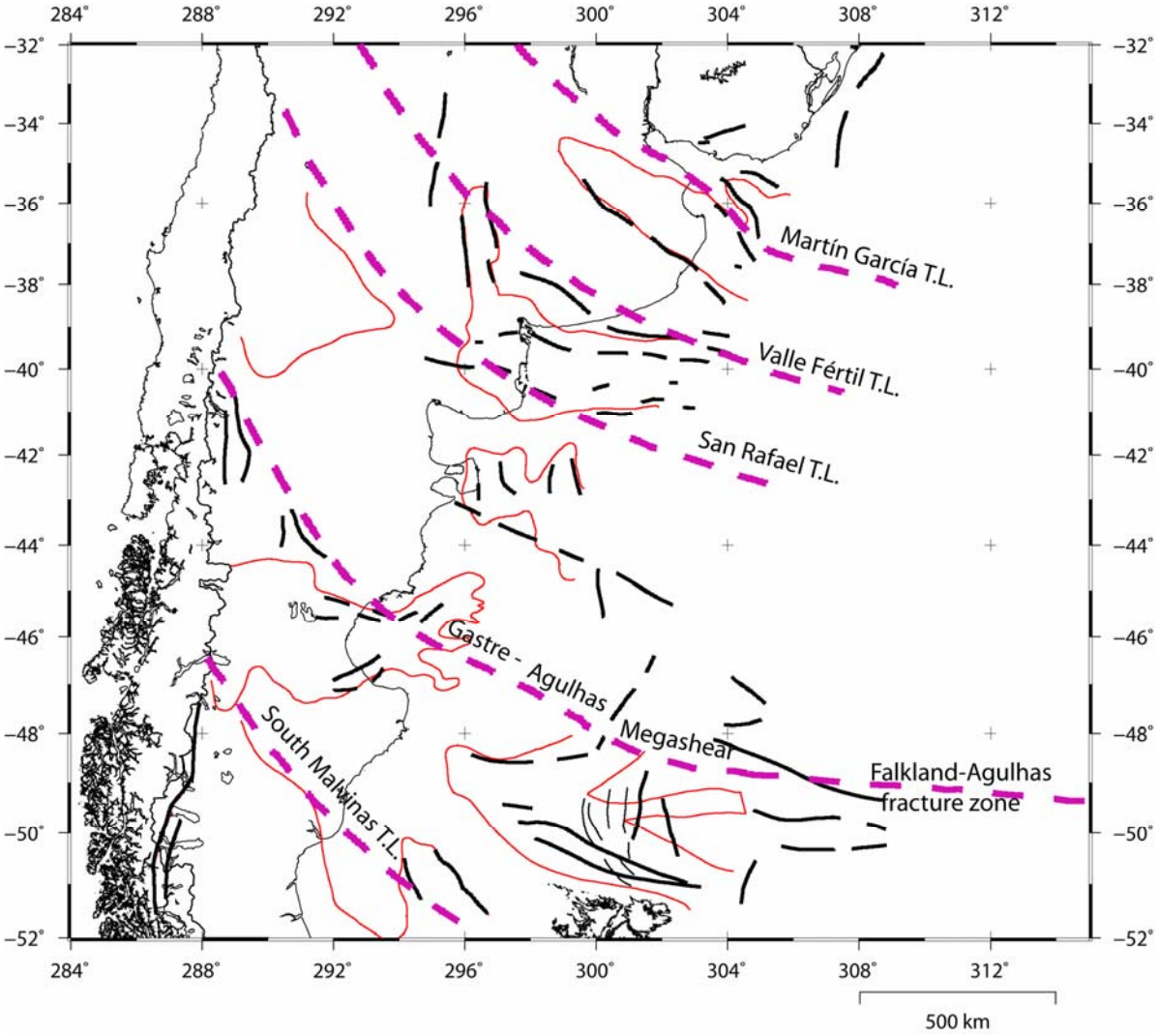

The Gastre-Agulhas Megashear extends onshore along the transcurrent Gastré Fault System in central Patagonia, which is associated with granite emplacement (Jacques, 2003), like the calc-alkaline granitoids of the North Patagonian Massif (Fig. 2.6). Its offshore extension corresponds to the Falkland-Agulhas Fracture Zone (Fig. 6.1). It was recognized as a major dextral shear zone, allowing displacement of the Southern Patagonian block relative to the rest of South America during the earliest rifting phase of Gondwana breakup. It also helps explain the postulated displacement of the Malvinas/Falkland islands (Macdonald et al., 2002).

The major basins and structural highs in the Argentine Margin are elongated at a high-angle to the direction of the margin (Figs. 3.1 and 6.1). They extend into the continental emerged areas, following the dominant NW-SE structural grain of the mainly Paleozoic and Precambrian basement orogenic belts. Offshore-onshore correlation based on refraction seismic and well data has historically been performed over the area (Ewing et al., 1963), showing good lithological correlation of the main stratigraphic units as well as the basement rocks under the sedimentary basins. In the Salado Basin area, the NW-SE elongation axis parallels a major morpho-structural basement feature, the Martín García High, with its eastward continuation as the Río de la Plata (or Plata) High, the latter separating the Salado and the Punta del Este basins (Fig. 2.6). The nature of the basement in this area was tentatively correlated with the Precambrian to Early Paleozoic gneissic, schistose and granitoid rocks described in the Tandilia High block (Fig. 2.6) (Zambrano & Urién, 1970). This basement high, extending to the south of the Salado Basin with the same orientation SW-NE, separates the latter from the Colorado Basin, to the south.

Fig. 6.1 (opposite page). Simplified tectonic map showing the main transverse tectonic lineaments (T.L.), attributed to zones of structural accommodation (purple, thick dashed lines after Jacques, 2003). Contours of the main basin and major fault lineaments are also indicated (modified after Urién & Zambrano, 1996). Basins: Co, Colorado; La, Laboulaye; Ma, Malvinas; Mc, Macachín; Mg, Magallanes; Ne, Neuquén; NMa, Northern Malvinas; PE, Punta del Este; Ra, Rawson; Sa, Salado; SJo, San Jorge; SJu, San Julián; Va, Valdés.

The basement of the Colorado Basin has been correlated with the Late Paleozoic deposits of the "Sierras Australes" (Southern Buenos Aires Hills, also called Ventana Hills) (Keeley & Light, 1991; Juan et al., 1996). These sediments represent the exposed portion of an older sedimentary basin (Claromecó Basin), buried between the Tandilia High and the Ventania Fold Belt hills (Fig. 2.6). The presence of these sediments at the bottom of the Colorado basin was confirmed by well drillings covering a wide area within the basin (Puelche x-1, Cruz del Sur x-1, Corona Austral z-1 and Estrella x-1) (Juan et al., 1996). The faults in the distal sectors of the Salado and Colorado basins are perpendicular to the continental margin (E-W and ESE-WNW) but, inland, they adopt the prevailing Paleozoic basement fabric, NW-SE (Max et al., 1999). Both basins are spatiallly constricted between the large transverse lineaments mentioned above.

6.2 Basin formation and evolution

Following the northward propagation of the continental rifting that led to the opening of the South Atlantic, a set of sedimentary basins were formed across the South American margin, displaying an arrangement of progressively younger basins from south to north. The wide range of orientations exhibited by the basins axis results from the strong control of the basement fabric (Keeley et al., 1993), and a time-varying stress field related to a multiple rifting phase evolution of the South Atlantic margin.

The southern basins, including the San Jorge, San Julián and Northern Malvinas basins (Fig. 2.6) have a more complex evolutionary history, since they were generated by a rift phase prior to the breakup-related Late Jurassic-Early Cretaceous main rift phase. The implications of basin evolution in the character of lithosphere extension in a rifted margin setting were studied from the perspectives of pre-breakup and post-breakup evolution. The southern parts of the Argentine margin exhibit a general thinning in the sedimentary cover over the outer shelf and slope. This was particularly observed in the transects over the San Jorge and the Valdés-Rawson basins (Fig. 4.6-4.8), and may be related to the uplift and subsequent erosion caused by the Andean Orogeny during Tertiary times (Rodríguez et al., 2001). In the San Julián Basin, reflection seismic revealed inverted tectonic structures attributed to a phase of oblique compression of probable

Aptian age, that produced a strong unconformity buried by non-deformed Maastrichtian sediments (Figueiredo et al., 1996). These authors related the inverted structures observed in the southern margin basins to the proximity to the Falkland-Agulhas Fracture Zone (Fig. 6.1).

6.2.1 Models of continental extension

After an early simplification in two categories of stretching, active rifting (controlled by a thermal plume impinging on the base of the lithosphere) and passive rifting (controlled by tensional stresses in the continental lithosphere), the focus changed towards a classification based on the strength and the rheological properties of the continental lithosphere (Allen & Allen, 2005). Both models agree that upper continental curst is deformed by brittle faulting although present different approaches on the accommodation of lithospheric extension in the lower crust to upper mantle and on the transfer mechanism of extension through the crust. Both models lead to crustal thinning and uplift of Moho, roughly coincident with the rift axis.

Pure shear uniform stretching model

Extension is due to take place uniformly and symmetrically in both the crust (by brittle fracture) and subcrustal lithosphere (by plastic flow) (Mackenzie, 1978). The total subsidence is made of two components: an initial (syn-rift) fault-controlled subsidence, which is dependent on the initial thickness of the crust and the amount of stretching β, and a subsequent thermal subsidence, caused by relaxation of the lithospheric isotherms to their pre-stretching position (Fig. 6.2a) (Allen & Allen, 2005).

Simple shear stretching model

This model explains lithospheric stretching assuming different mechanic responses between the crust and mantle lithosphere. Lithospheric extension takes place asymmetrically, by means of a large-scale, gently dipping shear zone that traverses the entire lithosphere and offsets the Moho (Wernicke, 1985). This shear zone transfers extension from the upper crust in one region to the lower crust and mantle lithosphere in another region. The elevated asthenosphere under the stretched lithosphere will control the location of the post-rift thermal subsidence. Ideally, there should be expected subsidence in the region of thin-skinned extensional tectonics, and uplift in the region overlying the thinned lower crust and mantle, i.e. over the zone of uplifted

asthenosphere (Fig. 6.2b) (Allen & Allen, 2005). Thermal subsidence should concentrate over the latter zone, leading to the formation of a shallow basin when erosion has previously flattened the uplifted crust (Allen & Allen, 2005). Uplift of the footwall is explained by unloading along major detachment faults, i.e. flexural cantilever effect of Kusznir et al. (1991) (Fig. 6.3).

Coupled simple-shear/pure-shear mode of deformation

This hybrid model considers that lithospheric extension is achieved by simple shear in the upper lithosphere, while pure shear is the dominant mechanism of deformation within the lower, plastic layer of the lithosphere. The fundamental architecture of continental lithosphere deformation is controlled by major basement faults that are restricted to the cool, brittle upper crust, i.e. the seismogenic layer, which has a thickness of 10 to 20 km (Kuznir & Egan, 1991). Since no faults have been observed in deep-seismic reflection cutting through the entire crust and offsetting the Moho, there must be a detachment level within or at the base of continental crust, above which the faults sole out (Fig. 6.2c) (Kusznir & Egan, 1990). These faults are directly responsible of extensional sedimentary basin formation, resulting in the formation of discrete rift basins within the collapsed hanging-wall of major basement faults.

Pure shear within the lithospheric mantle induces a passive rise of the lithosphere-asthenosphere boundary, transferring heat to the base of the thinned lithosphere. Subsequent cooling and contraction of the heated lithosphere will control the location and amplitude of the post-rift thermal subsidence (Fig. 6.3). In basins formed by several adjacent major faults, the resultant geometry is that of a set of sub-basins filled with syn-rift sediments, overlain by a laterally continuous blanket of post-rift thermal subsidence sediments. In this case, the ratio of post-rift to syn-rift sediment fill is greater.

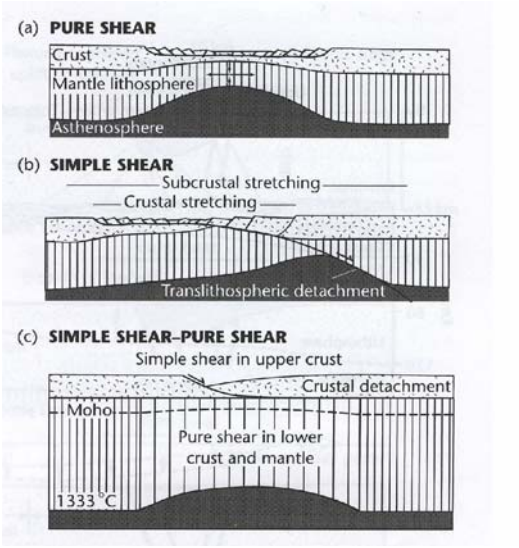

Fig. 6.2. Idealized representation of extensional lithospheric deformation models; (a) Pure shear (MacKenzie, 1978; Coward, 1986; Buck et al., 1988); (b) Simple shear (Wernicke, 1985; Royden et al., 1980); (c) Coupled model of simple-shear in the upper brittle crust and pure-shear in the plastic lower crust and mantle (Kusznir & Egan, 1991). Figure after Allen & Allen, (2005).

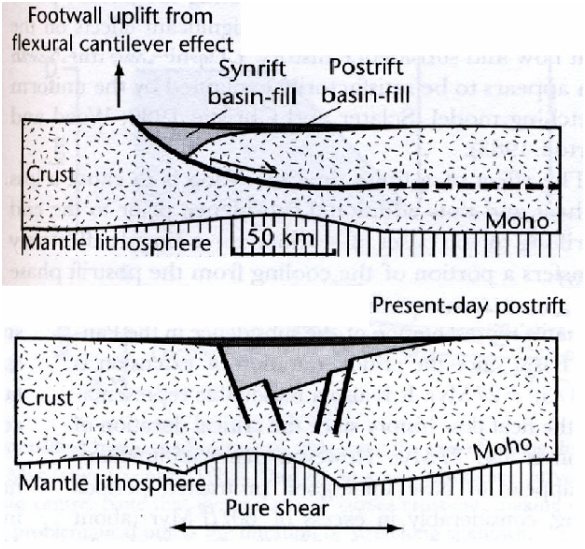

Fig. 6.3. Simplified spatial geometry of syn-rift and post-rift sedimentary basin fill on two different contexts of lithospheric extensional deformation: simple shear with intracrustal detachment, and pure shear (after Allen & Allen, 2005).

Karner & Driscoll (1999) proposed a method to describe the type of response of the lithosphere to extension, in relation to the distribution and magnitude of the various kinematically produced loads. Pre-rift to post-rift thickness ratios within crust (δ) and lithosphere (β) respectively, observed along a section of stretched lithosphere (Fig. 6.4) were plotted. The δ function determines the distribution of the rift-phase subsidence and the total thickness of sediments that can accumulate within the basin, whereas the β function controls the distribution of the post-rift subsidence (Karner & Driscoll, 1999). The relative distribution and magnitude of the estimated δ and β functions, obtained by matching the observed distribution and thicknesses of syn-rift and post-rift sequences, will help determine if some form of detachment was operative during the extension process (Fig. 6.4).

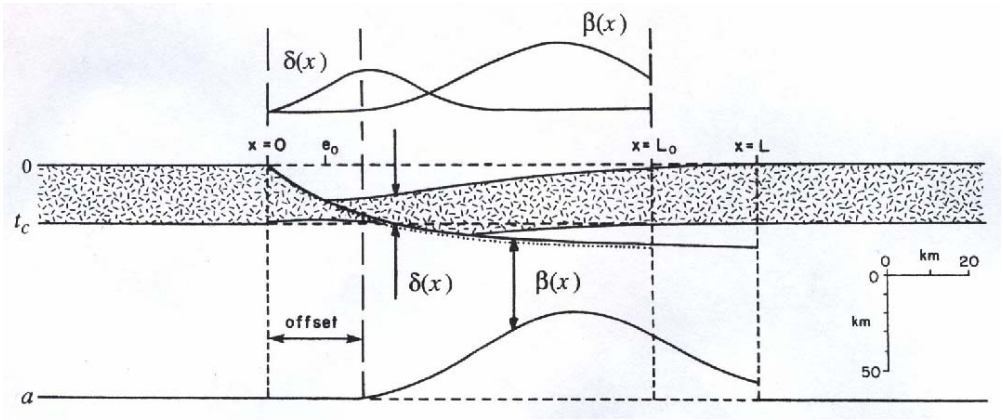

Fig. 6.4. Kinematic model of lithospheric extension by crustal simple-shear and lithospheric mantle pure-shear. The configuration of the model was inferred from the δ and β parameters shown above the model as mapping functions, which relate, respectively, the ratio between pre-rift to post-rift thickness of the crust and the lithosphere (after Karner & Driscoll., 1999).

6.2.2 Pre-breakup basin development

Several sedimentary basins that were developed prior to the breakup-related Late Mesozoic rift phase have been described across the Argentine margin. The presence of these rocks above the crystalline basement of the Salado and Colorado basins has been well documented and verified, especially in the deeply buried Claromecó Basin, under the sedimentary strata of the Colorado Basin (Fryklund et al., 1996). The Claromecó Basin is formed by Late Carboniferous weakly

metamorphosed sedimentary rocks. that have been correlated to onshore exposures in the Sierra de la Ventana, in southern Buenos Aires province (Fig. 2.6) forming the western extremity of the Cape Fold Belt (Keeley and Light, 1993). In general, these Late Paleozoic deposits are represented by an approximately 3000 m thick section (Juan et al., 1996), and were identified within the Salado and Colorado basins area as a set of parallel, steeply dipping and relatively strong reflectors (Fig. 3.8). These thick and deep sedimentary sequences are documented by both seismic reflection data and gravity modelling, and the position of these basins appears to be coincident or very close to the major depocentres of the Salado and Colorado basins, and correlate with a zone of relatively high-amplitude gravity anomalies (Fig. 5.2b and 5.3b). In both transects T1 and T2, the position of these depocentres were correlated to local shallowing of Moho (Fig. 5.2b and 5.3b). This fact may suggest that the position of the ancient Gondwana intracratonic basins exerted some control on the location of the younger breakup-related Salado and Colorado depocentres. To this respect, Fryklund et al. (1996) described a Permian phase of extension identified as E-W and NW-SE trending faulting within the basement of the Colorado Basin, followed by a transpressive episode that caused uplift and erosion. The direction of this faulting coincides with that of the major tectonic lineaments bounding the Salado and Colorado basins (Fig. 6.1).

6.2.3 Syn-rift evolution

The orientation of the seismic profiles utilized in this study, paralleling the strike of the major basins, as well as widespread presence of volcanic rocks within the syn-rift basins and a highly reflective basement prevents a good identification of the rift-related geological features. However, additional cross sections perpendicular to the strike of the basins, acquired from literature, display the spatial geometry between the main tectono-sedimentary sequences. Gravity modelling has contributed to refine the relief of the basement, from which, several inferred fault-bounded syn-rift structures, not imaged in the seismic profiles, have been interpreted (Figs. 5.1 and 5.3). As mentioned above, a different pattern of rift evolution is observed along the Argentine margin. The northern margin Salado, Colorado, Rawson and Valdés basins (Fig. 3.1), were formed during a single rifting episode related to the breakup of Gondwana in Late Jurassic-Early Cretaceous times. The southern margin basins (San Jorge, San Julián, North Malvinas) (Fig. 2.6) on the other hand, record a multiple-phase rifting evolution, that started in the early

Mesozoic. These basins were initially formed as back-arc basins during Permo-Triassic Pacific subduction along the SW margin of Gondwana (Keeley & Light, 1993; Ross et al., 1996).
The genetically Patagonian-related North Malvinas, San Julián and San Jorge basins (Fig. 2.6) exhibit a similar pattern of development, having been created by two successive rifting episodes (Fig. 2.10). The "early rift phase" was related to a phase of extension in Patagonia, in Early to Middle Jurassic times, after collision of the Deseado-Malvinas microplate against SW Gondwana (Ross et al., 1996). The "late rift phase" resulted from the Late Jurassic-Early Cretaceous breakup-related extension. The two rift phases are clearly identified in seismic sections across the North Malvinas and San Julián basins, separated by a prominent unconformity (Fig. 2.9) (Ross et al., 1996). The total thickness of the syn-rift deposits in the North Malvinas Basin reaches 7000 m in the deepest grabens, whereas the post-rift sediments are represented by a 1800 m thick succession. The San Jorge Basin (Fig. 3.1) however, exhibits a continued development of the two rift phases through Late Jurassic-Early Cretaceous. The early rift phase in the above mentioned basins is characterized by generalized volcanics and volcaniclastics of Middle to Late Jurassic age, widespread through the Patagonian region. In the San Jorge Basin, extension resulted in a series of fault-bounded half-grabens NW-SE oriented (Rodríguez et al., 2001).

The northern and central margin basins (Salado, Colorado, Rawson and Valdés) (Fig. 3.1) were originated during the Late Jurassic-Early Cretaceous breakup-related rift phase, and exhibit a variety of orientations, resulting from different structural grains of the basement. Extensional faulting controlled the development of the rift systems (Marinelli & Franzin, 1996). However, the seismic profiles of the transects do not image clearly enough recognizable syn-rift geometries as rotated fault-blocks or rift-related unconformities (Fig. 4.1-4.8). This is in part due to the orientation of some transects, paralleling the strike of the basins (Fig. 3.1). The pre-rift sequences in the northern region (Salado-Colorado basins) are made up of Upper Paleozoic metasedimentary rocks that, in the Colorado Basin area have an approximate thickness of 3000 m. The northern margin of the Colorado Basin experienced important uplift during and after the rift phase, with subsequent erosion of up to 2000 m of the pre-rift Paleozoic sequence (Juan et al., 1996). In both the Salado-Punta del Este and Colorado basins, thick (4000-5000 m) syn-rift deposits are filling a series of discrete fault-controlled half-graben-shaped depocentres (Stoakes et al., 1991; Franke et al., 2006) (Fig. 3.11). Deposition was synchronous with volcanism, as

extrusive volcanics and volcaniclastics are present at the base of the sequence (Stoakes et al., 1991; Franke et al., 2006).

6.2.4 Post-breakup basin development

Lithospheric stretching and crustal thinning eventually evolved in continental breakup between Africa and South America in Early Cretaceous time; inferred ages for Argentina/South Africa ranging from 127.7 to 135 Ma (Franke et al., 2006). Subsequent cessation of the fault activity that gave rise to the rift basins along the margin during continental rifting, was followed by the deposition of the post-rift sediments in a regime of regional thermal subsidence. These sediments are recognized by their lateral continuity and onlapping geometry over the underlying syn-rift sequences in some seismic profiles (Fig. 4.1-4.8) mostly orthogonal to the elongation of the basins. The maximum thickness should be coincident with the zone maximum relaxation of the isotherms, i.e. the zone of maximum crustal thinning during rifting. This appears to be the case in the Colorado Basin, according to the interpretation of transect T2b by Franke et al. (2006) (Fig. 3.11). In this figure, the post-rift sequence was identified between reflectors CO (Top Colorado) and BU (Breakup Unconformity), and exhibits maximum thickness at a distance of 300 km (Fig. 3.11), where the crust shows minimum thickness. This particular geometry could indicate pure shear as the mechanism of lithospheric stretching within this area (Figs. 6.2 and 6.3). Unlike the rift-fill sequence, the post-rift subsidence does not produce footwall uplift and subsequent erosion along the basin margins (Fig. 6.3), and the only variable is the amount of post-rift subsidence (Stoakes et al., 1991).

Post-rift sediments are documented to be preserved in all basins along the margin, with similar thicknesses to the syn-rift deposits. In the Salado and Colorado basins (Figs. 3.1, 4.1-4.4), the post-rift deposits range from Middle Cretaceous to Paleocene and are characterized by two units: a lower non-marine sequence and an upper interval of shoreface to marine sediments. The thickness of the post-rift sediments observed in the Salado area surpasses 2000 m, based on seismic information (Fig. 4.1 and 4.2) (Tavella & Wright, 1996). In the San Jorge Basin (Figs. 3.1, 4.7 and 4.8), the post-rift sediments have been divided into two sequences: early and late sag sequences (Rodríguez et al., 2001) that constitute the bulk of the sedimentation (Baldi & Nevistic, 1996).

Following the post-rift phase of subsidence that decreased exponentially with time, the onset of sea-floor spreading led to the deposition of the passive margin sequences, showing no relevant thickness variation. The passive margin phase is synchronous with sea-floor spreading of the expanding Atlantic Ocean. A thick layer of sediments from the continent progressively buried the newly formed continental margin of South America, as it rotated away from the active spreading centre, cooling and subsiding slowly (Stoakes et al., 1991). In the Salado-Colorado area, the passive margin phase is represented by an over 4500 m thick wedge of siliciclastic Eocene-Holocene sediments (Figs. 4.1-4.4).

In the seismic profiles along the transects, both post-rift and passive margin sequences are treated as a single unit called "post-breakup sediments", due to a certain ambiguity in the interpretation (Figs. 4.1-4.8). A main observation along the margin is the different thickness of the post-breakup cover over the outer shelf, showing a considerably thinning in the southern transects over the Valdés-Rawson and San Jorge basins, coincident with the position of the outer-shelf high (Figs. 4.6-4.8). The associated thick sedimentary wedge seaward of that high could be explained by intense sediment supply from the uplifted adjacent continental areas during the Tertiary Andean Orogeny (Figuereido et al., 1996).

6.3 Continent-ocean transition and boundary

Several crustal-scale studies have clearly shown that the location of the continent-ocean transition (COT) zone is associated with a rapid crustal thinning, reflecting a distinct shallowing of the Moho discontinuity (e.g. Keen & Dehler, 1997; Karner & Driscoll, 1999; Tsikalas et al., 2005). This is a fact if extension leading to breakup is short-lived and occurs with high strain-rates (e.g. Keen, 1987; Buck, 1991). Such a distinct COT zone is delineated as a strong negative-positive gradient on the Bouguer-corrected gravity field along the Argentine margin (Fig. 3.4). Within this zone, the continent-ocean boundary (COB) can be placed. The COB is defined as the line of maximum extent of continental crust material (e.g. Karner et al., 1999), representing the change from top continental crystalline basement to oceanic basement.

The initial prediction of COB along the transects, based on the analysis of the Bouguer-corrected gravity anomaly curves (Fig. 4.12), approximated roughly the positions obtained in gravity modelling for most of the transects (Figs. 5.1-5.6). Further refinement was required to satisfy the modelled results, leading to adjustments of up to 80 km in some transects (T0, T23). In all transects except T2 and T23, the best match of the models was achieved by introducing a slightly lower density (0.02-0.03 g/cm^3) within the portion of thickened oceanic crust that lies adjacent to the COB (Figs. 5.1-5.6).

As mentioned in Chapter 4, the initial proposals to locate the transition from continental to oceanic crust in passive margin settings, were based on correlated magnetic and gravity anomaly lineaments paralleling the continental margin (Rabinowitz and LaBrecque, 1979). The magnetic anomaly G was interpreted as an edge-effect caused by the contact between continental and oceanic crust, and was associated to the continental margin isostatic gravity anomaly (Rabinowitz & LaBrecque, 1979). All transects along the Argentine margin show a prominent free-air gravity high near the shelf edge paralleling a seaward low counterpart (Fig. 3.2, 3.3 and 4.12). This coupled anomaly, termed the gravity edge-effect, does not necessarily correlate with mass excesses or deficiencies within or below the crust, but can instead reflect a topographic edge-effect, caused by the steep bathymetry, present in most passive margins (Rabinowitz, 1982).

An attempt to infer the location of the COB along the margin, based on magnetic data is presented in Fig. 6.5. The locations of the seaward-dipping reflector wedge, depicted from the seismic profiles (Fig. 4.2-4.7), were marked over the transects tracks (Fig. 6.5). This position, marked in Fig. 6.5 by a thick, black dashed-line is highly coincident with an elongate, rather continuous magnetic high, at about 100 km seaward of the shelf edge (Fig. 6.5). This elongated anomaly has associated a seaward negative anomaly, which indicates a possible edge-effect related to the position of the magnetic bodies (Ghidella et al., 1995). Correlation between high-amplitude positive magnetic anomalies and the presence of seaward-dipping reflectors has been established on both the Argentine and the southwestern African margin (Austin et al., 1982; Bauer et al., 2000) and proposed as a possible continent-ocean boundary. Offshore the Salado Basin, the COB approaches the shelf-edge, and both lines appear to merge at 35°S, in a zone where the magnetic anomaly is most prominent. South of 45°S, the continuity of the COB location appears to be interrupted by a 100 km sinistral offset, that correlates with the Colorado Discontinuity (CD) (Fig. 6.5) (Ghidella et al., 1995). The

inferred position of the COB coincides closely with that of Rabinowitz & LaBrecque (1979). The southeastern offset segment of the COB coincides with the position of a conspicuous 300 km long, free-air gravity high elongated parallel to the margin (Figs. 3.2 and 3.3). This feature is represented in Fig. 6.5 as a thick orange line and was attributed to a deep igneous source with a probable volcanic expression, that could be related to leakage from the neighbouring and regionally prominent Falkland-Agulhas Fracture Zone (cfr. Fig. 6.7).

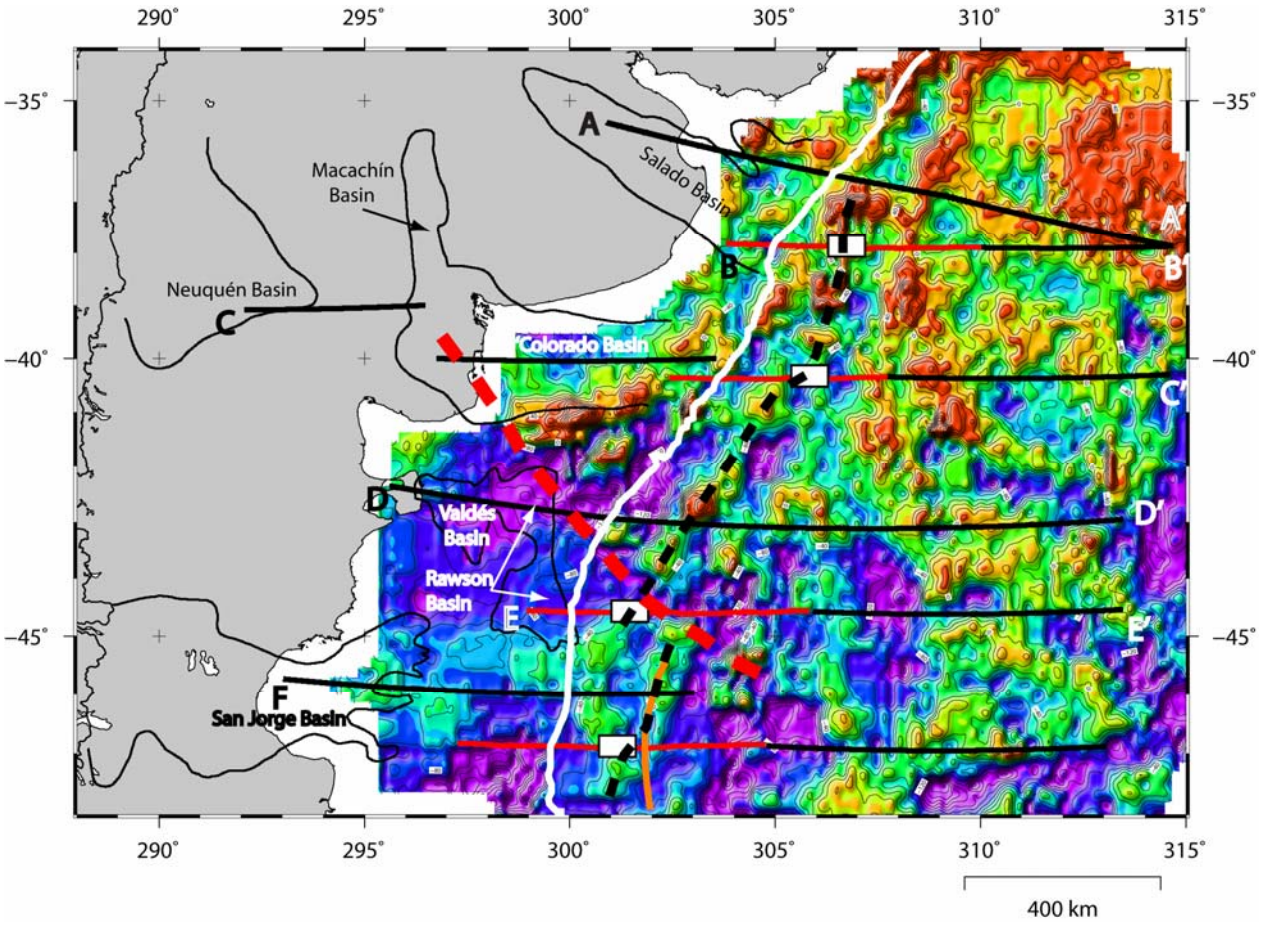

Fig. 6.5. Inferred continent-ocean boundary (COB) along the Argentine margin based on the magnetic anomaly field and the position of the seaward dipping reflection wedge depicted from seismic reflection profiles along the constructed transects in this study. Thick black dashed line, COB; thick red dashed line, Colorado Discontinuity (CD); thick continuous white line, 500 m isobath; white rectangular boxes, position of the SDRs wedge along the transects.

An additional constraint to the positioning of the COB/COT can be provided by the Bouguer-corrected anomaly map, by placing the superficial trace of this boundary along the trace of the maximum gradient shown by the anomaly. The thus inferred continent-ocean boundary line shows a considerable degree of coincidence with the position of the COB previously derived from magnetic anomaly and the SDRs wedge location (Fig. 6.6). Both lines display clearly the major offset at 45°S, coincident with the Colorado Discontinuity.

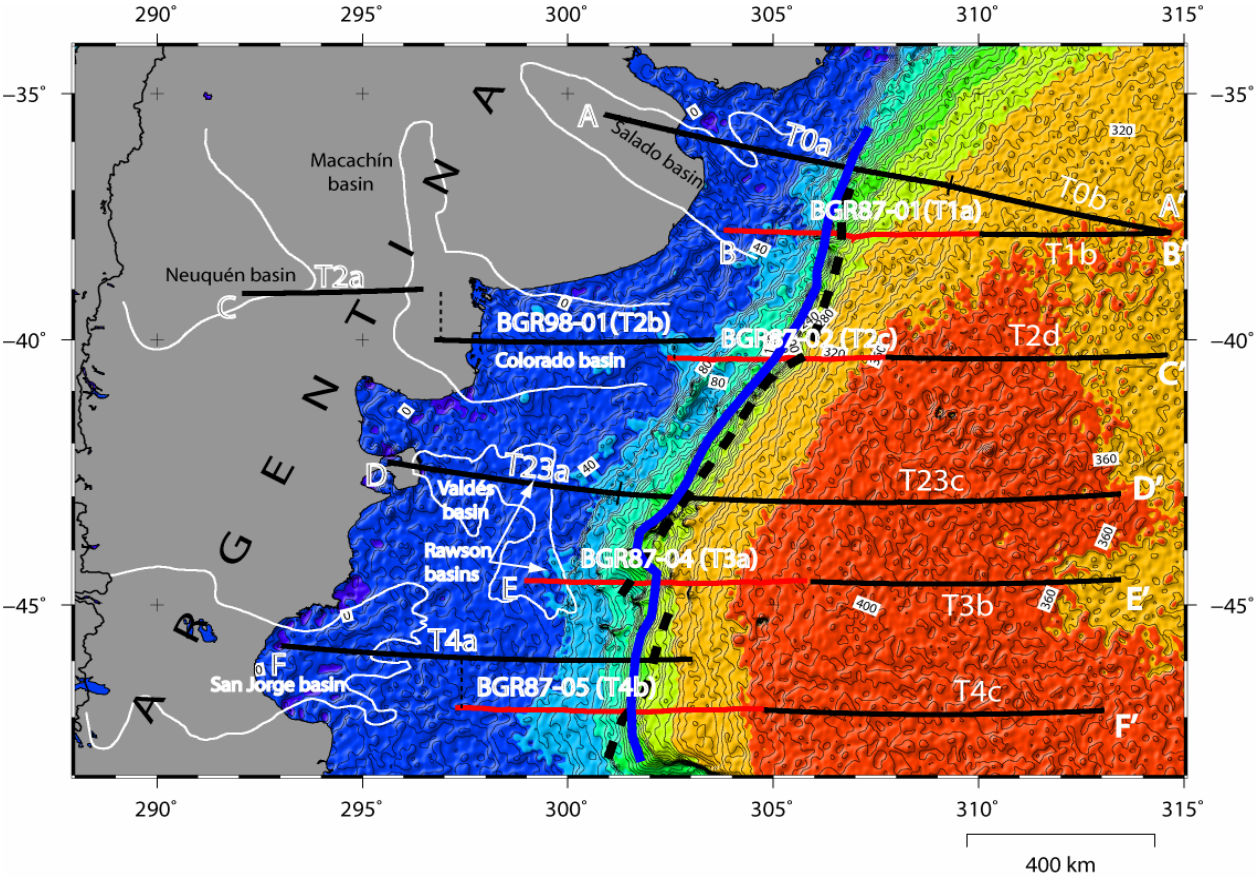

Fig. 6.6. Bouguer corrected gravity anomaly grid used to infer the continent-ocean boundary (COB). Thick, continuous blue line, COB trace based following line of maximum gravity gradient. Thick, black dashed line, estimated position of COB based on magnetic data and SDRs wedge location.

6.4 Breakup-related magmatism

Continental extension and breakup leading to the opening of the South Atlantic was strongly influenced by magmatism, resulting in the development of common crustal units and structural features within the newly formed margins (e.g. Eldholm et al., 2000). Within the Argentinian margin, the magmatic character of the crust is represented by both flow-basalts filling the base of the rift basins, as well as by a rather continuous belt of seaward-dipping reflectors sequences (SDRs), paralleling the margin (Hinz et al., 1999). Furthermore, underplating of presumed upper-mantle intrusives within the lower crustal bodies (LCB) has been inferred from gravity modelling results, in several transects across the margins (Figs. 5.1-5.3 and 5.5)

6.4.1 Continental Flood Basalts (CFB)

Extrusive volcanic flows of Late Jurassic-Early Cretaceous age, (inferred age of 129-134 Ma; Peate, 1997) have been described within the basal syn-rift fill sequence in the northern parts of the Argentine margin, i.e. in the Salado-Punta del Este basins, and, in minor quantity, in the Colorado Basin (Fig. 4.1-4.4) (Lesta, 1978; Tavella & Wright, 1996; Stoakes et al., 1991). These rocks are represented by flow-basalts of tholeitic composition interlayered with pyroclastic layers (Stoakes et al., 1991) and were considered as the southernmost expression of the Paraná-Etendeka volcanic province, related to the Tristan da Cunha mantle-plume. South of the Colorado Basin, no basaltic flows are found. Instead, rhyolitic lavas and pyroclastic flows of Early and Middle Jurassic age extend widely in the Patagonia region, forming an extensive “rhyolitic plateau” (Ramos, 1996). The origin of this large volcanic province was explained in a context of lower-plate passive margin controlled by simple shear lithospheric stretching (Ramos, 1996). These volcanic rocks constitute a thick basal syn-rift sequence within the southern basins of the Argentine margin (Rawson-Valdés, San Jorge, San Julián and Northern Malvinas basins) that was associated to a Middle Jurassic early rift phase (165 to 155 Ma) related to the initial stages of Gondwana breakup (Ramos, 1996).

6.4.2 Seaward-dipping reflector sequences (SDRs)

These wedge-shaped bodies of volcanic rocks have been identified in the BGR reflection seismic lines (Figs. 4.1-4.4) (Hinz et al., 1999), located beneath the outer continental margin. According

to several studies (Hinz et al., 1999; Gladczenko et al., 1999; Ghidella et al., 2005) the SDRs constitute continuous features along the margin, coincident with the magnetic anomaly G of Rabinowitz & LaBrecque (1979). A main observation from both the seismic interpretation and the gravity modelling (Figs. 4.1-4.4 and 5.1-5-6) is the decrease in volume of the SDRs wedges in the southern sector of the margin, approaching the transform margin (Fig. 6.7) together with the absence of significant associated magnetic anomalies, south of 43ºS (Fig. 3.5).

6.4.3 Lower crustal bodies (LCB)

Several lower crustal bodies of high-density and high-velocity rocks, derived from gravity model in this study, and from seismic data (Franke et al., 2006), were observed along the margin, with the most remarkable examples located in the northern transects,T0 and T1, within the Salado Basin area (Figs. 5.1-5.6). Further south, the presence of these features is almost non-existent, restricted to a small manifestation in Transect T3, east of the Rawson Basin (Fig. 5.5). This fact describes a first-order variation of the margin configuration along strike (Fig. 6.7).

Modelling results indicated elongated (up to 250 km long), relatively thin (up to 5 km) bodies, placed under the continent-ocean transition (COT) zone (Figs. 5.1-5.6). The position of the prominent LCBs of the northern Argentine margin correlates with the presence, in the upper crust, of the Paraná flood basalts, that are found in the Salado Basin. This may suggest that the emplacement of the LCBs in that area was controlled by the magmatic activity exerted by the Tristan da Cunha hot-spot.

Major margin variations along-strike can be visualized in Fig. 6.7, where the proportionally scaled transects are presented in correlative order from north to south, the latter being vertically aligned along the shelf-edge. The most striking variation, consisting of a southward reduction of the magmatic activity, is clearly shown by the diminishing volumes, in this direction, of the lower crustal bodies (LCB), which are indicated by the gray-coloured raster (Fig. 6.7).

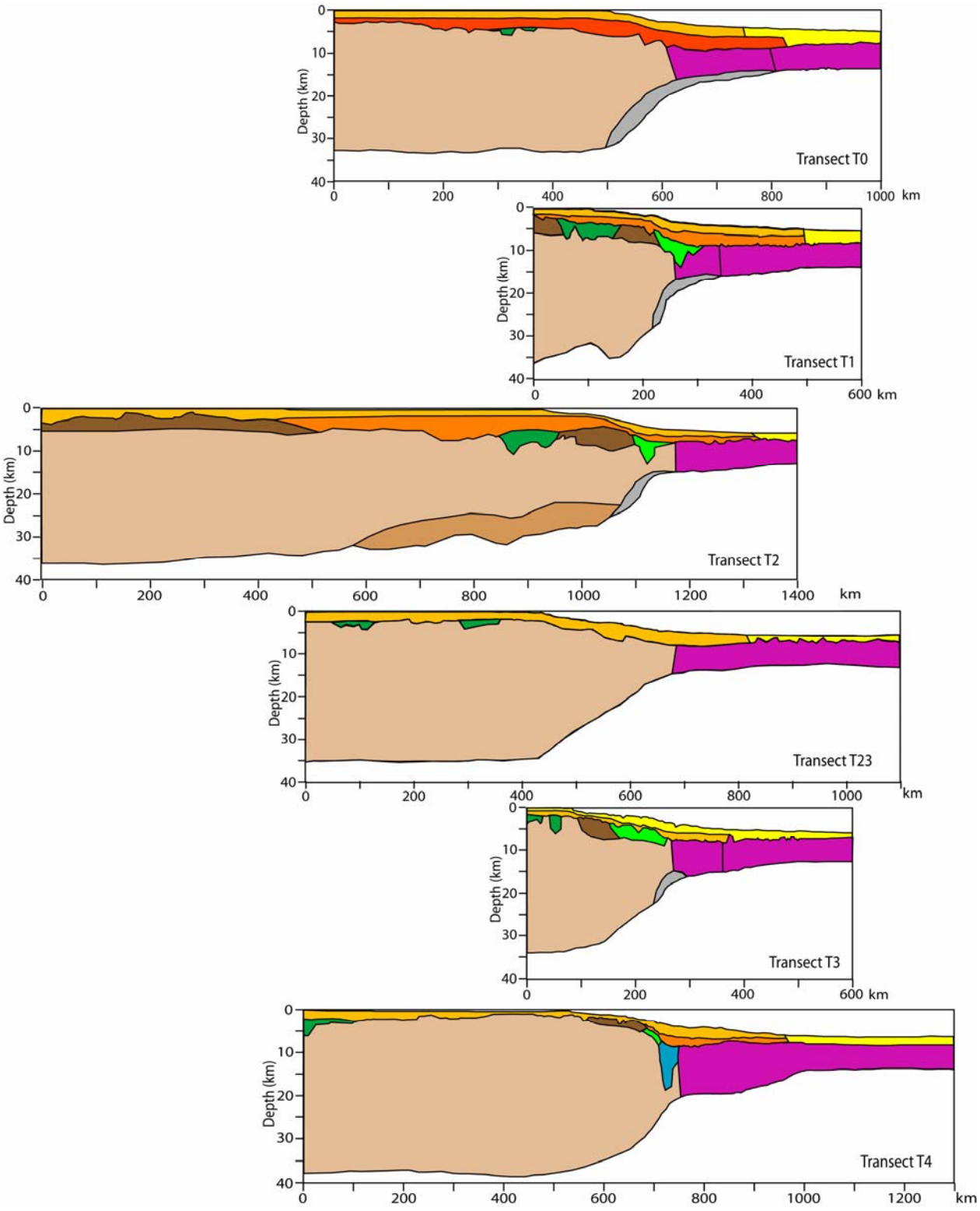

Fig. 6.7. Transects T0-T4 displayed in an along-margin array from north (above) to south (below), aligned with the shelf-edge.

6.5 Conjugate margin setting

The striking asymmetry between the two conjugate continental margins is denoted by their contrasted physiography. The continental shelf of Argentina extends hundreds of km between the coast and the shelf edge, the latter shown as a yellow line along the elongated edge-anomaly (Fig. 6.6). This wide platform exhibits an extremely smooth and flat relief (Parker et al., 1996) and is associated with a wide and flat coastal plain. In contrast, its counterpart African continental shelf stretches along a very narrow strip (Fig. 6.8) and is flanked by a prominent mountainous coastal relief.

An attempt to reconstruct the pre-breakup position of the continental plates across the South Atlantic was performed, with the aim of understanding the styles of deformation during rifting and come up with proposals of lithospheric stretching mechanisms (Figs. 6.8 and 6.9). Identification of the conjugate margin segment that correlates with that of the study area was based on the major oceanic fracture zone traces recognized in the free-air gravity map across the South Atlantic (Fig. 6.8). The continuity of these lineaments is poorly constrained within the Argentine and Cape basins, partially masked under the sedimentary cover.

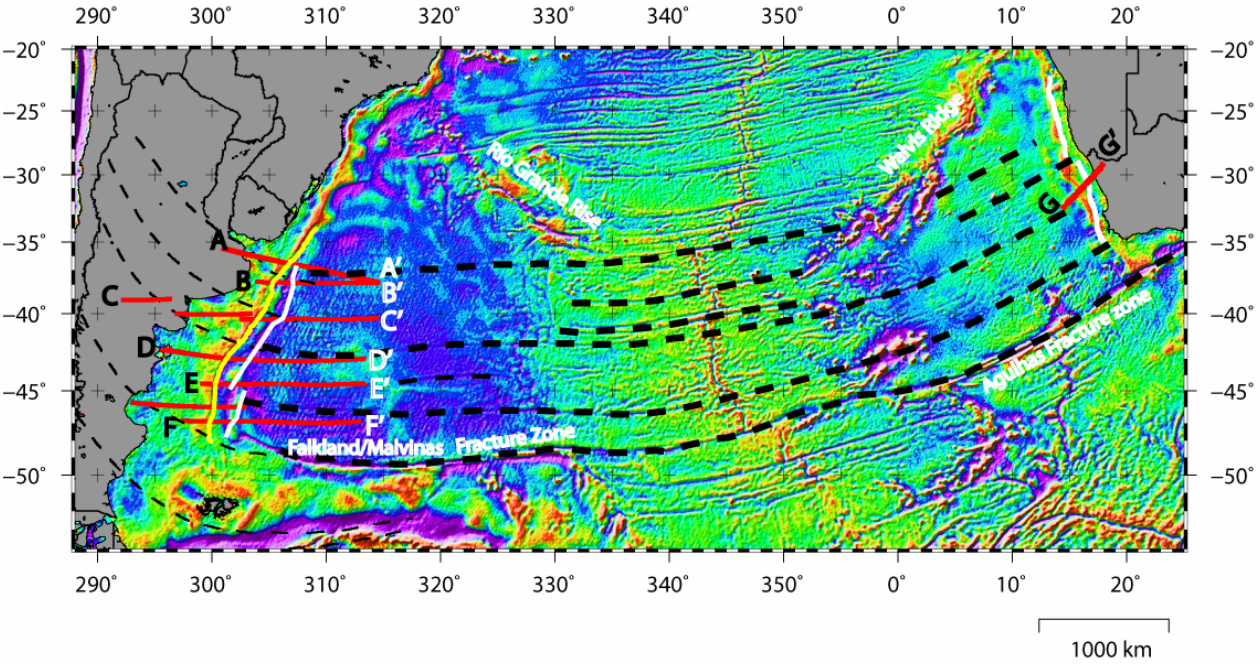

However, certain major lineaments could be traced across the entire width between the two continental plates, and corroborated with the correlation of Davison (1999). A crustal-scale geological section across the Orange Basin (Hirsch et al., 2007) in the Southwestern African margin (Transect G-G' in Fig. 6.8) was used in combination with its conjugate on the Argentine Margin (Transect C-C') to construct a synthetic composite section of the pre-breakup structure (Fig. 6.9).

Fig. 6.8 (previous page). Conjugate margin correlation based on oceanic fracture zones identified from the 2x2' KMS99 (Andersen & Knutsen, 1998) satellite free-air gravity grid across the South Atlantic. Onshore transform fault lineaments are shown from the South America side. Major lineament positions were elaborated after Davison (1999). Transect location on the conjugate SW African margin used in plate reconstruction is indicated as line G-G'. Inferred COB for the Argentine margin and COB derived from Rabinowitz & LaBrecque (1979) for the SW African margin are indicated with thick, continuous white line.

Fig. 6.9 (opposite page). Modelled crustal sections from the Colorado and Orange basins **(a)**. Estimated COB from both transects were used to reconstruct the continental plates at the time of breakup **(b)**. Observed and modelled free-air gravity anomalies are shown over the transects (transect across the Orange Basin modified after Hirsch et al., 2007). Transects locations in Fig. 6.7.

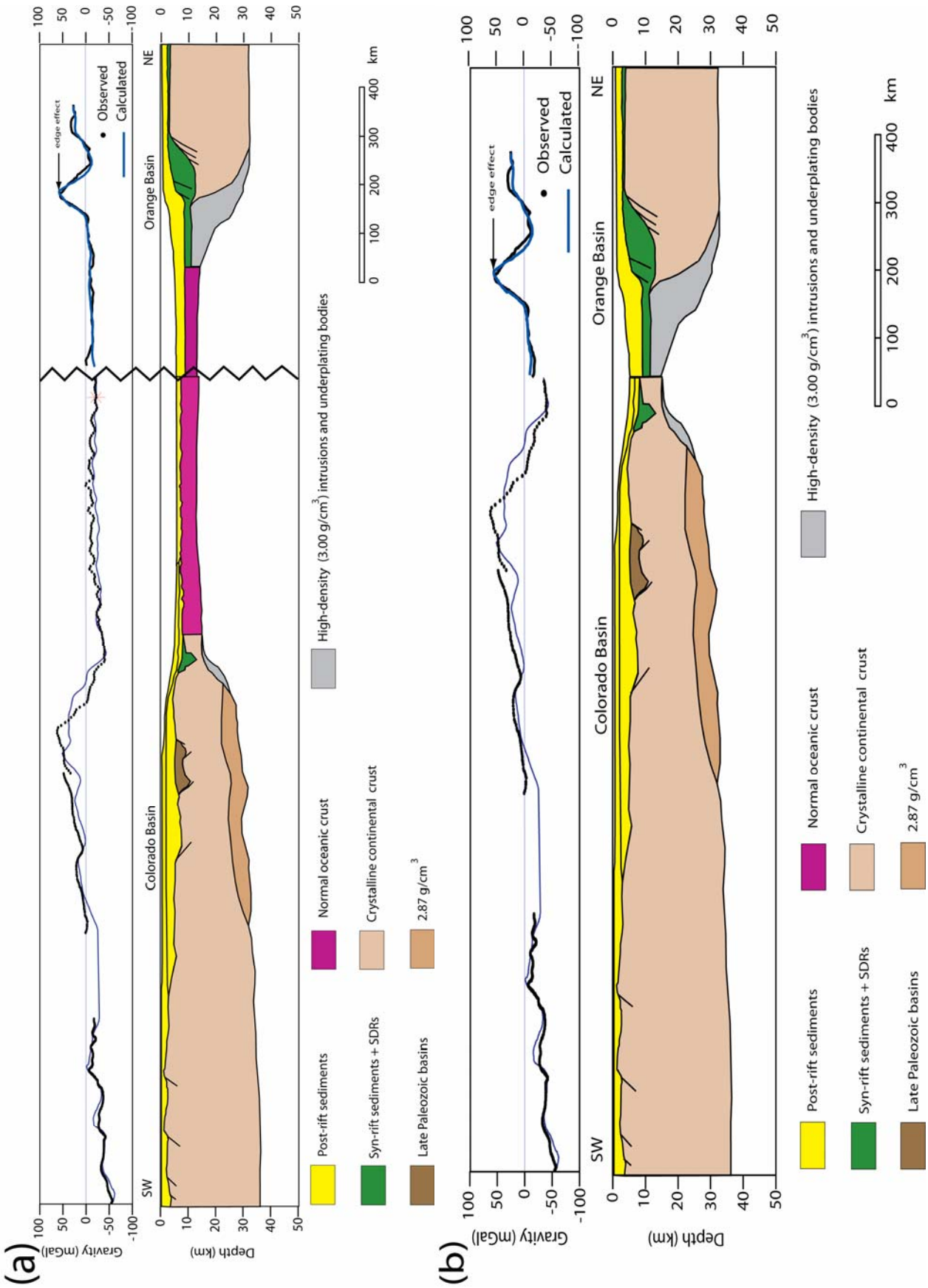
(a)
Gravity (mGal)
Depth (km)
edge effect
Observed
Calculated
Colorado Basin
Orange Basin
SW
NE
0 100 200 300 400 km
Post-rift sediments
Syn-rift sediments + SDRs
Late Paleozoic basins
Normal oceanic crust
Crystalline continental crust
2.87 g/cm3
High-density (3.00 g/cm3) intrusions and underplating bodies
(b)
Gravity (mGal)
Depth (km)
edge effect
Observed
Calculated
Colorado Basin
Orange Basin
SW
NE
0 100 200 300 400 km
Post-rift sediments
Syn-rift sediments + SDRs
Late Paleozoic basins
Normal oceanic crust
Crystalline continental crust
2.87 g/cm3
High-density (3.00 g/cm3) intrusions and underplating bodies

Several observations from the composite transect allow to elucidate the type of crustal scale mechanisms of extension that operated during rifting and breakup of the continental plates. Asymmetric extension is commonly observed in extensional settings and has been associated to contrasting conjugate types of passive margins, which led to their classification into two main groups: upper- and lower-plate margins (Fig. 6.10) (Lister, 1991). Considering simple shear as the cause of the asymmetry, the two end-member types of passive margins can be visualized from the lithospheric stretching model of Wernicke (1985) (Fig. 6.2). A more detailed graphic description is given in Fig. 6.10, where the upper-plate margin comprises the crust above a deep detachment, whereas the lower-plate margin corresponds to the footwall of the detachment, overlain by faulted upper-plate remnants (Lister, 1991).

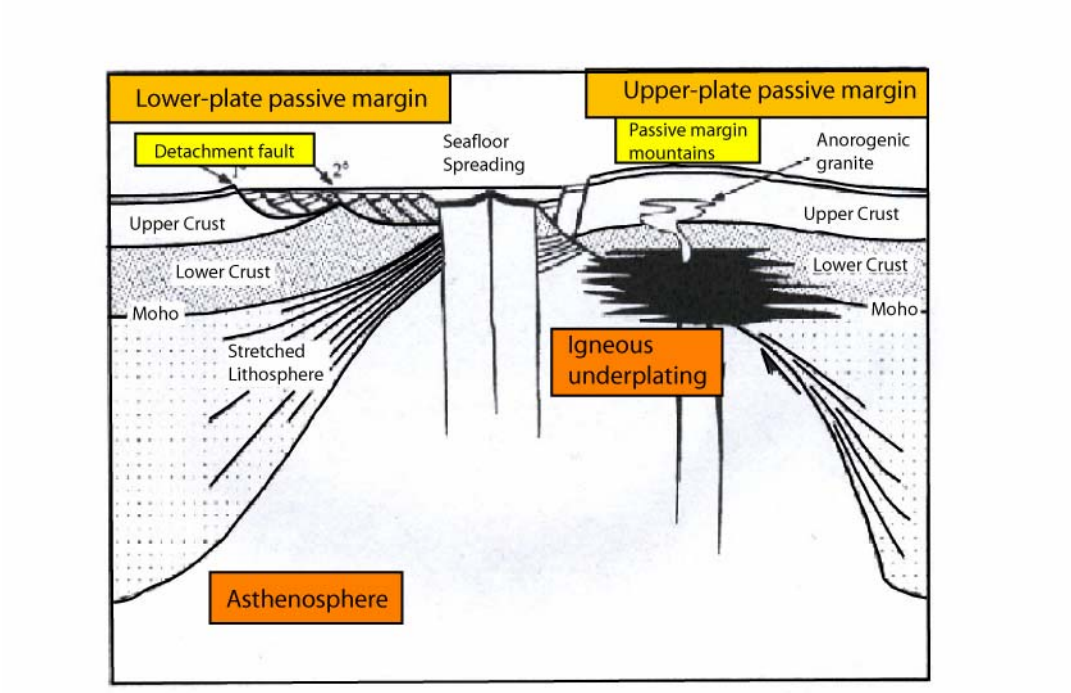

Fig. 6.10. Upper-plate and lower-plate passive margin settings resulting from simple shear lithospheric stretching (modified after Lister et al., 1991).

The most remarkable feature within the African margin is a voluminous high-velocity and high-density zone (7.00 km/s; 3.00 g/cm³) in the lower crust beneath the position of the SDRs outer wedge (Fig. 6.9) (Bauer et al., 2000). This unusual zone was interpreted as exclusively igneous crust, reaching a thickness of up to 25 km, formed by igneous underplating due to shallowing of

the asthenosphere (Bauer et al., 2000). The vertical correspondence between the large igneous underplating in the lower crust and the pronounced positive relief of the above continental hinterland adjacent to the margin, has been causally associated to the context of upper-plate passive margins (Fig. 6.10) (Lister, 1991).

In such context, the margin uplift, triggered by asthenospheric rise in the initial stages of extension, is preserved long after the thermal anomaly has decayed, this fact being attributed to the effects of igneous underplating (Lister et al., 1991). The high lateral velocity gradient landward of the igneous intrusion led Bauer et al. (2000) to redefine the COB at this position, consistent with the G-anomaly of Rabinowitz & LaBrecque (1979). This led to the interpretation of a relatively abrupt continental rupture over a narrow rift zone, as shown by the steeply dipping contact between the basement and the syn-rift sediments (Fig. 6.9).

The presence of such "transitional crust" (Bauer et al., 2000) between pure continental crust and pure oceanic crust, has not been observed on the modelled transects along the Argentine margin (Figs. 5.1-5.6). This is in agreement with the detailed OBS studies of Franke et al. (1999) over the same area. In contrast, these features appear to be common on the African side of the South Atlantic, as revealed by deep seismic and potential field data studies of the Angola margin (Contrucci et al., 2004; Moulin et al., 2005) and the South Gabon margin (Meyers et al., 1996; Rosendahl, 1999). In these areas, a so-called transitional crust that cannot be recognized as purely oceanic nor continental, was associated to coincident free-air gravity and magnetic highs (Meyers et al., 1996) and to a lower crust anomalous high-velocity zone (Contrucci et al., 2004). Although not full agreement has been reached in interpreting this transition zone, the above mentioned authors support the model of a zone of highly attenuated crust with anomalous high velocities and densities at its lower level. The concept of transitional crust was further reviewed by Rosendahl et al. (2005) under the term "proto-oceanic crust" (POC). This term was used to describe a crust that is fundamentally oceanic in nature, coupled to the oceanic crust. Furthermore, these authors relate the origin of the proto-oceanic crust to leaky transform faults (Rosendahl et al., 2005).

The observed asymmetry (Fig. 6.9) suggests the interpretation of the Argentine margin as a lower-plate margin, in the model of Lister (1991) (Fig. 6.9). When joining the two continental

blocks of South America and Africa (Fig. 6.9) the evidences of asymmetric extension are more visible, and the most remarkable of those is the considerable thinning of the crystalline crust on the South American plate over a wide area. In comparison, the African margin exhibits a much more abrupt transition between the thinned and the normal thickness crust (Fig. 6.9). The rather homogeneous crustal thinning, inferred from the widely distributed post-rift sediments implies the presence of a mid-crustal detachment surface beneath the brittle, upper crust (Fig. 6.11). Evidence for a zone of detachment that accommodated the crustal extension are sparse, since reflection seismic profiles along the constructed transects do not resolve the deep structure. Furthermore, the absence of a density contrast between the blocks at either side of the detachment prevents gravity modelling from detecting this structure. Several faults interpreted from the basement geometry derived from gravity modelling appear to dip relatively gently seawards (Fig. 6.9), suggesting a detachment present at some level underneath. On the African side, in contrast, upper crustal deformation appears to have taken place through steeply dipping faults that produce little horizontal extension and define an abrupt continent-ocean transition (Bauer et al., 2000). The presence of a continuous basement high along the margin, as observed in most transects (Fig. 4.1 -4.6) is consistent with the lower-plate margin model, and could be an indirect indicator of a detachment surface, as postulated by Lister (1991).

The above mentioned indications, and further literature references (Ramos, 1996) suggest a model of lithospheric stretching and breakup controlled by crustal scale simple shear (Wernicke, 1981) (Fig. 6.11). A large translithospheric detachment triggered by first order crustal discontinuities, such as sutures, is needed to explain this idealized model. Pre-existing structures and major intracratonic lithological boundaries may have controlled the line of continental rupture (Macdonald, 2003). Observations from the crustal geometries of the modelled transects suggest differences in the type of extensional regimes along the margin. Conspicuous local shallowing of the Moho discontinuity is present beneath the Salado and Colorado basins (Fig. 5.2, 5.3). Both basins exhibit great sedimentary thicknesses and an unexpectedly high gravity anomaly response (Introcaso, 2003), suggesting isostatic uncompensation. The assumption of localized pure shear stretching is in agreement with the position of the elevated Moho, beneath the basins major depocentres (Fig. 5.2, 5.3 and 6.7).

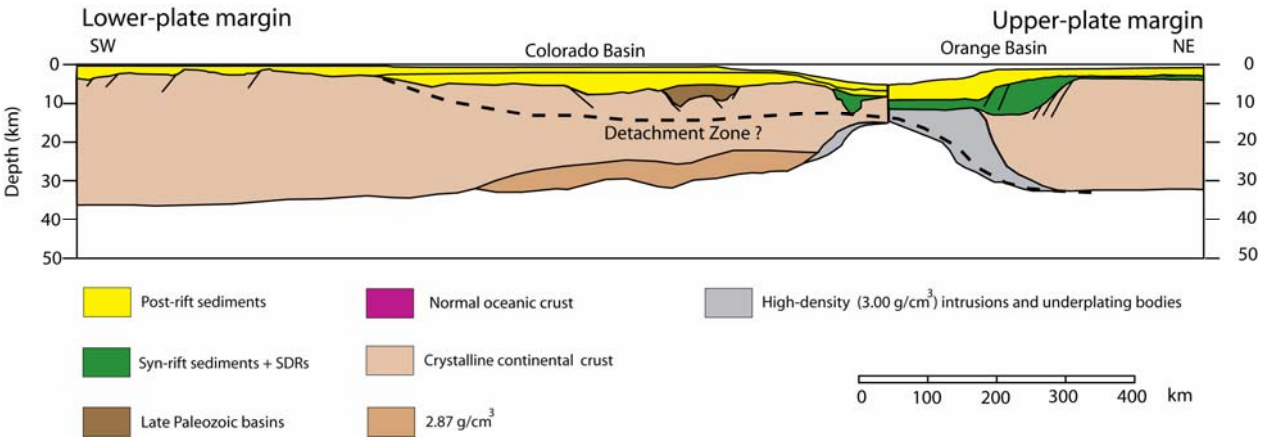

Fig. 6.11. Proposed model of simple shear controlled lithospheric stretching along composite conjugate margin transect CC'-GG'. Transect location in Fig. 6.7.

Finding the position of the COB has important consequences in the rheological characterization of the lithosphere, since that boundary should form at the location of greatest crustal and lithospheric mantle thinning, that is, within the region of maximum depth-independent lithospheric extension (Karner et al., 1992). As mentioned above, the post-rift thermal subsidence is controlled by the spatial distribution of lithospheric mantle thinning. To this respect, the presence of an intracrustal detachment surface can be inferred from the distribution and thickness of syn- and post-rift sequences (Karner & Driscoll, 1999). Such crustal scale detachments develop in response to diferential lithospheric extension, with greater thinning within the lithospheric mantle rather than within the crust (Karner et al., 1992).

An example of inferred intra-crustal detachment was demonstrated by Karner et al. (1999) in the Brazilian margin basins of Tucano and Sergipe-Alagoas. The absence of post-rift sediments within the Tucano Basin, and the subsequent lack of thermal subsidence was related to an intracrustal detachment that concentrated the extension on the upper crust, while enhancing the lithospheric mantle thinning in the Sergipe-Alagoas basins area (Karner et al., 1992). On the Argentine margin, however, the widespread distribution of post-rift sediments observed over all the transects (Figs. 4-1-4.8) in this study (and confirmed by literature) implies to argue the

presumed presence of an intracrustal detachment from a different approach. In this aspect, a reduced flexural strength of the lithosphere compared to that of the Brazilian margin, could have allowed developing the subsidence to accommodate the thick post-rift sedimentary cover, while the detachment surface was operative. A lower flexural lithospheric strength would be in agreement with the younger basement rocks exhibited by the Argentine margin, compared to the Brazilian margin.

Further constraints to the conjugate margin setting across the South Atlantic have been provided by the results of a parallel study on the North Namibia margin (Sakariassen, 2007). This study reveals a volcanic-type margin south of the Walvis Ridge, as interpreted from the presence of a lower crustal body (LCB), large volumes of seaward-dipping reflectors (SDRs), and a wide transitional crust, composed of accreted igneous material (Sakariassen, 2007). Likewise the Argentine margin, the volcanic character of the Namibe margin has been related to the Tristan da Cunha hot-spot. The presence of an extensive transitional crust along the Namibe margin is the major contrasting feature in relation to the Argentine side. Sakariassen (2007) places the COB at the seaward edge of the inferred COT. These general observations in the SW African margin appear to confirm the asymmetric character of the conjugate margin setting, suggesting a simple-shear controlled lithospheric breakup.

Chapter 7

Summary and conclusions

An integrated approach involving seismic reflection/refraction and potential field data and modelling has been successfully implemented in the geological characterization of the Argentine margin. The methodology constitutes a robust tool to complement the limitations of the seismic profiling approach, providing additional constraints to the imaging of the crustal structure. A variety of data sets were compiled and processed, consisting of: (a) reflection seismic profiles from BGR (Bundesanstalt für Geowissenschaften und Rohstoffe); (b) gridded data, including bathymetry, free-air and Bouguer-corrected gravity anomalies, magnetics and sediment thickness. These data were presented in a set of seismic sections (in both two-way traveltime and depth converted sections), gridded anomaly maps and along-track extracted profiles. Depth conversion of the seismic reflection profiles was performed using a simplified seismic velocity-depth function derived from regional considerations and earlier studies. A total of six composite crust-scale regional transects along the Argentine margin were constructed. All transects span the entire continental margin, from the coastline to the abyssal plain, and some have onshore extensions. Initial Moho relief estimates along the transects were inferred by both forward isostatic balancing and inverse gravity modelling, since seismic reflection data did not resolve the deep crustal structure.

All constructed transects were 2D-gravity modelled utilizing the initial constraints from the seismic reflection profiles and the Moho relief estimates. By defining crustal-blocks of geologically representative density values, iterative corrections of both block geometry and density were implemented until the modelled gravity response satisfactorily matched the observed gravity anomalies. The crustal structure thus inferred along the transects shows a more complex configuration, revealed by the presence of discrete blocks of anomalous density, and a varied geometry of the Moho relief. In particular, high-density lower crustal bodies represent a common feature along the Argentine margin, being more developed in the northern parts.

By evaluating and comparing the constructed geological models both in along-margin and conjugate margin settings, the main aspects of the crustal architecture and margin development could be tested, and new insights added. In this context, inheritance of

Precambrian and Paleozoic structures appears to have played an important role in the pattern of continental rupture, with the development of basins along preferential directions, at high-angle with the direction of the margin, like the Salado and Colorado basins. The basins along the Argentine margin were thus formed parallel to large zones of structural accommodation, following lines of weakness between ancient accreted blocks of SW Gondwana, exhibiting a variety of orientations. Furthermore, continental rifting and subsequent breakup along the Argentine margin propagated from south to north, with the southern San Jorge, San Julián and North-Malvinas basins developing through a more complex extensional history, starting in early Mesozoic time in a back-arc setting. The main Late Jurassic-Early Cretaceous breakup rift phase developed thick syn- and post-rift sedimentary sequences, preserved within the margin basins. The major syn-rift depocentres are not well resolved by the seismic profiles along the transects, due in part to non-favorable orientation of the latter. Instead, the thick post-rift sediments are well imaged, showing thick development and widespread distribution over the margin.

A particular focus in constraining the margin geometry was made in this study, by inferring the position of the continent-ocean boundary (COB) along the margin. A COB location was tentatively derived from magnetics, Bouguer-corrected gravity anomaly, and the location of the seaward-dipping reflectors wedge (SDRs) showing good correspondence with the inferred COB of Rabinowitz & LaBrecque (1979). Lithospheric breakup was accompanied with widespread magmatism along the Argentine margin, exhibiting a stronger character in the northern parts of the margin, due to the proximity of the Tristan da Cunha hot-spot. In addition to the continuous wedge of seaward-dipping reflectors paralleling the margin in its entire length, the presence of high-density lower crustal bodies has been observed with considerable development to the north of the margin. Southwards, the margin appears to be more influenced by the Falkland-Agulhas Fracture Zone, and exhibits reduced magmatic manifestations.

Physiographic and crustal-scale analysis of the conjugate Argentine and SW Africa margins reveals a striking asymmetry. The most appropriate conceptual tectonic model is that interpreting lithospheric extension as controlled by simple-shear deformation mode, the Argentine margin evolved as the lower-plate margin. Pure-shear controlled lithospheric extension may have also taken place beneath some major rift depocentres, like in the Salado and Colorado basins, as expressed by local shallowing of Moho derived from gravity

modelling. This is observed particularly in the the Salado Basin area. The existence of a presumed intracrustal detachment within the Argentine margin can only be inferred on the basis of indirect evidence, since the seismic reflection data have limited resolution at deep crustal levels.

Based on the integrated seismic reflection and potential field data and modelling approach, six regional transects were constructed that, in turn, contribute to the better understanding of the crustal-scale structure and architecture of the Argentine margin. The comparative analysis of the modelled transects provides crucial information regarding the along-margin evolution in both time and space and, to a certain degree, provides additional insights to the conjugate margin setting evolution.

References

Allen, P.A. and Allen, J.R., 2005. Basin analysis. Principles and applications.

Andersen, O.A., and Knudsen, P., 1998. Global marine gravity field from the ERS-1 and Geosat geodetic mission. Journal of Geophysical Research 103, 8129-8138.

Austin, J.A. Jr., and Uchupi, E., 1982. Continental-oceanic crustal transition off southwest Africa. The American Association of Petroleum Geologists Bulletin, V.66, No. 9, p. 1328-1347.

Baldi, J.E. and Nevistic, V.A., 1996. Cuenca costa afuera del Golfo San Jorge. In Ramos, V.A. and Turic, M.A. (eds.) Geología y Recursos Naturales de la Plataforma Continental Argentina, XIII Congreso Geológico Argentino y III Congreso de Exploración de Hidrocarburos, Relatorio 3: 29-65, Buenos Aires.

Bauer, K., Neben, S., Schreckenberger, B., Emmermann, R., Hinz, K., Notker, F., Gohl, K., Schulze, A., Trumbull, R.B. and Weber, K., 2000. Deep structure of the Namibia continental margin as derived from integrated geophysical studies. Journal of Geophysical Research, V. 105, No. B11, p., 25,829-25,853.

Biddle, K.T., Snavely, P.D. and Uliana, M.A., 1996. Plateau de las Malvinas. In Ramos, V.A. and Turic, M.A. (eds.) Geología y Recursos Naturales de la Plataforma Continental Argentina, XIII Congreso Geológico Argentino y III Congreso de Exploración de Hidrocarburos, Relatorio 3: 29-65, Buenos Aires.

Buck, W.R., 1991. Modes of continental lithospheric extension. Journal of Geophysical Research, V. 96, No. 12, p. 20,161-20,178.

Cawood, P., 2004. Terra Australis Orogen: Rodinia breakup and development of the Pacific and Iapetus margins of Gondwana during the Neoproterozoic and Paleozoic. Earth-Science Reviews 69, p. 249-279.

Condie, K., 1989. Plate tectonics and crustal evolution.

Contrucci, I., Matias, L., Moulin, M., Geli, L., Klingelhofer, F., Nouze, H., Aslanian, D., Olivet, J.L., Rehault, J.P. and Sibuet, J.C., 2004. Deep structure of the West African continental margin (Congo, Zaire, Angola), between 5°S and 8°S, from reflection/refraction seismics and gravity data. Geophysical Journal International 158 (2), p. 529-553.

Dalziel, I.W.D., Lawver, L.A. and Murphy, J.B., 2000. Earth and Planetary Science Letters 178 (2000), p. 1-11.

Davison, I., 1999. Tectonics and hydrocarbon distribution along the Brazilian South Atlantic margin. In: Cameron, N.R. Bate, R.H. & Clure, V.S. (eds) The Oil and Gas Habitats of the South Atlantic. Geological Society, London, Special Publications, 153, 133-151.

de Wit, M., Jeffrey, M., Bergh, H. and Nicolaysen, L., 1999. Gondwana reconstruction and dispersion. Search and discovery article #30001 (1999). www.searchanddiscovery.net.

Direen, N.G. and Crawford, A.J., 2003. Fossil seaward-dipping reflector sequences preserved in southeastern Australia: a 600 Ma volcanic passive margin in eastern Gondwanaland. Journal of the Geological Society, London, Vol. 160, p. 985-990.

Eldholm, O., Gladczenko, T.P., Skogseid, J. and Planke, S., 2000. Atlantic volcanic margins: a comparative study. In Nødvedt, A. et al., (eds.) Dynamics of the Norwegian Margin. Geological Society, London, Special publications, 167, p. 411-428.

Ewing, M., Ludwig, W.J. and Ewing, J.I., 1963. Geophysical Investigations in the submerged Argentine coastal plain. Geological Society of America Bulletin, V.74, p. 275-292.

Figuereido, A.M.F., Pellón de Miranda, A., Ferreira, R.F. and Zalán, P.V., 1996. Cuenca de San Julián. In Ramos, V.A. and Turic, M.A. (eds.) Geología y Recursos Naturales de la Plataforma Continental Argentina, XIII Congreso Geológico Argentino y III Congreso de Exploración de Hidrocarburos, Relatorio 3: 29-65, Buenos Aires.

Franke, D., Neben, S., Schreckenberger, B., Schulze, M.S. and Krawczyk, C.M., 2006. Crustal structure across the Colorado Basin, offshore Argentina. Geophysical Journal International 165, p. 850-864.

Fryklund, B., Marshall, A and Stevens, J., 1996. Cuenca del Colorado. In Ramos, V.A. and Turic, M.A. (eds.) Geología y Recursos Naturales de la Plataforma Continental Argentina, XIII Congreso Geológico Argentino y III Congreso de Exploración de Hidrocarburos, Relatorio 3: 29-65, Buenos Aires.

Ghidella, M., Paterlini, C.M., Kovacs, L.C. and Rodríguez, G., 1995. Magnetic Anomalies on the Argentine Continental shelf. Proceedings of the 4th International Congress of the Brazilian Geophysical Association and 1st Latinoamerican SEG/ULG Conference (Río de Janeiro).

Gladczenko, T.P., Hinz, K., Eldholm, O., Meyer, H., Neben, S. and Skogseid, J., 1997. South Atlantic volcanic margins. Journal of the Geological Society, London, Vol. 154, p. 465-470.

Hinz, K., Neben, S., Schreckenberger, B., Roeser, H.A., Block, M., Goncalves de Souza, K., and Meyer, H, 1999. The Argentine continental margin north of 48ºS: sedimentary successions, volcanic activity during breakup. Marine and Petroleum Geology 16, p. 1-25.

Hirsch, K.K., Scheck-Wnderoth, M., Paton, D.A., di Primio, R., Horsfield, B., Cloetingh, S.A.P.L. and Beekman, F., 2007. 3D Gravity modelling and subsidence analysis in the Orange Basin, southwest African Continental Margin. Geophysical Research Abstracts, V.9, 06275, 2007.

Introcaso, A., 2003. Significativa descompensación isostática en la Cuenca del Colorado (República Argentina). Revista de la Asociación Geológica Argentina, 58 (3), p. 474-478.

Jacques, J.M., 2003. A tectonostratigraphic synthesis of the Sub-Andean basins: inferences on the position of South American intraplate accommodation zones and their control on South Atlantic opening. Journal of the Geological Society, London, V.160, p.703-717.

Juan, R., de Jager, J., Russell, J. and Gebhard, I., 1996. Flanco norte de la cuenca del Colorado. In Ramos, V.A. and Turic, M.A. (eds.) Geología y Recursos Naturales de la Plataforma Continental Argentina, XIII Congreso Geológico Argentino y III Congreso de Exploración de Hidrocarburos, Relatorio 3: 29-65, Buenos Aires.

Keeley, M.L. and Light, M.P.R., 1993. Basin evolution and prospectivity of the Argentine continental margin. Journal of Petroleum Geology, vol. 16(4), p. 451-464.

Karner, G., Egan, S.S. and Weissel, J.K., 1992. Modelling the tectonic development of the Tucano and Sergipe-Alagoas rift basins, Brazil. Tectonophysics, 215, p. 133-160.

Karner, G. and Driscoll, N.W., 1999. Tectonic and stratigraphic development of the West African and eastern Brazilian Margins: insights from quantitative basin modelling. In: Cameron, N.R., Bate, R.H. and Clure, V.S. (eds.) The Oil and Gas Habitats of the South Atlantic. Geological Society, London, Special Publications, 153, 11-40.

Keen, C.E. and Dehler, S.A., 1997. Extensional styles and gravity anomalies at rifted continental margins; some North Atlantic examples. Tectonics 16 (5), p. 744-754.

Kostadinoff, J., Gregori, D.A. and Raniolo, A., 2005. Configuración geofísica-geoloógica del sector norte de la provincia de Río Negro. Revista de la Asociación Geológica Argentina 60 (2), p. 368-376.

Kusznir, N.J. and Egan, S.S., 1990. Simple-shear and pure-shear models of extensional sedimentary basin formation: Application to the Jeanne d'Arc Basin, Grand Banks of Newfoundland. In: Tankard, A.J. and Balkwill, H.R. (eds.) Extensional Tectonics of the North Atlantic Margins. American Association of Petroleum Geologists Memoir 46, p. 305-322.

Lesta, P., Mainardi, E. and Stubelj, R., 1980. Plataforma continental argentina. In Turner, J.C.M. (ed.) Segundo Simposio de Geología Regional Argentina. Academia Nacional de Ciencias II: p. 1577-1601, Córdoba.

Lesta, P., 2003. La exploración de la plataforma continental argentina: presente, pasado y futuro. Petrotecnia, 3, p.16-23.

Lister, G.S., 1991. Detachment models for the formation of passive continental margins. Tectonics, V.10, No. 5, p. 1038-1064.

Macdonald, D., Gómez-Pérez, I., Franzese, J., Spalletti, L., Lawver, L., Gahagan, L., Dalziel, I., Thomas, C., Trewin, N., Hole, M. and Paton, D., 2003. Mesozoic breakup of SW Gondwana: implications for regional hydrocarbon potential of the southern South Atlantic.

Marinelli, R.V. and Franzin, H.J., 1996**.** Cuencas de Rawson y Península de Valdés. In Ramos, V.A. and Turic, M.A. (eds.) Geología y Recursos Naturales de la Plataforma Continental Argentina, XIII Congreso Geológico Argentino y III Congreso de Exploración de Hidrocarburos, Relatorio 3: 29-65, Buenos Aires.

Max, M.D., Ghidella, M., Kovacs, L., Paterlini, M. and Valladares, J.A., 1999. Geology of the Argentine continental shelf and margin from aeromagnetic survey. Marine and Petroleum Geology 16, p. 41-64.

McKenzie, D., 1978. Some remarks on the development of sedimentary basins. Earth and Planetary Science Letters. V. 40, p.25-32.

Meyers, J.B., Rosendahl, B.R. and Austin, J.A. Jr, 1996. Deep-penetrating MCS images of the South Gabon Basin: implications for rift tectonics and post-breakup salt remobilization. Basin research, 8, (1), p. 65-84.

Milsom, J., 2003. Field geophysics. The geological field guide series.

Mjelde, R., Kodaira, S., Digranes, P., Shimamura, H., Kanazawa, T., Shiobara, H., Berg, E.W. and Riise, O., 1997. between a Regional and Semi-regional crustal OBS model in the Vøring Basin, Mid-Norway margin. Pure and Applied Geophysics 149, p. 641-665.

Mjelde, R., Kasahara, J., Shimamura, H., Kamimura, A., Kanazawa, T., Kodaira, S., Raum, T. and Shiobara, H., 2002. Lower crustal seismic velocity-anomalies; magmatic underplating or serpentinized peridotite? Evidence from the Vøring Margin, NE Atlantic. Marine Geophsical Researches 23, p. 169-183.

Moulin, M., Aslanian, D., Olivet, J.L., Contrucci, I., Matias, L., Geli, L., Klingelhoefer, F., Nouze, H., Rehault, J.P. and Unternehr, P., 2005. Geological constraints on the evolution of the Angolan margin based on reflection and refraction seismic data (ZaiAngo Project). Geophysical Journal International 162 (3), p. 793-810.

Nafe, J. E., and C. L. Drake, 1957. Variation with depth in shallow and deep water marine sediments of porosity, density and the velocities of compressional and shear waves. Geophysics, v. 22 Issue3, p. 523-552.

Nürnberg, D. and Müller, R.D., 1991. The tectonic evolution of the South Atlantic from Late Jurassic to present. Tectonophysics, 191, 27-53.

Pankhurst, R.J., Rapela, C.W., Fanning, C.M. and Márquez, M., 2006. Earth-Science Reviews 76, p. 235-257.

Parker, G., Violante, R.A. and Paterlini, M.C., 1996. Fisiografía de la plataforma continental. In: Ramos, V.A. and Turic, M.A. (eds.) Geología y Recursos Naturales de la Plataforma Continental Argentina, XIII Congreso Geológico Argentino y III Congreso de Exploración de Hidrocarburos, Relatorio 3: 29-65, Buenos Aires.

Peate, D.W., 1997. The Paraná-Etendeka Province. In: Mahoney J.J. and Coffin M.F. (eds.) Large Igneous Provinces: continental, oceanic, and planetary flood volcanism, Geophysical Monograph 100, American Geophysical Union, Washington, DC, 247-272.

Planke, S., 1993. Section: Section plotting, digitizing and utility program. Version 1.0. Computer program/database documentation series no. 4, Geophysics Research Group, Department of Geology, University of Oslo.

Rabinowitz, P.D. and LaBrecque, J., 1979. The Mesozoic South Atlantic Ocean and evolution of its continental margins. Journal of Geophysical Research 84, p. 5973-6002.

Rabinowitz, P.D., 1982. Gravity measurements bordering passive continental margins. In Scruton, R.A. (ed.). Dynamics of passive margins. Geodynamics series Vol. 6, p. 91-114.

Ramos, V.A., 1996. Evolución tectónica de la plataforma continental. In: Ramos, V.A. and Turic, M.A. (eds.) Geología y Recursos Naturales de la Plataforma Continental Argentina, XIII Congreso Geológico Argentino y III Congreso de Exploración de Hidrocarburos, Relatorio 3: 29-65, Buenos Aires.

Rodríguez, J.F.R. and Littke, R., 2000. Petroleum generation and accumulation in the Golfo San Jorge Basin, Argentina: a basin modelling study. Marine and Petroleum Geology 18, p. 995-1028.

Rosendahl, B.R. and Groschel-Becker, H., 1999. Deep seismic structure of the continental margin in the Gulf of Guinea; a summary report. In: Cameron, N.R., Bate, R.H. and Clure, V.S. (eds.) The Oil and Gas Habitats of the South Atlantic. Geological Society, London, Special Publications, 153, 11-40.

Rosendahl, B.R., Mohriak, W.U., Odegard, M.E., Turner, J.P., Dickson, W.G., 2005. West Africa and Brazilian Conjugate Margins: Crustal Types, Architecture and Plate Configurations, 25th annual GCSSEPM Foundation Bob F. Perkins Res. Conference, Petroleum Systems of Divergent Continental Margin Basins, Houston, Texas.

Ross, J.G., Pinchin, J., Griffin, D.G., Kinkelman, M.G., Turic, M.A. and Nevistic, V., 1996. Cuenca de Malvinas Norte. In Ramos, V.A. and Turic, M.A. (eds.) Geología y Recursos Naturales de la Plataforma Continental Argentina, XIII Congreso Geológico Argentino y III Congreso de Exploración de Hidrocarburos, Relatorio 3: 29-65, Buenos Aires.

Sakariassen, R., 2007. North Namibia margin: regional tectonic evolution based on integrated analysis of seismic reflection and potential field data and modelling. MSc Thesis Department of Geosciences, University of Oslo.

Sandwell, D.T., and Smith, W.H.F., 1997. Marine gravity anomaly from Geosat and ERS-1 altimetry. Journal of Geophysical Research 192, 10039-10054 (v. 15.1).

Soares, J.R.S., Miranda, A.P. and Figueiredo, A.M.F., 2000. Geological and geophysical interpretation of the San Julián Basin, offshore Argentina. In: Atlantic Rifts and Continental Margins.

Stoakes, F.A., Cambell, C.V., Cass, R. and Ucha, N., 1991. Seismic stratigraphic analysis of the Punta del Este Basin, offshore Uruguay, South America. The American Association of Petroleum Geologists Bulletin V. 75, No. 2, p. 219-240.

Talwani, M. and Eldholm, O., 1973. Boundary beween continental and oceanic crust at the margin of rifted continents. Nature V. 241, p. 325-330.

Tavella, G.F. and Wright, C., 1996. Cuenca del Salado. In Ramos, V.A. and Turic, M.A. (eds.) Geología y Recursos Naturales de la Plataforma Continental Argentina, XIII Congreso Geológico Argentino y III Congreso de Exploración de Hidrocarburos, Relatorio 3: 29-65, Buenos Aires.

Tsikalas, F., Eldholm, O. and Faleide, J.I., 2005. Crustal structure of the Lofoten-Vesterålen continental margin, off Norway. Tectonophysics 404, p.151-174.

Urién, C.M. and Zambrano, J.J., 1996. Estructura de la Plataforma Continental. In Ramos, V.A. and Turic, M.A. (eds.) Geología y Recursos Naturales de la Plataforma Continental Argentina, XIII Congreso Geológico Argentino y III Congreso de Exploración de Hidrocarburos, Relatorio 3: 29-65, Buenos Aires.

Watts, A.B. and Stewart, J., 1998. Gravity anomalies and segmentation of the continental margin offshore West Africa. Earth and Planetary Science Letters 156, p. 239-252.

Wernicke, B., 1985. Uniform-sense normal simple shear of the continental lithosphere. Canadian Journal of Earth Sciences 22 (1), p. 108-125.

White, R.S., McKenzie, D.P. and O'Nions, K.R., 1992. Oceanic crustal thickness from seismic measurements and rare earth element inversions. Journal of Geophysical Research, V. 97, B13, p. 19683-19715.

Zambrano, J.J. and Urién, C.M., 1970. Geological outline of the basins in southern Argentina and their continuation off the Atlantic shore. Journal of Geophysical Research, V. 75, No. 8, p.1363-1396.